Free Space Optical Wireless Communication with Physical Layer Network Coding

Zina Mohammed Hassan Mohammed Ali Abu-Almaalie

A thesis submitted in partial fulfilment
of the requirements of the
University of Northumbria at Newcastle
for the degree of

Doctor of Philosophy

Research undertaken in the
Faculty of Engineering and Environment

June 2016

Abstract

Terrestrial free-space optical (FSO) communications is an emerging low-cost, license-free and high-bandwidth access solution for a number of applications including the "last mile" access network. However, for a transmission range from a few meter to longer than 1 km, a number of atmospheric phenomena, such as rain, haze, fog, snow, scintillation and pointing errors become a major performance limiting factors in FSO systems resulting in link deterioration and ultimately complete link failure. Relay-assisted technique is capable of mitigating the signal fading and maintain acceptable performance levels. In this thesis, a two-way relay (TWR) channel technique is adopted to increase system spectral efficiency, which in turn boosts the network throughput. This is achieved by using a physical layer network coding (PNC) technique, where network coding (NC) is applied at the physical layer. It takes advantage of the superimposition of the electromagnetic waves, and embraces the interference, which was typically deemed as harmful, by performing the exclusive-OR mapping of both users' information at the relay. Therefore, the main contribution of this thesis is to study the design of the TWR-FSO communication system that embraces PNC technique for the full utilization of network resources based on the binary phase shift keying (BPSK) modulation. Moreover, error control coding (ECC) in conjunction with interleaving can be employed in FSO communications to combat turbulence-induced fading, which can enhance the performance of the proposed TWR-FSO PNC system. A comparative study between convolutional code (CC) and bit-interleave coded modulation with iterative decoding (BICM-ID) code are carried out. The result shows that the BICM-ID code outperforms the CC for TWR-FSO based PNC over strong turbulence regime by ~10dB of SNR to achieve a BER of 10^{-4}. However, the number of users that can be simultaneously transmitted to the relay is considered the main constraint in PNC system. Therefore, to overcome this challenge, a new scheme that integrates the iterative multiuser detection (I-MUD) technique with the PNC system over RF and FSO links are introduced as another achievement. The results show that the I-MUD offers improved performance about 8, and 22dB of SNR to get a BER of 10^{-4} over RF and FSO channels, respectively, for number of simultaneously users equal to 14 with respect to TWR-PNC system.

Table of Contents

List of Figures

List of Tables

Glossary of Abbreviations

1G	First generation
2G	Second generation
3G	Third generation
4G	Fourth generation
ACNC	Arithmetic-sum CNC
AF	Amplify-and-forward
ANC	Analogue network coding
APD	Avalanche photodiode
APP	A posteriori probability
ARQ	Automatic repeat request
AWGN	Additive White Gaussian Noise
BC	Broadcast phase
BCID	Convolutional encoding with iterative detection
BCJR	Bahl, Cock, Jelenik, and Raviv algorithm
BER	Bit error rate
BICM	Bit-interleaved coded modulation
BICM-ID	BICM with iterative decoding
BPSK	Binary phase shift keying
BWA	Broadband wireless access
CC	Convolutional code
CCI	Co-channel interference
CDMA	Code division multiple access
CDMA	Code division multiple access
CF	Compress-and-Forward
CH_4	Methane
CM	Coded modulation
CNC	Channel decoding network-coding
CO_2	Carbon dioxide
CSI	Channel state information

DD	Direct detection
DECs	Decoders module
DF	Decode-and-forward
DS-SS	Direct sequence spread spectrum
DVB-S2	Digital video broadcast satellite standard
ECC	Error control coding
EM	Electromagnetic wave
ENC	Non-recursive systematic CC encoder module
ESA	European space agency
EXIT	Extrinsic information transfer
FDMA	Frequency division multiple access
FEC	Forward error correction
FED	Free Euclidean distance
FIR	Finite impulse response
FOV	Field-of-view
FSO	Free space optical
GaAs	Gallium arsenide
Gbps	Gigabits per second
GF (.)	Galois field
GSM	Global system for mobile communication
H_2O	Water vapour
HBS	Hub base station
HDTV	High-definition television
He-Ne	Helium-neon
HWN	Hierarchical wireless networks
IC	Interference cancellation
ICI	Inter-channel interference
IDMA	Interleave division multiple access
IM	Intensity modulation
I-MUD	Iterative MUD
IP	Internet protocol
IR	Infrared

IrDA	Infrared Data Association
ISI	Inter symbol interference
IUI	Inter-user interference
JD-XOR-F	Jointly demodulate-and-XOR forward
JNCC	Joint design of network-channel coding
km	kilometer
LANs	Local area networks
LDPC	low-density parity-check codes
LDs	Laser diodes
LEDs	Semiconductor light-emitting diodes
LLR	Log-likelihood ratio
LO	Local oscillator
LOS	Line-of-sight
MA	Multiple access phase
MAI	Multiple access interference
MAP	Maximum a posterior probability criterion
Mbps	Migabits per second
MED	Minimum Euclidean distance
mrad	milliradian
MHD	Minimum Hamming distance
MIMO	Multiple-input multiple-output
MISO	Multiple-input single-output
ML	Maximum likelihood
MLCD	Mars laser communication demonstration
MLPNC	Multi-level PNC
MMSE	Minimum mean square error
MPPM	Multipulse PPM
MSs	Mobile stations
MUD	Multiuser detector
nm	nanometer
N_2	Nitrogen
NASA	National aeronautics and space administration

NC	Network coding
NI-MUD	Non-iterative MUD
NLOS	Non Line-of-sight
NRS	Non-recursive systematic
NRZ-OOK	Non return-to-zero on-off keying
O_2	Oxygen
O_3	Ozone
OFDM	Orthogonal frequency division multiplexing
ONUs	Optical network units
OOK	On-off keying
OPNC	Optical PNC
OWC	Optical wireless communications
P2P	Point-to-point
P2P FSO	Point-to-point FSO
PBC	Peak basis correlation
PDF	Probability density function
PDs	Photodetectors
PIN	positive-intrinsic-negative
PNC	Physical layer network coding
PON	Passive optical network
PPM	Pulse position modulation
PSD	Power spectral density
PSK	Phase shift keying
QF	Quantize-and-Forward
QoS	Quality of service
RA	Repeat accumulate
RF	Radio frequency
RN	Relay node
RSC	Recursive systematic convolutional codes
SC	Selection combining
SEP	Symbol-error probability
SILEX	Satellite link experiment

SIMO	Single-input multiple-output
SISO	Soft-input-soft-output
SNR	Electrical signal-to-noise ratio
SP	Simple spreading code module
SUB	Single user bound
TCM	Trellis-coded modulation
TCMA	Trellis-code multiple access
TCs	Turbo Codes
TDM	Time-division multiplexing
TDMA	Time division multiple access
THz	Terahertz
TIA	Trans-impedance amplifier
TWR	Two-way relay
TWR-FSO	Two-way relay FSO
USDC	United states digital cellular
VA	Viterbi algorithm
VCSEL	Vertical-cavity surface-emitting laser technology
VPN	Virtual private network
WANs	Wide area networks
WDM	Wavelength division multiplexing
WDMA	Wavelength division multiple access
XOR	Exclusive-OR

Glossary of Symbols

A	Ampere
A_o	Error function of v
$\mathcal{A}_d$	Photodetector area
α	Effective number of large-scale turbulent eddies
b_0	Direct current level bias
β	Effective number of small-scale turbulent eddies
β_c	Spread signal bandwidth
β_d	Information signal bandwidth
$\mathfrak{B}(.)$	Branch metric associated with the next transition
$\widetilde{\mathfrak{B}}(.)$	Natural logarithm of $\mathfrak{B}$
C	Encoder output associated with the state transition
$\hat{c}$	XOR of coded bits
C_n^2	The reflection index
c_a	The XOR coded sequence
c_k	Coded bit sequence
$\gamma(.)$	Branch metric associated with the current transition
$\tilde{\gamma}(.)$	Natural logarithm of γ
$\gamma_{th1}, \gamma_{th2}$	Optimal decision for PNC
D	Delay
D.C.	Direct current
D_k	Hard-decision of the LLR of the decoder
$\hat{d}$	The network-coded symbol
d_k	The information bits from each users
$\hat{d}_k$	The estimated bits for each users
d_R	Receiver aperture diameter
d_T	Transmitter aperture diameter
$\delta(\lambda)$	Attenuation coefficient of the atmosphere at wavelength λ
E_b	Bit energy

$E[.]$	Mean operator
$\mathbb{E}(.)$	Expectation
ε	Constant
f_c	The frequency of the transmission object
f_d	Doppler shifts
G	Spreading factor
G_{loss}	Geometric loss
$\mathbb{g}_i(t)$	Signature waveform
$g(t)$	Rectangular shaping pulse
$g(D)$	Generator polynomials
ζ	Optical modulation index
$He_z(.)$	z^{th} order Hermit polynomial
h	Channel state of the RF and FSO systems
h_l	Channel atmospheric loss
h_p	Pointing error loss
h_s	Attenuation due to scintillation
h_x	Large-scale irradiance fluctuations
h_y	Small-scale irradiance fluctuations
η_k	The distortion term
I	Interleave sequence
$\mathbb{I}$	The signal light intensity at the transmitter with turbulence
$\mathbb{I}_o$	The signal light intensity at the transmitter without turbulence
$\hat{I}_{p1,p2}$	Deinterleaver sequence of the superimposed symbol at RN
θ_s	Optical source divergence angle
K	The number of users
K_c	Constraint length
$K_n(.)$	Modified Bessel function of the second kind of order *n*
L	Link distance
$L(.)$	Soft-bit decision of the log-likelihood ratio (LLR)

$L(\hat{c})$	LLR of XOR coded bits at relay
L_d	Binary data length
$L_{dec(k)}(.)$	LLR a priori information from decoder
$L_{dem(k)}(.)$	LLR extrinsic information from demapper
L_{desp}	The despreader prior information
L_k	A posteriori LLR on the information data from the decoder
L_{map}	The chip-level extrinsic information
L_n	The number of the propagation path
L_s	Spreading length
M	Constellation size
$m(.)$	Minimum Euclidean distance
M_c	Memory of encoder
M_p	Length of the shift register
$\widetilde{m}$	Modulated signal at relay node
m_k	BPSK Modulation signal for k^{th}user
m_{PNC}	Network-coded symbol
λ	Wavelength
N	Symbols length
N_c	Code word length
N_o	Noise power spectral density
N_p	The length of the packet
μ_x	Mean of variable χ
P	Users pairs
$p(.)$	Conditional probability distribution
$p(h_s)$	PDF of turbulence-induced fading
$p(h_x)$	Gamma distribution of the large-scale irradiance fluctuations
$p(h_y)$	Gamma distribution of the small-scale irradiance fluctuations
P_{max}	Maximum optical Power
P_o	Received optical power

$P_r(.)$	The priori distribution
p_{ra}	Probability density function of Rayleigh distribution
P_t	Transmitted optical power
P_{uncon}	Unconditional bit error rate
$p(h_P)$	Probability density function of misalignment
$p_h(h)$	Probability density function of the optical channel
p_c	Correct packet rate
$p_e(.)$	Probability of error
p_e^{NC}	Probability of error for NC
p_e^{pnc}	Probability of error for PNC
$\mathcal{P}_{\mathcal{C}}$	Probability to receive one correct packet
$\widehat{\Pi}$	The chip-level deinterleaver module
Π	Chip-level interleaver module
ξ	Ratio between the equivalent beam radius at the receiver and the Pointing error displacement (jitter) standard deviation at the receiver
$Q(.)$	The complementary error function
q	Parameter related to the particle size distribution and visibility
R	Detector responsivity
R_c	Code rate
$\mathfrak{r}$	Radial distance from the optical axis
r	Aperture radius
S_1	Node represents User 1
S_2	Node represents User 2
s_k	Spreading code sequence
$\mathbb{s}_i$	Initial state
$\mathbb{s}_{i+1}$	Next state
$\mathbb{s}_{i-1}$	Previous state
$\mathbb{S}$	A state sequence of Markov process
T	Time duration
t	Instantaneous time

T_b	Bit interval
T_c	Chip duration
T_s	Symbol interval
$\mathcal{TH}_{(.)}$	Throughput for the transmission mode
$\mathcal{T}_p$	Time to exchange data between the two nodes
ρ_{auto}	Autocorrelation function
ρ_{ij}	Cross-correlation function
V_c	The speed of the light
V_u	The speed of the user
V	Visibility
$Var[.]$	Variance operator
σ^2	Noise variance
σ_I^2	Scintillation index
σ_R^2	Log irradiance variance
σ_s	Pointing error induced jitter standard deviation
σ_x^2	Variance of variable χ
σ	Atmospheric loss
$\mathscr{o}(.)$	Branch metric associated with the previous transition
$\tilde{\mathscr{o}}(.)$	Natural logarithm of $\mathscr{o}$
τ	Time varying path delay
$\emptyset$	The angle phase
ψ	Signal-to-noise ratio (SNR)
W	Watt
w_c	Carrier angular frequency
w_L	Beam width at the receiver plane
w_k	AWGN from RN to the sources
w_{Leq}	Equivalent beam radius at the receiver
w_r	AWGN from the source to the RN
$x(t)$	Modulation transmitted signal

$\hat{x}_p^r(n)$	Chip modulated transmitted signal for each *P*
x_k	Transmitted symbols from the k^{th} sources to the RN
x_p	Superposition of the n^{th} partners' transmitted symbols
x_R	The modulated transmitted symbols from the RN
χ	Gaussian distributed log-amplitude fluctuation
y	Observation symbols vector from the sources at the RN
y_d	Signal coherent demodulator output as a function of time
y_r	Received optical signal at RN
y_{sk}	Received signal at k^{th}destination from RN
$(\mathbb{w}_i)_{i=1}^{\mathbb{z}}$	Weight factors of the z^{th}order Hermite polynomial
$(\mathbb{x}_i)_{i=1}^{\mathbb{z}}$	Zeros of the z^{th}order Hermite polynomial

Dedication

I dedicate this thesis to my precious husband and children, Abdullah, Raniya and Dalya, who have supported me throughout the years of my study.

Acknowledgements

The journey through my PhD studies, which bears enlightening life and research experiences, fruitful technical achievements and timely completion of this thesis, is impossible without the wonderful people who have walked with me and uplifted me through numerous good and difficult moments.

I shall begin to thank my God for upholding me with perseverance, wisdom and strength throughout this journey, and allowing everything to happen miraculously such that I could learn, grow and show appreciation in every aspect of my life. His blessings have brought me success and smooth accomplishment to this research project.

First of all, I would like to express my heartfelt gratitude to my supervisor Prof. Zabih Ghassemlooy for giving his most sincere and thoughtful advice, guidance and support, particularly in justifying proper research direction of the project and ensuring that the research aims and objectives are fulfilled. It is an honour for me to study and do research under his supervision.

In addition, I would like to thank to my co-supervisor, Dr. Hoa Lee Minh and Dr. Nauman Aslam, for the insightful guidance and support, which have enabled me to acquire the fundamental knowledge to carry out this work.

Moreover, I would like to express my utmost appreciation to my Employer-Ministry of Higher Education and Scientific Research-University of Kerbala for providing the much needed financial support during my leave of study. Next, I would like to convey my sincere acknowledgement to my Mum and siblings and their spouses for their understanding and moral support, especially during the most challenging moments of my research. Last but not least, I am deeply thankful to my husband who has persistently

accompanied me in completing this journey, sharing my tears and cries and showering upon me with love, joy and laughter. Also, I dedicate this thesis to my lovely children, and I appreciate all their patience and support during mommy's study. Finally, I would like to express my heartfelt gratitude to my colleagues for sharing their experiences and opinions, which have inspired me with more feasible ideas and solutions to overcome the roadblocks encountered in my research studies.

Declaration

I declare that the work contained in this thesis has not been submitted for any other award and that it is all my own work. I also confirm that this work fully acknowledges opinions, ideas and contributions from the work of others.

Name: ZINA M. HASSAN M. ALI ABU ALMAALIE

Signature :

Date:

Chapter 1

INTRODUCTION

Optical wireless communications (OWC), which is also known as free space optical communication (FSO) is a technology that entails the transmission of information-laden optical radiation through the free-space channel. FSO gives a flexible networking solution that delivers the truly broadband services. The FSO technology only provides the essential combination of virtues vital to bring the high-speed traffic to the optical fiber backbone. Furthermore, FSO is offering a license-free spectrum with almost an unlimited data rate, a low cost of development and ease and speediness of installation. However, the primary factors limiting the performance of FSO communication systems are linked to the short wavelengths of the optical system and they include atmospheric attenuation in form of scattering and absorption, and optical scintillation. In addition to the atmospheric effects, FSO communication systems can also be affected by the pointing errors due to weak earthquakes, strong winds, and thermal expansion and cooling, resulting in misalignment of the transceivers, and, consequentially, degradation of the FSO communication system performance. Therefore, to address these challenges, relay-assisted communications has been recently considered in the context of FSO, where both amplify-and-forward (AF)

and decode-and-forward (DF) relaying schemes have been studied. Unlike the radio frequency (RF) channel, the severity of the small–scale fading in the optical wireless channel is distance-dependent. Furthermore, since FSO is a line-of-sight (LOS) technology, relaying is attractive in situations where source and destination do not have LOS paths. Recently, a two-way relay (TWR) channel has attracted many researchers' attention due to the potential of improving spectral efficiency based on the one-way relaying system. Thus, the proposed work unfolds new insight on the FSO system design in the context of the physical layer of a TWR communication model. By utilizing broadcasting nature of wireless medium, physical layer network coding (PNC) has been proposed, which can improve the network throughput. PNC is a technique that allows two users to exchange their messages in less time via an intermediate relay. This takes place at a relay node and exploits the interference caused by the noisy incoming signals by performing special demapping/mapping and then by broadcasting again to the users.

The rest of the chapter outlines the challenges and motivation of this work. A brief background of the FSO systems for outdoor applications as a complementary technology to the existing schemes is also presented in this chapter. The point-to-point FSO wireless channel topology is described throughout the chapter. The chapter looks into the optoelectronic devices used in FSO alongside with usage wavelength. The functionality of the transmission mode in wireless networks is illustrated in this chapter. The chapter highlights on the principle of the PNC technique and its application in wireless communication. The final part of this chapter summarizes our contributions and includes an overview of the following chapters of this thesis.

1.1 Challenges and Motivation

As the vehicular communication technologies grow rapidly in the coming years, there will be demands for more RF spectral resources. Unfortunately, wireless spectrum is a limited natural resource and the growing demands on its usage in various applications will eventually put constraints on developing future high data rate systems. One approach to relieve the pressure on the RF spectrum is to utilize the available FSO spectrum that has enormous unlicensed bandwidths, immunity to electromagnetic interference, and provide a significant degree of secrecy. In spite of the existing RF is widely used in wireless communications, FSO communications is poised to become a promising broadband wireless access (BWA) candidate to use extensively in communication.

This thesis deals with exchanging the information over TWRC. For this issue, a numerical number of network coding (NC) strategies have been considered in the literature. In this work, the relay computes a function of the two messages directly from the channel output without intermediate decoding. This strategy so called PNC when the network coding is applied to the physical layer. This scheme relies on two phases, namely, a multiple access (MA) and a Broadcast (BC) phases. Through reliable theoretical analysis and simulation studies, feasible mitigation techniques and/or optimization methods can be proposed and examined with improved accuracy, in order to address the effective mitigation of the adverse atmospheric channel effects on FSO systems. Therefore, the central idea of this study attempts to address some of the issues in the context of the physical layer of TWRC communications model over a FSO link. Consequently, the communication network can be considered as being two nodes connected by FSO links. The information is sent as one packet at a time from the source to the destination via an intermediate node acting as a relay in the MA phase. The PNC technique takes advantage of the additive nature of

electromagnetic waves (EM), and embraces interferences by performing coding operations to combine the bit-wise convoluted messages and sends back to both sources in the BC phase. In such a way, both the communication time and the bandwidth are utilized more efficiently, which in turn boosts the network throughput. Furthermore, atmospheric turbulence is usually categorised in terms of its strength depending on the magnitude of index of refraction variation and inhomogeneities. The turbulences regimes are a function of the propagation path travelled by the optical radiation through the atmosphere and are classified as weak, moderate, strong and saturation. The log-normal distribution channel is widely used to describe the scintillation under weak atmospheric turbulence conditions. For moderate to strong turbulence, gamma-gamma distributions are commonly preferred. However, these models used in the simulation to characterize the behaviour of the system under consideration.

Channel coding may be applied in PNC techniques by using the link-by-link or end-to-end code schemes. The difference between the two coding methods lies in how the relay processes the received signal. The purpose of this research is to investigate the general problem, which is addressed by adopting a relaying network and to propose a new design/application of a relaying scheme in the area of the FSO communications scenario. The potential benefits of considering an end-to-end coded PNC system is the guaranteed security, high data rate information reliability, and a new implementation principle within the context of FSO communications. The development of practical iterative detection algorithms will have much broader application throughout the field of communications.

PNC in the TWRC communications can only support exchange of data between two users. Therefore, as a natural and enriched extension, redesigning the PNC to accommodate multiple user pairs to swap their messages is seen as an attractive topic.

Hence, the work in this thesis tries to adopt the principle of PNC technique over FSO and then increase the number of users that can share the relay process to exchange information. For this purpose, one of the powerful iterative multiuser detection techniques with chip-interleaving is used to perform the PNC mapping at the intermediate node.

1.2 Literature Review

1.2.1 FSO communication link

The field of wireless communications has been extensively researched in order to exploit the advantages they have over wired networks such as mobility and flexibility. The main challenge is to design more adaptive and scalable networks that can provide high data rates to support the increasing demand for bandwidth. In view of this, several wireless networks have been developed to address the demand for high information carrying capacity. The FSO technology was introduced in wireless communications for transferring the information by providing larger bandwidths and high data rates [1, 2] . FSO communication or laser communication is a LOS technology based upon the transmission of optical laser beam waves.

In early 1790s the optical telegraph was devised by C. Chappe, which was able to transmit and receive information in the shortest time possible by changing the orientation of signalling (arms) on a large tower. Thereafter, a code book of orientations of the signalling arms was developed to encode letters of the alphabet, numerals, common words and control signals. As a result, messages could be sent over a distance 120 miles (193 kilometer (km)) in a matter of minutes [3, 4]. In 1792, the first message was sent between Paris and Lille where the semaphore line was used to relay messages during the war between France and Austria. The semaphore lines spread widely in Europe and the

network was used not only for military purposes but also for relaying commercial messages. This was followed by the invention of the earliest optical wireless communication device using electronic detector by A. G. Bell and C. S. Tainter in 1880 [5]. This system could transmit an operator's voice over a distance by modulating a reflected light from the sun on a foil diaphragm. Consequently, it was possible to transmit an audible signal over a distance of 213 meters [5, 6]. Since 1960, the fortune of FSO changed with the discovery of the laser as an optical source. In [7], F. E. Goodwin recorded that a spectacular transmission of a television signal over a distance of 30 mile (48 km) using a gallium arsenide (GaAs) light emitting diode was given by Lincoln Labs, prior to a significant laser communication systems demonstration. In 1963, he recorded that the transmission of voice modulated using helium-neon (He-Ne) laser between Panamint Ridge and San Gabriel Mountain in United States over a distance of 118 miles (190 km). Laser was first used for television transmission by the North American Aviation research group in 1963, and the first laser link to handle commercial traffic was built in Japan around 1970 over a distance of 14 km [7].

Moreover, FSO has continued to be researched and used essentially by the military for covert communications, secure, relevant, and timely information. The United States military used sun-light based power devices to send signals from one mountain top to another mountain top in the early 1800. National Aeronautics and Space Administration (NASA) and the European Space Agency (ESA) have been doing in FSO for deep space applications with programmes such as Mars Laser Communication Demonstration (MLCD) and the Semiconductor Laser Inter Satellite Link Experiment (SILEX) [8, 9]. FSO was also successfully demonstrated in space between satellites at data rates of up to 10 gigabits per second (Gbps) [10]. With the bandwidth available to FSO anywhere from

100 to 100,000 times higher than RF or microwave transmitters, the use of the FSO technology could give a military force much leverage over their rivals.

Hence, the recorded successes of FSO in military applications have rejuvenated interest in its civil applications within the access network. At the present time, FSO has emerged as a commercially viable complementary technology to RF and millimeter wave wireless systems for consistent and fast deployment of data, voice and video within the access networks [11]. RF and millimeter wave based wireless networks can provides data rates from a few megabits per second (point-to-multipoint) up to several hundred of megabits per second (point-to-point) [12]. However, there is a limitation in market penetration due to the spectrum congestion, licensing issues and interference from unlicensed and licensed bands. The future emerging license-free bands were promising, but still have certain bandwidth and range limitations compared to the FSO [13].

A common commercial use-case implements FSO as a solution to the last mile access network problem. The short-range FSO links are used as an alternative to the RF links for the last or first mile to provide broadband access network to homes and offices as well as a high bandwidth bridge between the local area networks (LANs) and wide area networks (WANs) [14, 15]. Furthermore, full duplex FSO systems running at 1.25 Gbps between two static nodes are now common sights in today's market just like FSO systems that operate reliably in all weather conditions over a range of up to 3.5 km. In [16] the first 10 Gbps FSO system was introduced to the market, making it the highest-speed commercially available wireless technology. Terrestrial FSO has now proven to be a viable complementary technology in addressing the contemporary communication challenges, most especially the bandwidth/high data rate requirements of end users at an

affordable cost. Table 1.1 summarizes the main differences between FSO and RF systems [17, 18].

1.2.2 Optoelectronic components

Outdoor optical wireless link using more expensive transmitters, receivers and pointing mechanisms, therefore, multi-gigabit per second transmission was possible over 4 km [17-19]. The design of terrestrial FSO communication systems must consider the atmospheric conditions such as rain, fog and snow and high levels of atmospheric turbulence across the horizontal path, which affects the system performance in different points. Optical wireless transmit information by modulating the instantaneous optical intensity in response to an input electrical current signal as the information sent on this channel is not contained in the amplitude, phase or frequency of the transmitted optical waveform, but rather in the intensity of the transmitted signal. Therefore, optical wireless transmits information by employing an optoelectronic light modulator. This process is termed electro-optical conversion and is usually accomplished by a light-emitting diodes (LEDs) or laser diodes (LDs).

Table 1.1 The comparison between RF and FSO communication links.

Parameter	**RF link**	**FSO link**
Bandwidth regulated	licensed	Free license
Security	Low	High
Data rate	<1.25 Gb/s	<10 Gb/s
Eye safety	N/A	Required
Multipath distortion	Yes	Only in diffuse indoor systems
Source of Signal degradation	Multipath fading, rain, and user interferences	Atmospheric turbulence and obscuration
Network architecture	Non-scalable	Scalable
Signal-to-noise ratio	Depends on RF signal amplitude	Depends on optical signal power
Path loss	High	High

However, LED is fundamentally a semiconductor P-N junction, where the light is generated by radiative recombination of minority carriers injected across a forward-biased P-N junction through the spontaneous emission process. In this process, the recombination of injected carriers occurs in a random manner, causing the output light generated by a LED would be incoherent. Also, the modulation bandwidth of LEDs is limited to a few hundred megahertz and provides low optical output powers. Furthermore, device self-heating remains as another key concern affecting the performance of LEDs. Consequently, LEDs are used where low data rates and short haul communications are required, such as indoor FSO systems [19].

LDs are more recent technology that evolved from the underlying LED fabrication techniques, which can be created by placing an LED in an optically resonant cavity. These laser devices still depend on the transition of carriers over the bandgap to produce radiant photons, but with modifications to the device structure, in order to enable the efficient production of coherent light over a narrow optical bandwidth. LD are the most important light sources for outdoor FSO communications since early 2000 [20]. The superior characteristics of the LDs encompassing high modulation bandwidth (for achieving higher data rate), efficient electrical-to-optical conversion and high optical launch power capability. These features make LDs very popular as a light source for optical communication systems. On other hand, LDs are more difficult to construct and as a result can be more expensive than LEDs. Recently, wide range of LDs is available to perform various applications. Some of the applications of LDs include surgery, cutting of metals, distance determination, projection of 3-dimensional holographic images and computer printing. The optical detectors, also referred to as photodetectors (PDs) or photodiodes, are solid-state devices, which operate essentially as reverse-biased diodes, to perform the

inverse operation of optical sources (LEDs, LDs) by converting the incident radiant light into an electrical current [6]. The two common types of photodiode include the positive-intrinsic-negative (PIN) photodiode and avalanche photodiode (APD) [21]. The latter is a popular and widely used detector because of its small portable size, relatively low cost, good responsivity and high accuracy. The basic construction of APDs is very similar to that of a PIN photodiode. The difference is that the APDs are capable of providing various gains in the resultant photocurrent through the carrier multiplication process, while PIN photodiodes can generate at most one electron-hole pair per photon absorbed. Care must be taken in the selection of photodiode receivers to ensure that cost, performance and safety requirements are satisfied.

1.2.3 Point-to-point FSO links

FSO has been used for more than 30 years to provide fast communication links in remote locations. Therefore, much work has been done in the area of communications system design and in characterizing communication links, such as; developing novel channel topologies, designing receiver for transmitter optics and electronics. However, the characteristics of the optical wireless channel can vary significantly depending on the topology of the link considered. Each channel topology is suited to a different application depending on required data rates and channel conditions. It may also be advantageous to combine the operation of the various topologies to form a more robust link.

Point-to-point (P2P) FSO links operate when there is a direct path between a transmitter and a receiver. A link is established when the transmitter is oriented toward the receiver. In narrow field-of-view (FOV) applications, this oriented configuration allows the receiver to reject ambient light and achieve high data rates and low path loss. A typical example of these links is the standard Infrared Data Association (IrDA) Fast infrared (IR)

4 migabits per second (Mbps) link [6]. Ultra-long range P2P links for outdoor link are being considered for earth-to-space communications at rates in excess of 1 Mbps [22]. The main disadvantage of this link topology is that it requires pointing and is sensitive to blocking and shadowing.

1.2.4 Choice of the optical wavelength

The majority of FSO communication systems use the transmission windows of 780-850 nanometer (nm) and 1520-1600 nm. The wavelengths 780-850 nm are suitable for FSO operation in which higher-power LDs optical sources can be used. In network and transmission equipment, reliable, inexpensive, and high-performance transmitter and detector components are commonly used within the wavelength around 850 nm. For instance, the APD detector and advanced vertical-cavity surface-emitting laser (VCSEL) technologies can be used for operation in this wavelength. On other hand, the 1550 nm band is well suited for free space transmission due to its low attenuation, as well as the proliferation of high-quality transmitter and detector components. It is also allowed to transmit more power than its 850 nm counterpart for eye safety reasons (i.e., more power can be transmitted to overcome attenuation by aerosols), compatibility with wavelength division multiplexing (WDM) and reduced background solar radiation and scattering in light haze or fog [1, 23]. However, its disadvantages include reduced receiver sensitivity and higher component cost.

1.2.5 Relaying communication systems

In communication networks the information transfer from the source to the destination terminals without the use of any other communicating terminal is called direct communications, where these two terminals located within each other's transmission

range [24]. However, a direct link condition might not be always available due to the obstacles such as high buildings and terrains, so that a message from a source to a destination can be delivered through an intermediate node served as a relay between the two sources. Hence, wireless relay networks are a communication system that possess transmit and receiving capabilities. In wireless networks, the physics of the EM lead to multipath propagation of wireless signals causing a variation in the received signal generally called fading, in space, frequency, and time. Therefore, the channel impairment can be mitigated through the use of diversity techniques by effectively transmitting or processing independently fading copies of the signal [25, 26]. These techniques aim to provide multiple, independent, signal paths between the transmitter and the receiver that can significantly improve the overall reliability of the link [27].

On other hand, a cooperative communication, which can be considered as a new form of spatial diversity, generate this diversity with different terminals. These terminals collaborate to form a virtual-multiple antenna array system to achieve a better performance. V. D. Meulen was the first to introduce the three-node model consisting of a source node, a destination node and a relay node, which was then investigated extensively by T. Cover and A. Gamal [28, 29]. Later, J. N. Laneman *et al.* studied the mutual information and the outage probability between a pair of nodes using cooperative communications under different relay modes [30]. Based on their fundamental work, cooperative communication has been extensively studied from the perspectives of both physical layer and network layer [31-34]. The key idea behind cooperative communications at the physical layer is sharing the physical layer resources and cooperating to forward each node's packet to the intended destination node [35]. Sendonaris *et al.* introduced the concept of user cooperation diversity, which used in lieu

of relaying, enabling the relay mobile to simultaneously transmit its own independent information over the ad-hoc network towards their destinations [36]. They concluded that such a scheme provides higher throughput and robustness to channel variations for both the transmitting and relaying mobiles.

1.2.6 Two-way relay channels

One-way communication was attracted the attention of the research community as a means to extending the coverage and providing robustness against channel variations with reduced infrastructure deployment costs in wireless networks [37, 38]. Recently, bidirectional communications or TWRC has received considerable attention because of its improved bandwidth efficiency in half-duplex relaying systems that are due to the two channel uses required for the transmission from the source station to the destination station compared with one-way communications. The original study of the TWRC problem traced back to Shannon's work in 1961[39]. However, TWRC can be considered as a sub-branch of relay channel that two or more terminals exchange their messages using a relay, where all terminals assumed to be half-duplex nodes implying that they cannot simultaneously transmit and receive [30, 40]. Hence, it can identify itself from the traditional relay protocols by considering bidirectional information flows in the process of relaying and was simple to implement in practical systems [41]. On other word, TWRC protocols combined the uplink and downlink data transmission together by ingeniously mixing the data from different sources at the relay, instead of simply forwarding the received data from one source at a time. Therefore, the TWRC protocol only needs two phases, namely, the MA phase and the BC phase [41]. Whereas, the traditional relaying protocols require four channel uses to exchange the data between the source and the

destination via the relay, which leads to loss in the spectral efficiency due to the application of half-duplex relays.

1.2.7 Physical layer network coding

Relaying strategies are promising technological advancements for future wireless networks in which it can take advantage of ad-hoc deployments that exploit cooperative communications. Consequently, depending on how the information is encoded, the exchange of information can occur in four, three, or two orthogonal time slots. In ad-hoc networks, the nodes communicate with each other using peer-to-peer links. In such systems, the information delivery is performed by store-and-forward routing schemes, where the intermediate nodes store and forward their received data. Hence, in such transmission schemes for TWRC, the exchange of information between a pair of source terminals, without a direct link requires four time slots through an intermediate relay node [42]. With each of the first two time slots, one of the terminals transmits information to the relay node, while with each of the last two time slots; the relay node transmits information to each of the terminals, as shown in Figure 1.1(a).

Recently, NC has been proposed as a promising technique at the network layer of the protocol stack to replace the store-and-forward routing in these networks and to improve the network capacity. It was proposed in [43] for improving the throughput in multicast scenarios. It allows the relay node to manipulate its received data from multiple sources and generate new packets containing data for other nodes. With NC, the required number of transmissions to send data from a source to a destination can be reduced. This is illustrated by the third and fourth time slots, which are combined into one-time slot. In contrast to the store-and-forward approach to network operation, where an intermediate node replicates the received information and delivers it to its neighbour nodes, NC allows

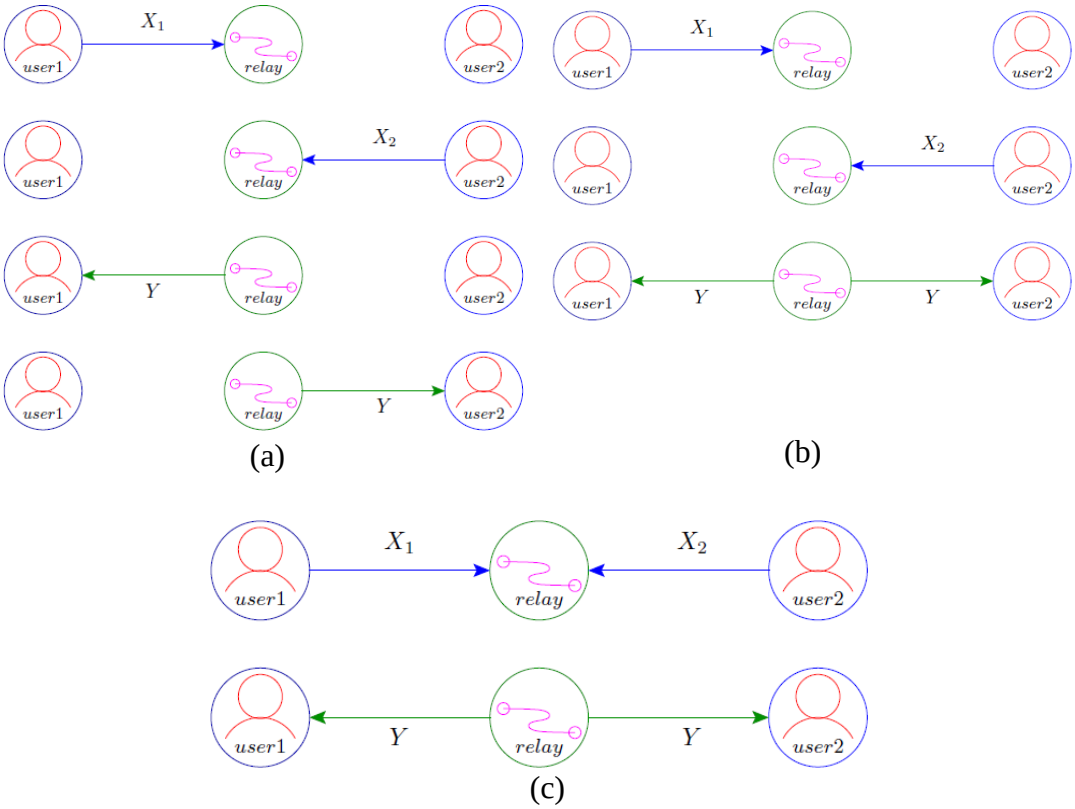

Figure 1.1 The type of the transmission mode over wireless channels: (a) store-and forward, (b) NC, and (c) PNC.

an intermediate node to process the incoming data from multiple sources. Therefore, it enables each connection to use the whole capacity of the overlapped paths as if there is existing only one connection in the network. Hence, this technique having the relay add modulo-2 to the information that it receives from the two terminals, as shown in Figure 1.1(b). Therefore, the interference signal of the two source terminals and the effect of the channel becomes part of the arithmetic operation in NC. Therefore, the relay node sends the sum of the two sources information during the third time slot and each terminal is able to recover the information from the other terminal by adding/subtracting modulo-2 for its own message from the received information.

However, a prospective technique in the wireless TWRC communications is the PNC, which exploits interference to improve the throughput [44]. The main idea of PNC

technique is achieved through a special demapping and mapping process at the relay node, where EM wave can be mapped to digital bit streams of a Galois field of two elements (GF (2)). In this scheme, the overall communication occurs during two phases, MA and BC. In the first phase, both end terminals transmit to the relay node simultaneously in which it directly transforms the received waves to the network coding form without individually detecting them as shown in Figure 1.1(c). Then, in the BC phase, the relay node broadcasts the network coded signal to both end terminals. Specifically, PNC has proven to have the ability to approach the capacity of the TWRC in high signal-to-noise ratio (SNR) regions as well as the throughput upper bound of wireless networks [42, 43]. PNC may be implemented using two different schemes. The relay may simply amplify then forward the received signal sum directly, without performing demodulation and decoding. This scheme is referred to as the analogue network coding (ANC) [45]. Another scheme for the relay node is to detect the received signal sum, and clean the noise by performing demodulation and decoding in an effort to estimate the network code word.

1.2.7.1 PNC employing error correction coding

Wireless communications suffer from high and time-varying packet losses due to the detrimental effect of fading of wireless channels compared to wireline communications. One method to provide reliable communications is using redundant information to recover errors in the original information. This scheme is called error control coding (ECC), which has a history dating back to the middle of the twentieth century when C. Shannon introduced the basic theory on bounds for communications [46]. Channel coding is a conventional error-correction technique used for P2P communications over a single channel. It is implemented at the physical layer to recover erroneous bits/symbols through redundant parity-check bits/symbols appended to a packet. Thus, to apply PNC in

wireless systems, channel coding must be adopted to combat the effect of the wireless channels.

The channel decoding network-coding (CNC) process involves both channel and network coding operations to transform the received signal at the relay [47]. Hence, this scheme in a PNC system can either be done link-by-link or end-to-end basis. With the former technique, the channel encoding and decoding was performed at the end nodes as well as the relay node [47] and the latter accomplished the channel coding only at the end nodes, and not at the relay node [48] .

In terms of practical design, there have been extensive research activities on the effective coding schemes for PNC. S. Zhang and S. C. Liew performed a novel coded PNC using link-by-link approach, where the decoding algorithm was re-designed for repeat accumulate (RA) code to decode exclusive-OR (XOR) messages at relay [47]. This was called the arithmetic-sum CNC (ACNC) scheme, which aimed to obtain the soft version of the arithmetic summation of the two source packets rather than individual packets as in CNC. Hence, it could help to avoid decoding extraneous information not related to XOR messages and made full use of the information contained in the received signal to help decode the network-coded packets. Therefore, ACNC outperforms CNC by about 0.5dB of SNR at a BER of 10^{-4} when the RA code was used.

However, the first use of the convolutional coding for TWRC with coded PNC using link-by-link approach was studied by D. To and J. Choi [49], in which the decoding performed by Viterbi algorithm (VA) at the relay. It is well known that the complexity of VA based decoder depended on the trellis structure, therefor; the authors proposed a reduced-state trellis structure by merging every disjoint group of states in the full-state trellis into a signal merged state to reduce decoding complexity. Nevertheless, simulation result

showed that there was a performance gap of about 2dB of SNR at a BER of 10^{-5} paying for the complexity reduction compare to the conventional coding.

There were several publications in the literature that investigated the combination of low-density parity-check (LDPC) codes and PNC for a MA channel [50-52]. Moreover, a bit-interleaved coded modulation (BICM) scheme in a Gaussian TWRC joint with PNC was examined by X. Li *et al.* using RA code [53], taking the advantage of the iteration processing between the demapping and decoding at the relay. The simulation result presented that the BER performance of the iterative CNC outperformed by 1.8dB of SNR at a BER of 10^{-5} with respect to the conventional coding. Additionally, Z. Chen *et al.* employed BICM with multi-level PNC (MLPNC) for TWRC to address the problem on how to develop a cooperative coded modulation scheme in PNC [54]. Whereas, Li Chen *et al.* proposed BICM with iterative decoding (BICM-ID) for the TWRC operated with PNC at the relay [55]. With iterative decoding, the transmitted symbol pair probabilities provided a better estimated so that the demapper offered well coded bit information for the decoder. The simulation results showed that significant iterative decoding gain about 18 dB of SNR was achieved at a BER of 10^{-4} with respect to the non-iterative scheme over fading channels.

Furthermore, the joint design of network-channel coding (JNCC) for PNC in TWRC was adopted by Z. Lian-chi and X. Chun-di, where the turbo code (TC) and binary phase shift keying (BPSK) modulation were considered [56]. The authors depended on the linearity of TC and soft detection module to reduce the complexity of encoding and decoding and achieve good performance in high SNR. The result outlined that the proposed scheme achieved 50% throughput increase compared with traditional network coding.

1.2.7.2 Multiple access technique employing PNC

The systems employing TWRC have attracted increasing research attention due to the potential of improving spectral efficiency upon one-way relaying systems. Therefore, many works were proposed NC protocols for TWRC that outperform the traditional four-phase relaying communications in terms of throughput and achievable rate. The near future for wireless ad-hoc networks are most likely to consist of many more than two nodes wishing to exchange information, potentially having to share intermediate relays. Based on this technique, a crucial aspect of implementing PNC system is the formulation of a simple relay receiver in which the relay forwards the summation of the received signal directly and all of the processing was performed at the end nodes. However, the PNC technique uses a dedicated demapping and then mapping scheme at the relay to construct a new output NC signal from transmitted signals. Therefore, increasing the number of nodes in PNC system that can simultaneously be transmitted to the relay is still considered as the main constraint in such a system. This is mainly due to the PNC demapping and mapping process at the relay, which only support two nodes for exchanging their messages at the same time in TWRC. This leads to some researchers studied the impact of growing the number of communication pair in PNC technique. S. Shukla *et al.* designed a new modulation schemes for the PNC three-way wireless relaying scenario, where three nodes exchange their message through relay in two phases. A mathematical structure called Latin Cube was used in this model to construct new NC mapping at relay, in which XOR operation for decoding three messages were satisfied at the relay [57]. The aforementioned work was extended in [58] to four user nodes with PNC mapping at the cost of increased relay system complexity. Their results showed that adaptively changing the NC mapping used at the relay according to the channel conditions

that satisfies the XOR operation greatly reduced the impact of multiple access interference (MAI), which occurred at the RN during the first transmission phase. Moreover, multiple access techniques have been proposed jointly with PNC technique. Hence, M. Chen and A. Yener proposed and investigated the performance of the model, where multiple user pairs exchanging information with the help of the relay node [59]. To reduce MAI comes from multiple transmitted, code division multiple access (CDMA) technique was proposed in this model, where each pair of users shares a common spreading signature. Relaying scheme referred to as jointly demodulate-and-XOR forward (JD-XOR-F) was proposed to enable the relay to perform multiuser detection at relay, which increased the computational complexity of the relay. Additionally, ANC technique combined with asynchronous CDMA was proposed by S. Mao *et al.* [60]. This work focused on the relationship between the inter-user interference (IUI) resulting from asynchronous transmission and the number of users. However, the result showed that the proposed system improved the performance over the traditional four-phase when large spreading factor and low number of users were used. A combination of CDMA with PNC scheme was proposed by D. Fang *et al.* in [61]. It was employed to take advantage of the interference mostly present at relay during the exchange of messages between the hub base station (HBS) and mobile stations (MSs) in hierarchical wireless networks (HWN). As co-channel interference (CCI) severely limits the system performance, when the incoming signals reach the RNs, this scheme exploited CCI to provide a diversity benefit while PNC was used to encompass the inter-channel interference (ICI). However, MAI is a major concern for CDMA cellular networks, which can mitigate by using multiuser detection. The high computational cost involved in multiuser detection, which may increase in an exponential order with the number of users, limits its application in

practical systems [62]. Therefore, an alternative interesting technique for multiple access referred to as interleave division multiple access (IDMA) was introduced. The essential feature clue of IDMA is to use dissimilar interleaver to distinguish between multiple users [63]. The design of irregular RA codes for IDMA to support multiple pair of nodes for the TWRC system was presented by F. Lenkeit *et al.* in [64]. The authors gave a description of the general code design process based on extrinsic information transfer (EXIT) analysis and compared it with conventionally coded IDMA systems based on CCs. However, multiple access techniques such as time division multiple access (TDMA), frequency division multiple access (FDMA), CDMA and IDMA are allowed multiple simultaneous transmissions in the same time and divided channel capacity between multiple users. In contrast, PNC expands the capacity of the network.

1.2.7.3 PNC with optical communication

Although the promising effects of PNC technique in RF communications have been considered so far in the context of wireless ad-hoc networks, its application in optical wireless networks are fairly limited. As these two wireless networks extremely different in network structure, system components and physical characteristics, therefore, the knowledge from RF wireless communications cannot be directly applied to the optical communications. Recently, optical PNC (OPNC) was proposed and experimentally demonstrated with various features including boosting network efficiency, reducing resources needed for network protection, and increasing system throughput [65]. Conventionally, two optical network units (ONUs) in the same passive optical network (PON) cannot communicate with each other directly. Therefore, wasting bandwidth occurred through the upload and download phases. Accordingly, all optical virtual private network (VPN) was introduced to enable direct communication among ONUs. Due to the

half-duplex constraint, this limits the capacity of VPN. Therefore, PNC for boosting network efficiency was verified experimentally for the first time by W. Qike *et al.* over time-division multiplexing (TDM) PON in all optical VPN [66]. The authors concluded that PNC increased the capacity of VPN communication as well as provided more secure service. Zhixin Liu *et al.* explored the application of PNC in optical systems and networks for the first time [67, 68]. OPNC based on polarization multiplexing with 10 Gbps non return-to-zero on-off keying (NRZ-OOK) signal for packet switching networks was proposed. It was shown that an OPNC saved on the resources requirement for network protection in a multicast network with no need for bit synchronization and could be easily implemented. Whereas Z. Liu *et al.* proposed for the first time OPNC in a star-topology fiber-wireless system to double the system throughput [69]. The network coding process was similar to that in [68] except that the modulation format was changed to orthogonal frequency division multiplexing (OFDM).

1.3 Research Contribution and Publications

This section outlines the main contributions of this thesis, which can be highlighted as:

- The application of the PNC technique over two-way relay free space optical (TWR-FSO) links is presented in **Chapter 3**, which can be considered as the original contribution of this chapter. This new scheme is called TWR-FSO PNC. However, the turbulence-induced effects result in the aggravation of optical irradiance fluctuations and random signal losses at the receiver side; in which such stochastic behavior can be appropriately modelled by the log-normal and gamma-gamma distributions, valid in the weak-to-moderate and moderate-to-strong scenarios, respectively. Hence, the performance of the new model is

evaluated by taking into account the influence of the atmospheric loss, weak and strong turbulence fading channels together with misalignment effects using BPSK modulation. The implementation of the new model with three system parameters (propagation path, wavelength and beam width) are investigated and compared with the point-to-point (P2P) FSO system in terms of the bit error rate (BER).

- The performance of the TWR-FSO PNC system using end-to-end iterative decoding algorithms is considered in **Chapter 4**. The original contribution of this chapter is to evaluate the system performance with state-of-art iterative decoding scheme, in order to examine the resulting impact of channel coding on the performance of the TWR-FSO PNC link, in the presence of scintillation effects. The performance of the non-iterative channel coding using convolutional code (CC) with TWR-FSO PNC system in terms of BER is also studied in **Chapter 4**. The implementation of the coded TWR-FSO PNC is investigated and compared with non-iterative CC and P2P FSO in terms of BER performance.

- A PNC based bi-directional data exchange in TWRC over RF communication link, where multiple pairs of communication nodes exchange their information between each other through an intermediate node, is proposed in **Chapter 5**. This new model allows the network coded symbols of the useful signal and interference signal are jointly decoded and iteratively processing at the receiver side. Non-iterative multiuser (NI-MUD) detection with PNC over TWRC is also deliberated and compared with the iterative multiuser (I-MUD) detection in **Chapter 5**, in order to examine the effects of adoption the I-MUD alongside

with chip-interleaving on the performance of the system. In the proposed system, both of Gaussian and Rayleigh fading channels are considered. Additionally, to allow multiple pairs of user to swap their data between them within a single relay over FSO link when there is no direct path between them with the aim of maximizing the utilization of network resources, I-MUD detection is introduced and applied on TWR-FSO PNC system as another contribution in **Chapter 5**. The implementation of the proposed system is investigated and compared with TWR-FSO PNC in terms of BER performance by considering link impairments imposed by the atmospheric attenuation as a result of beam extinction and channel fading caused by turbulence (ranging from weak to strong).

1.3.1 Related publications

Journals:

- **Z. Abu-Almaalie**, Z. Ghassemlooy, M. R. Bhatnagarh, H. Le-Minh, N. Aslam, S-K Liaw and I. E. Lee, " Investigation on iterative multiuser detection physical layer network coding in two-way relay free-space optical links with turbulences and pointing errors ", *Journal of Applied Optic*, vol. 55, Issue 33, pp.9396-9406, 2016.

Conferences:

- **Z. Abu-Almaalie,** Z. Ghassemlooy, H. Le-Min and N. Aslam," Investigating the impact of mobility and traffic loads on energy consumption of MANETs,"14th Annual *Post Graduate Symposium on the Convergence of Telecommunications, Networking and Broadcasting* (*PGNET*), 2013.

- **Z. Abu-Almaalie,** Z. Ghassemlooy, H. Le-Minh and N. Aslam," Implementation the chip-level interleaver with physical layer network coding," *Northumbria Research Conference, Northumbria University,* 2014.

- **Z. Abu-Almaalie,** Z. Ghassemlooy, H. Le-Minh and N. Aslam," Performance evaluation of IDMA implementation with physical layer network coding," 9*th International Symposium on Communication Systems, Networks & Digital Signal Processing* (*CSNDSP*), pp.700-705, 2014.

- **Z. Abu-Almaalie,** Z. Ghassemlooy, H. Le-Minh and N. Aslam," Physical layer network coding with two-way relay free space optical communication link," 6th *International Conference on Internet Technologies and Applications* (*ITA*), pp.292-297, 2015.

- **Z. Abu-Almaalie,** Xuan Tang, Z. Ghassemlooy, It Ee Lee and Alaa A. S. Al-Rubaie," Iterative multiuser detection with physical layer network coding for multi-pair communications," 10*th International Symposium on Communication Systems, Networks & Digital Signal Processing* (*CSNDSP*), pp. 1-6, 2016.

- **Z. Abu-Almaalie**, Z. Ghassemlooy, Alaa A. S. Al-Rubaie, It Ee Lee and H. Le-Minh," Forward error correction with physical layer network coding in two-way relay free space optical links," 8*th Computer Science and Electronic Engineering (CEEC),* pp. 1-5, 2016.

Poster:

- **Z. Abu-Almaalie,** Z. Ghassemlooy, H. Le-Minh and N. Aslam," Evaluation the performance of the large wireless transmission using physical layer network coding," *Northumbria Research Conference (winner), 2013.*

1.4 Organization of the Thesis

The rest of the thesis is organized as follows:

Chapter 2 describes the two-way communications technique and the most popular strategies for relaying system are also outlined in this chapter. A comprehensive review and discussion pertaining to the key aspects of FSO technology links for long-distance terrestrial are also presented. The relevant components encompassing the optical transmitter and receiver blocks together with the important characteristics and modelling of the atmospheric channel are introduced and the functions of each block highlighted. In this chapter, the principle of PNC technique together with the modulation and channel model are introduced in the implementation of the system.

Chapter 3 gives a detailed description of optical wave propagation in TWRC free space with PNC. An aggregated optical channel between two sources and relay is defined, which starts from the FSO output at the transmit node and ends at the FSO input at the receiver node through the relay. It is assumed that the output laser beam at the transmitter has a Gaussian transverse profile. The Beers-Lambert law is used to model atmospheric attenuation of optical fields. Moreover, a weak log-normal atmospheric turbulence regime is considered whose log-amplitude and phase are normally distributed and their statistical moments are mathematically described. Also, gamma-gamma atmospheric turbulence is used to model the moderate-to-strong turbulence alongside with its BER performance analysis. Different parameters are taken into account to characterize the system behavior.

Chapter 4 presents the encoder and decoder for channel coding in digital transmission with its algorithms that are used to decode the data encoded using convolutional codes.

Also, it discusses general concepts about coded modulation (CM) techniques, with particular focus on bit-interleaved coded modulation with iterative decoding (BICM-ID). Then, it introduces the channel coding in TWR-FSO PNC model with iterative decoding. The conventional code technique for non-iterative scheme and BICM-ID code in TWR-FSO PNC systems are compared when the relay role is as simple as possible.

Chapter 5 presents an overview for multiple access schemes and provides preliminaries on spreading code and interleaver with their mechanism and characteristics along with conditions for orthogonality. In addition to it, the mechanism of choosing interleaver is also outlined in details for single path along with literature review on multiuser detection technique. The detailed challenge of PNC in multi-user networks is investigated in this chapter for RF and FSO communication links, where multiple nodes exchange their information through one relay. This chapter, therefore, outline in details the full structure of the transmitter, relay and receiver of the proposed systems with its mathematical expression.

In Chapter 6 the conclusion of the thesis is presented along with the possible directions for further research related to PNC technique over TWR-FSO links.

Chapter 2

BACKGROUND

This chapter presents the general fundamental and techniques, which are essential to support the research work carried out. Firstly, the chapter gives a brief concept on the cooperative communication technique, where the common relaying strategies are also defined. FSO technology alongside its relevant features that make it a viable complementary access network technology is also introduced in this chapter. The fundamental structure of the FSO communication system is outlined and the optical detection methods are described in which noise sources at the receiver are demonstrated for their influence on the performance of the system. Emphasis is placed on the explanation of the system model of the PNC architecture. A mathematical representation of the relay demapping and mapping processes are also explained and illustrated. The comparisons between the PNC throughputs with other transmissions mode are also clarified to demonstrate the benefit for the use of this technique.

2.1 Cooperative communication systems

Cellular systems employed advanced algorithms and techniques that not only increase the data rate, but also enable the system to guarantee the quality of service (QoS) desired by the various media classes such as coding, modulation and detection. Among these techniques, diversity was acknowledged as the most effective techniques due to the nature of the wireless environment by combating fading effects in wireless communications [36]. Spatial diversity showed to be very effective in increasing network capacity. However, equipping a wireless node with multiple antennas may not always be practical, as the footprint of multiple antennas may not fit on a wireless node and the cost will be increased. On other hand, relays that receive and retransmit the signals between base stations and mobiles can be used to extend the coverage of cellular networks. Infrastructure relays do not need wired connection to network thereby offering saving in operators backhaul costs. In relaying networks, the relay located either in a central or a series of central elements whose main purpose is for gathering data from other terminals and either broadcasting the received signal or performing signal processing operations on it before forwarding. Mobile relays can be used to build LAN between mobile users under the umbrella of the wide area cellular networks. Moreover, in relaying systems, energy can potentially be conserved. Otherwise, when the relay terminal provides the communication between two terminals in a half-duplex transmission mode, they cannot transmit and receive data simultaneously using the same frequency channel, this leads to an inefficient in spectral efficiency [30]. Therefore, it has been recognized recently that effective relaying protocols can be devised to facilitate cooperation between two terminals when they want to exchange information simultaneously over relay terminals. Based on the availability of the links, the relaying system has popular variants such as

cooperative communication and TWRC. A cooperative communications have the ability to increase channel capacity without using multiple antennas at each terminal and attain broader cell coverage with single antenna terminals.

The basic idea of cooperative communication is that the two mobile agents propagate the signal arriving to the same destination through independent path, which is generated spatial diversity via the introduction of a relay channel [70]. Figure 2.1 shows a simplified cooperative communication model. This model comprises of a source, relay and the destination nodes and the data communication occurs as follows. At the first hop, signals are broadcasted by the source node to the neighboring nodes, which are heard by both the destination node and the involved relay nodes at the same instant. While in the second hop, the relay node processes its received signal and forwards it to the destination node. At the destination node, it has now received multiple copies of independent fading channel so that the process of diversity combination will be performed for the received signal from both source and relay nodes. However, the advantage of cooperative communications becomes clear when information is recovered at the destination. Without relays, when the source-destination link is bad, the information may not be decoded accurately. Therefore, in cooperative communications, the destination can use additional information from the relays, resulting in an improved decoding. However, there are two

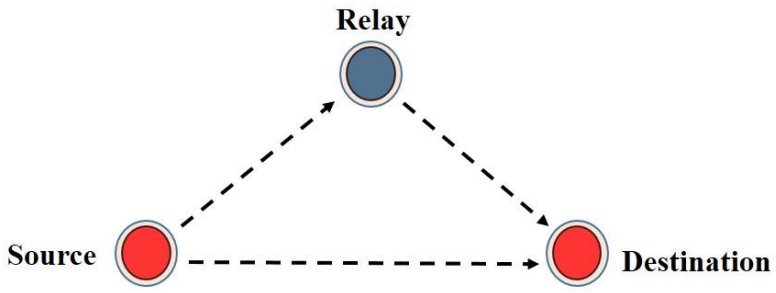

Figure 2.1 Simplified cooperation communication model.

topologies for transmission for relaying system. The first one is serial-relay transmission where the signal propagates from the source to the destination through multihop relay as shown in Figure 2.2(a). This topology is valuable when the distance between two terminals is far away. Furthermore, for outdoors and non-LOS (NLOS) communication, signal wavelength may be large and the installations of multiple antennas are not possible. Alternative one is the parallel-relay transmission in which the signals between the two terminals propagate through multiple relay paths in the same hop and the destination combines the signals received with the help of various combining schemes, as shown in Figure 2.2(b). This type may be used when the serial-relay transmission suffers from multipath fading effects.

2.2 Relaying strategies

Relay strategy is defined by the way the received signal is processed at the relay. These strategies that used in conventional relaying systems can also be applied to TWRC protocol. The relay node applies either, a very simple mathematical operation, or modifies

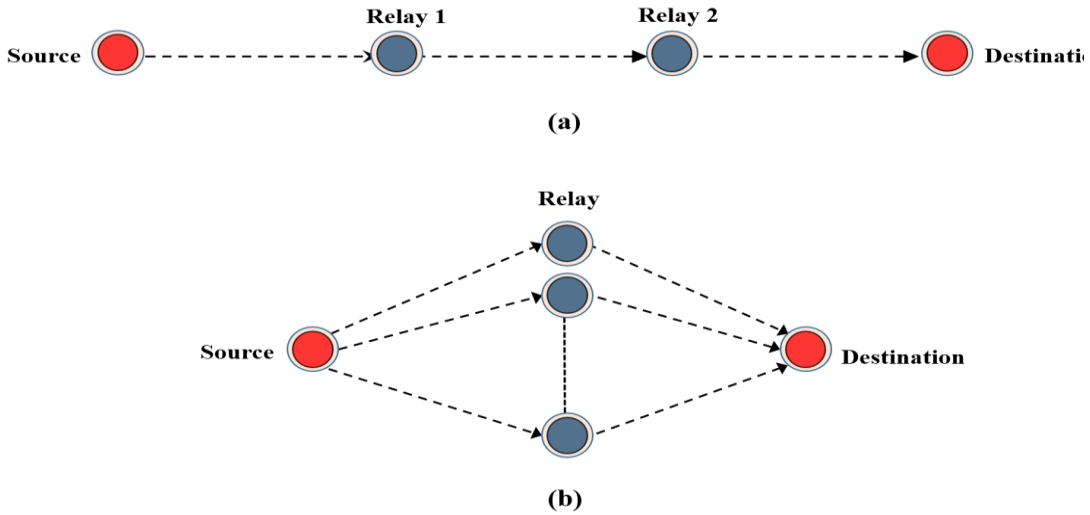

Figure 2.2 The classification of the relay transmission topologies: (a) serial-relay transmission, and (b) parallel-relay transmission.

the received signal and then forwards the new version of the signal to its destination. In these sub-sections, some of the particular relay strategies for relaying network will be discussed.

2.2.1 Amplify and forward

In amplifier-and-forward (AF) scheme, the relay simply retransmits an amplified version of the received signal with a gain factor and forwards the resulting signal to the destination. At the receiving side, it subtracts the known data symbols transmitted by it from the received signals so that the remaining signal only contains the data symbols from the other side. Although the AF relaying scheme is simple to implement, it forwards the signal as well as the amplified noise to the destination and may be subject to noise enhancement, which makes it unsuitable for multihop scenarios. Recently, the performance analysis of AF strategy with TWRC has been one of the most important research directions, which offer low complexity [29, 30, 40, 71-73].

2.2.2 Decode and forward

The decode-and-forward (DF) scheme was first introduced by T. Cover and A. E. Gamal for the traditional relaying communications network, which also referred to as the regenerative signalling scheme [29]. The DF protocol attracted a lot of attention and interest in the wireless communications community, which provides a more reliable solution but at the cost of increased complexity. In a DF relaying communication system, the source node transmits its information to the relay, which tries to regenerate the information by detecting and correcting the errors in the received data then re-encoded it prior forwards a new version of the data to the destination [70, 74, 75]. In this strategy, relay made a hard decision about what symbol was transmitted by the source and forward

this estimated symbols to the destination, which did not include any additional information about the reliability of the source-relay link. Error propagation occurs when the relay fails to correctly estimate the source's symbol, and thus forwarding the wrong symbol to the destination. For cooperative system, the destination uses a combined version of its two received symbols to estimate the information sent by the source [30, 70, 76].

2.2.3 Estimate and forward

This protocol is also known as Compress-and-Forward (CF) or Quantize-and-Forward (QF) [29]. At the relay, a transformation is applied to the received signal, which provides an estimate to detect the information at the destination. This estimation is called soft information, and it is forwarded to the destination. It is useful when the relay cannot decode the source information very well. The quality of the link between the source and the relay has a significant effect on the performance of this scheme [77]. Therefore, when the relay is near to the destination, this protocol has improved BER performance compared to the DF relay network [78].

2.3 Features of FSO Technology

The development of the wireless communications standards into the fourth generation (4G) has detected recent rapid progress in information and communication technologies. This in turn discovered a plenty of mobile broadband facilities, such as internet protocol (IP) telephony, high-definition television (HDTV) broadcasting services, streamed multimedia applications and gaming services [79, 80]. Transporting an exponentially increasing amount of data to the end users within an acceptable amount of delay time, will inadvertently result in severe congestion of the RF spectrum and wireless traffic

bottleneck. Complementing the existing RF and millimeter wave wireless systems, FSO has now emerged as a reliable and rapid deployment of data, voice and video within the access networks. FSO communications is poised to become a promising broadband wireless access candidate to resolve the existing last mile access network problems that entails the transmission of information laden optical radiation through the atmosphere channel [81]. FSO communications refers to any two transceivers LOS transmitting modulated visible or IR beams through the atmosphere to establish a full duplex communication link and there cannot be any obstructions. The basic feature of the FSO technology is that, it permits huge modulation bandwidth excess 2000 terahertz (THz) using an optical carrier whose frequency ranges from 10^{12} - 10^{16} Hz. Therefore, it promises an increased information capacity compared to RF based communication systems with a usable frequency bandwidth comparatively lower by a factor of 10^{5} [82, 83]. Further attractive feature include low cost and fast installation compared to the other communication technologies, which does not incur cost of digging up tunnels and trenching of roads to install bulky copper cables and it is much faster to deploy [82, 84-86]. Moreover, it is becoming increasingly expensive and difficult to allocate additional RF frequencies because of the congested spectrum. In contrast, the FSO technology provides unlicensed spectrum because of its spectrum band doesn't required regulations and therefore are relatively inexpensive compared to the RF licensed spectrum [86-88]. The main advantage of the FSO is the immunity to electromagnetic interference [82]. Furthermore, the confined beam of FSO communications is the ability to provide a significant degree of secrecy unlike many RF systems that radiate signals in all directions, thus making the signal available to all within the receiving rang [83, 89].

2.4 FSO Block Diagram

FSO is one of the most promising new access technologies that provides P2P link, a ring and star or mesh network architectures [90, 91]. An FSO link requires a LOS communication, where there is no obstacle between the transmitter and receiver. A physical model of a typical terrestrial FSO communication system is depicted in Figure 2.3. The diagram is composed of standard communication blocks, which are endemic to any communication system in terms of transmission, modulation, reception, and processing of data. The following sub-sections present a further discussion of each of the main blocks related to the FSO link: an optical transmitter, an optical receiver separated by an atmospheric channel.

2.4.1 The optical transmitter model for P2P FSO system

The objective of any communication system is the transfer of information from point to point. Therefore, the functionality of this block is to modulate the source information onto optical carrier using LEDs or LDs. This carrier is then transmitted as an optical light field,

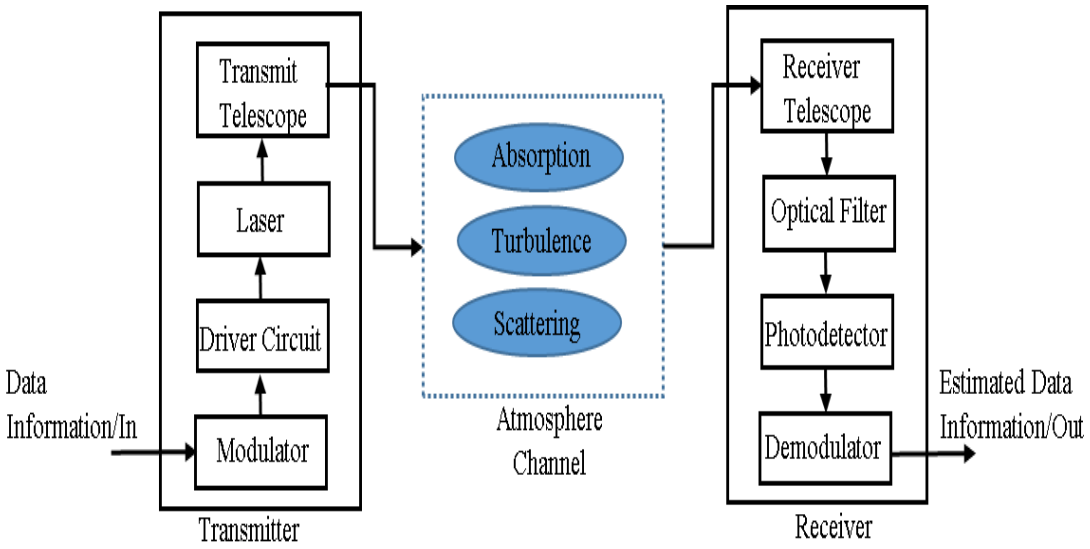

Figure 2.3 The point-to-point (P2P) FSO communication system block diagram.

or beam, through the atmosphere channel. The modulation of the source information onto the optical carrier can be in form of amplitude, intensity, frequency and phase.

For an optical wave, another modulation scheme is also often used, namely intensity modulation (IM) in which the source information is modulated onto the irradiance of the optical radiation. This can be achieved by varying the driving current of the optical source directly in line with the transmitted data or using the external modulator. The functionality of the driver is to regulate current flowing through the LD and stabilizes its performance. It also neutralizes temperature and aging effects on the performance of the laser. LD and LED are widely employed as the optical sources for wireless optical communications in order to convert an electrical input signal into the corresponding optical signal. Then, the transmitter optics (lens, telescope) collects, collimates and directs the optical radiation towards the receiver optics at the other end of the channel.

2.4.2 The channel characteristics for FSO

The reliability of the terrestrial FSO communications depends on the conditions of the optical atmospheric channel. For an optical radiation travelling through the atmosphere, some of the photons are absorbed by the molecular constituents, while others experience the scattering, which changes the initial propagating direction, shape, and electromagnetic properties of the laser resulting in power loss. Furthermore, the beam is also spread out while propagating through the channel leading to the size of the received beam wider and it is typically greater than detector aperture area [92]. These optical transmission power losses can be determined through Beer-Lambert law [1]. Another feature of interest is the atmospheric turbulence, which is mostly based on velocity and temperature fluctuations. In the context of optical propagation, the air's density experiences random space and time fluctuations induced by solar heat and wind that produced an inhomogeneous refractive

index distribution. The temperature inhomogeneity of the atmosphere causes corresponding changes in the index of refraction of the atmosphere, resulting in eddies, cells or air pockets having varying sizes. The propagating optical radiation is therefore fully or partially diverged and fluctuated from its original path [93].

In contrast to the conventional RF channel, where SNR is proportional to the average received power, in optical communication systems, it is proportional to the square of the average received optical signal power. When the shot noise is dominant, SNR is also proportional to the photodetector area $\mathcal{A}_d$ because the received electrical power and the variance of the shot noise are proportional to the receiver detector area [97]. However, the transmitted signal $x(t)$ represents the power rather than amplitude and should fulfil the followings: the non-negative and the average value of the transmitted signal must not exceed a specified maximum power P_{max} , where [94]:

$$P_{max} \geq \lim_{T\to\infty} \frac{1}{2T} \int_{-T}^{T} x(t)\, d(t). \tag{2.1}$$

A further description of the channel characteristics will be fully explained in the next chapter.

2.4.3 Noise in optical detection

To accurately characterise the system performance, a good understanding of origins of noise is required, in which the capability of a PD to identify an input signal is limited by intrinsic fluctuations or noise. Correspondingly, the design, performance evaluation and optimization of terrestrial FSO links would require in-depth understanding pertaining to the occurrence, characteristics and inter-relationships of various noise sources present in the optical receivers. Noise in the detection process of WOC system arises from the

radiation entering the receiver and from internally noise. Therefore, the receiver front-end typically constitute from the PD and pre-amplifiers in order to enable the detection of the weakest possible optical signals that subjected to the interference and distortions arising from various fundamental noise sources as shown in Figure 2.4 [95]. A number of noise sources are associated with the optical communication systems, which include the thermal noise caused by thermal interaction between the free electrons and the vibrating ions in a conducting medium [96]. Thermal noise obeys the Gaussian distribution with zero mean and unit variance and is regarded as a 'white' noise mainly because the power spectral density (PSD) of this noise source is independent of frequency. While using a low resistance R_L in the front end is capable of improving the frequency response, an excessive amount of thermal noise is generated by the pre-amplifier independent of the resultant photocurrent. The second type called the dark current shot noise which is arising from the transition of electrons from the valence to the conduction band, includes tunnel, leakage, diffusion currents and generation-recombination taking place in the space-charge region and is proportional to the volume of the depletion region [97]. Furthermore, the appropriate channel model for FSO communication system using IM will depend on the background light. The background radiation, also called background noise or ambient noise, can degrade the performance of FSO links. It is due to the detection of photons

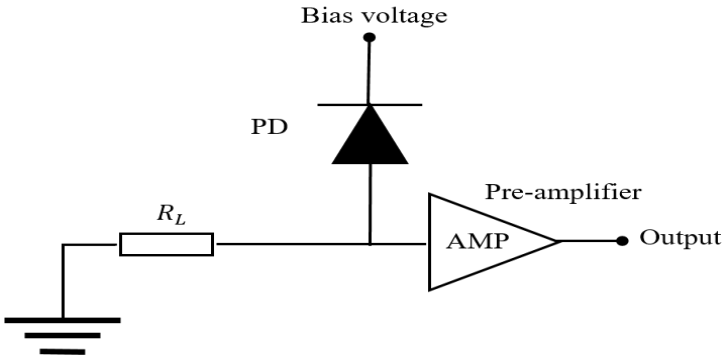

Figure 2.4 Optical receivers front-end, which consist from photodetector and pre-amplifier and resistance (R_L).

generated by the environment (sun and sky). In general, the background radiation is greater than other noise processes so that it dominates the total shot noise, which is the summation of all type of noises [97]. However, the unwanted background radiation is collected together with the desired signal at the receiver, which is statistically modelled as additive white Gaussian noise (AWGN) in time and space with zero mean and variance $\sigma^2 = N_0/2$, where $N_0/2$ is the two-sided PSD. The collected background noise is processed along with the desired signal and affects the overall system performance.

2.4.4 The optical receiver model for P2P FSO system

The receiving side of the FSO link, which recovers the transmitted data from the incident optical field, is composed from optics system, PD, and a trans-impedance amplifier (TIA) followed by a demodulator as shown in Figure 2.5. The main advantage of the optics is to help to collect and focus the received optical beam to the PD, which converts the optical signal into the electrical signal before it is amplified. Following amplification the original signal is recovered using a suitable demodulation process [98]. In optical systems, an optical band pass filter is normally used before the signal is passed through the PD to minimize the effects of the background noise, which is collected from the large optic receiver aperture [99]. The receiver detection process can be classified into direct detection (DD) as shown in Figure 2.5 in which the receiver detects the instantaneous intensity or power of the optical radiation impinging on the PD. Its implementation is

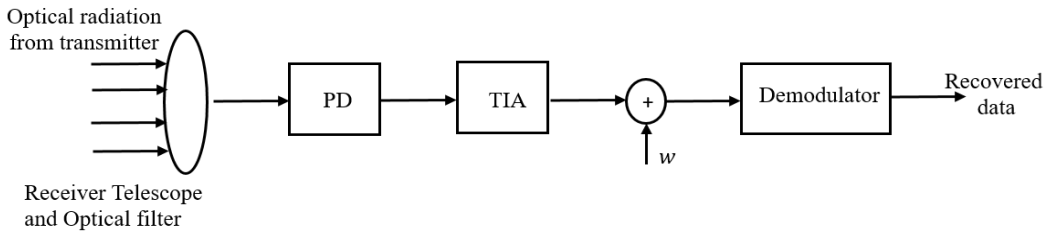

Figure 2.5 The block diagram of DD structure of the P2P FSO receiver.

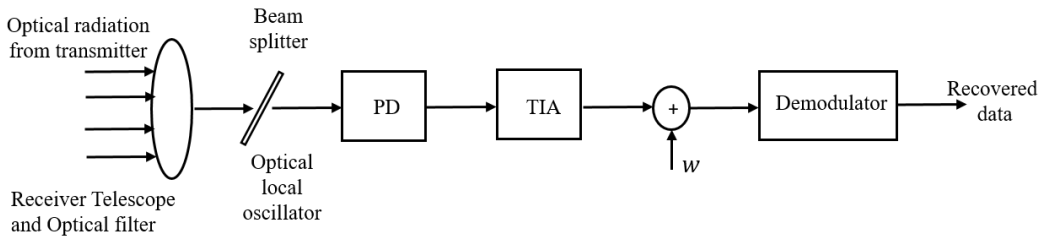

Figure 2.6 The block diagram of the coherent detection at the receiver side of the FSO.

simple and suitable for IM optical systems [92, 96]. Whereby in coherent detection, the receiver computes decision variables based on the recovery of the full electric field, which contains both amplitude and phase information. The schematic way in which coherent detection is carried out is shown in Figure 2.6. Coherent detection allows the greatest flexibility in modulation formats, as information can be encoded in amplitude and phase [100]. Coherent detection requires the receiver to have knowledge of the carrier phase, as the received signal is demodulated by a local oscillator (LO) that serves as an absolute phase reference. The coherent receiver can be further divided into homodyne and heterodyne receivers. In homodyne receivers the frequency/wavelength of the LO is exactly the same as that of the incoming radiation [96], while in heterodyne detection the incoming radiation and the LO frequencies are different [81]. In contrast to RF coherent detection, the output of the LO in an optical coherent detection is not required to have the same phase as the incoming radiation.

2.5 Physical Layer Network Coding System

For decades, wireless communication has seen tremendous developments in technology and application. It has penetrated into every aspect of our life and has become essential to the modern society such as mobile cellular telephones, pagers, Wi-Fi local networks and terrestrial microwave networks. Nowadays, the demand in network capacity has continued to increase to support high data rate services such as video conference, internet

and multimedia applications. The upcoming of the wireless communication systems are compulsory to meet such growing demands with high spectral efficiency, low energy consumption and high mobility. The main impediments to high performance wireless communications are the interference from other users called MAI, the inter symbol interference (ISI) and signal fading caused by multipath propagation [101]. In wireless communication networks, interference is typically treated as a destructive phenomenon. When multiple transmitters transmit RF waves to their particular receivers, a receiver collects signals from its transmitter as well as from other communication terminals, which are often treated as interferences that corrupt the intended signal. Therefore, wireless networks strive to avoid scheduling multiple transmissions at the same time in order to prevent interference. Thus, one of the major problems facing wireless networks is the reduction of capacity because of interference due to simultaneous transmissions. As a new formed in the NC techniques, PNC takes advantage of the superimposition of the EM [44, 102], and embraces the interference, which was typically deemed as harmful, by performing XOR-operation. Therefore, the spectral efficiency is utilized, which in turn boosts the network throughput. The crucial concept of the PNC system is that the two users swap their information, but they are out of each other's transmission range, therefore the relay is essential. However, the link from the two users to the relay can be seen as a MA phase, while the link from the relay to the two users can be seen as a BC phase, where all the nodes operate in half- duplex mode. The following sub-sections present in details the structure of the PNC technique along with its mathematical expression of the demapping and mapping at the relay.

2.5.1 The transmitter structure

The fundamental structure of the PNC system consisting of three-node linear network; two users (S_1, S_2) and the relay node (RN) was considered as represented in Figure 2.7. In MA phase, the transmitted signal for the two users produce a sequence of information bits $(d_k(l))_{l=0}^{L_d-1} \in GF(2)$ of random binary data length L_d, where $k \in (1,2)$ is the number of users. In digital transmission, the information bits are mapped into a suitable modulation scheme before performing baseband modulation. This is achieved by an array technique, *M*-ary, for phase shift keying (PSK) modulation schemes. Thus, *M* can be defined as the constellation size of the utilized modulation scheme. The *M*-ary scheme groups the $log_2 M$ bits for each constellation point. For instance, the scheme with $M = 2$ is known as BPSK, which maps one consecutive bits to a symbol taken from the BPSK alphabet. In TWRC structure with binary data transmission, the users send only one of two possible signals during each bit interval T_b. In this case, we have two symbols, each representing a particular bit value as shown in Figure 2.8. Consequently, the transmitters may send one of M possible signals during each signalling interval of duration T_s. Therefore, the information bits are mapping to a constellation diagram using BPSK to

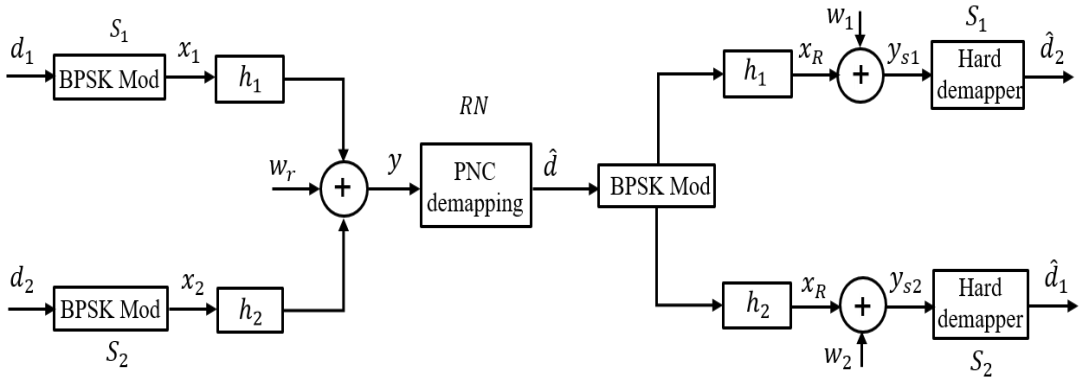

Figure 2.7 The transmitter and receiver structure of the TWRC for the PNC system using BPSK modulation, where (h_1, h_2) are denoted the channel gains and x_R the modulated transmitted signal from the RN. Wheares $\hat{d}$ represents the network-coded symbol.

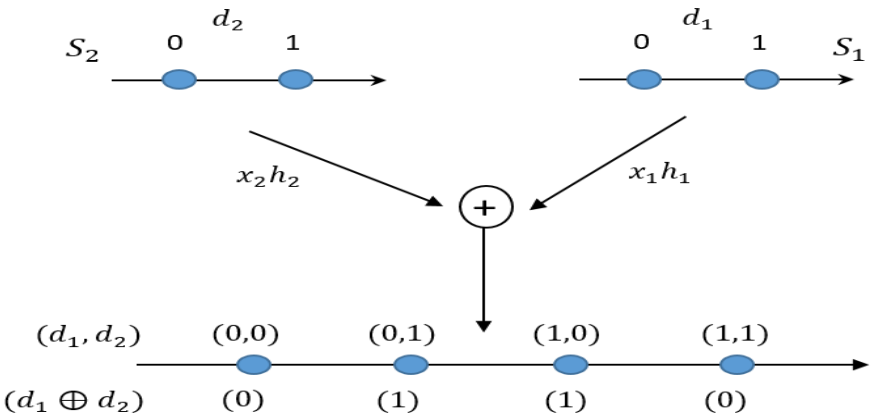

Figure 2.8 The module-2 sum is the XOR operation of the two information bits.

generate the transmitted input symbols sequence $(x_k(n))_{n=0}^{N-1}$ of symbol length N. For BPSK signal requires the bandwidth, which is equal $1/T_s$ for the bit rate equal to $(\log_2 M)/T_s$. Finally, the symbol is transmitted simultaneously by the two users over the channels.

2.5.2 The channel model and characteristics

The physical characteristics of wireless communication channels can vary widely because of relative mobility between the transmitter and receiver, which changes the amplitude and phase of the transmitted signal over a short period of time or travel distance. In mobile communication system, a signal can travel from transmitter to receiver over multiple reflective paths; this phenomenon is referred to as multipath fading propagation. When there is NLOS condition between the transmitter and the receiver, the signals will be attenuated, reflected, refracted, and diffracted before they arrive at the receiver. This propagation environment is known as Rayleigh fading. These variations can be modelled by assuming that the transmitted signal passes through a linear filter with a time varying impulse response. The impulse response $h(t)$ characterizes the channel and is a function of both time variations t and channel multipath delay τ. By applying the central limit theorem, $h(t)$ of the channel can be modelled as a complex-valued Gaussian random

process. Thus, the channel impulse response of the flat fading and NLOS propagation can be described as [102]:

$$h(t) = \sum_{l=1}^{L_n} \exp(j\ 2\pi\ t\ f_d\ \cos(\alpha_l) + \emptyset_l\ , \tag{2.2}$$

where L_n is the number of the propagation paths, $\emptyset_l$ is the angle phase of the l^{th} multipath component, which is uniformly distributed over $[0,2\pi]$, and f_d is Doppler shifts defines as the relative motion between the transmitter and receiver, which can be described as:

$$f_d = (V_m/\lambda) = V_u f_c/V_c\ , \tag{2.3}$$

where λ is the wavelength of the carrier signal, V_u is speed of the user, f_c is the frequency of the transmission, and V_c is the speed of the light [103]. Generally, the received signal $y(t)$ is described in terms of the transmitted signal $x(t)$ convolved with the impulse response of the channel as:

$$y(t) = x(t) * h(t) + w(t) = \int_{-\infty}^{\infty} h(\tau)x(t-\tau)d\tau + w(t). \tag{2.4}$$

The constructive and destructive nature of the arriving multipath components of the fading channels at the receiver caused the rapid amplitude and phase fluctuations of the received signal, which in turn influenced the transmission performance. It is well known that the envelope of the sum of two quadrature Gaussian noise for the received signal is statistically described by Rayleigh distribution, which probability density function (PDF) is given by [102]:

$$p_{ra}(y) = \begin{cases} \dfrac{y}{\sigma^2}\exp\left(\dfrac{-y^2}{2\sigma^2}\right), & y \geq 0 \\ 0, & \text{otherwise} \end{cases} . \tag{2.5}$$

2.5.3 Relay node for the PNC system

RN receives the noisy signal which is given as:

$$y = h_1 x_1 + h_2 x_2 + w_r, \tag{2.6}$$

where w_r is AWGN from the source to the RN and (h_1, h_2) are denoted the channel gains from two users to the RN. The RN maps the received signal y to produce the modulo-2 sum in another constellation diagram to yield the modulated transmitted output symbols x_R, where the PNC mapping is implemented as $PNC: y \rightarrow x_R$ as shown in Figure 2.7. The superimposed signal is mapped as the XOR combination of the information from the two users, given by $\hat{d} = d_1 \oplus d_2$, where $\hat{d}$ denote the network-coded symbol and $\oplus$ represents the bit-wise XOR operation, which is broadcast back to the destination nodes after BPSK modulation.

In PNC technique, there are two approaches of processing the received signals at the RN. These approaches are end-to-end PNC and link-to-link PNC. In the first one, the RN does not try to perform channel decoding and re-encoding. Instead, the RN may simply try to recover $d_1 \oplus d_2$ in a symbol-by-symbol manner and pass the symbols along to the end nodes. The latter approach, the RN tries to decode the successive symbols to recover the desired network coded symbol. However, in this research work, the goal is to make the process at the RN as simple as possible by using the approach end-to-end PNC technique. During a particular signalling interval, the received signal at the RN at the time instant *t* can be expressed as:

$$y(t) = \sum_{k=1}^{K} x_k(t) + w_r(t). \tag{2.7}$$

For the PNC communication system, the most interesting process for the system is the PNC demapping at the RN to produce $\hat{d}$ and then mapping to recover x_R, which have the information sent by the two users. Without loss of generality, the noise is ignored to simplify the process. Therefore, (2.7) can be rewritten as:

$$y = x_1 + x_2 \ . \tag{2.8}$$

Due to the system using BPSK modulation in all the nodes and according to (2.8), the signal y has corresponding bits mapping, which can be summarized in Table 2.1. For PNC demapping process $y = 0$ when $x_1 \neq x_2$ and $y = 2, -2$ when $x_1 = x_2$. According to Table 2.1, the signal space is $-2, 0, 2$ with corresponding probabilities of $25\%, 50\%, 25\%$, respectively, as shown in Figure 2.9 (a).

Whereas the PNC mapping process, $\hat{d} = 0$ should be set to -1 when $x_1 = x_2$ and $\hat{d} = 1$ should be set to 1 when $x_1 \neq x_2$, as shown in Figure 2.9 (b). This is done by:

$$x_R = \begin{cases} -1 & \hat{d} = 0 \\ 1 & \text{otherwise} \end{cases} \ . \tag{2.9}$$

Afterward, the mapping signal forwards back to the end users. However, the well-known challenge for PNC in TWRC is the fading and the noise in the MA phase, which in turn made S_1 and S_2 under the effect of fading channel. Therefore, the transmitted signal over Rayleigh fading channel in the MA phase can be expressed as:

$$y = h_1 x_1 + h_2 x_2 + w_r. \tag{2.10}$$

Table 2.1 The demapping/mapping at the RN for PNC system.

Modulation mapping at each users		Demapping /mapping at RN		
x_1	x_2	$y = x_1 + x_2$	$\hat{d}$=$d_1 \oplus d_2$	x_R
-1	-1	-2	0	-1
-1	1	0	1	1
1	-1	0	1	1
1	1	2	0	-1

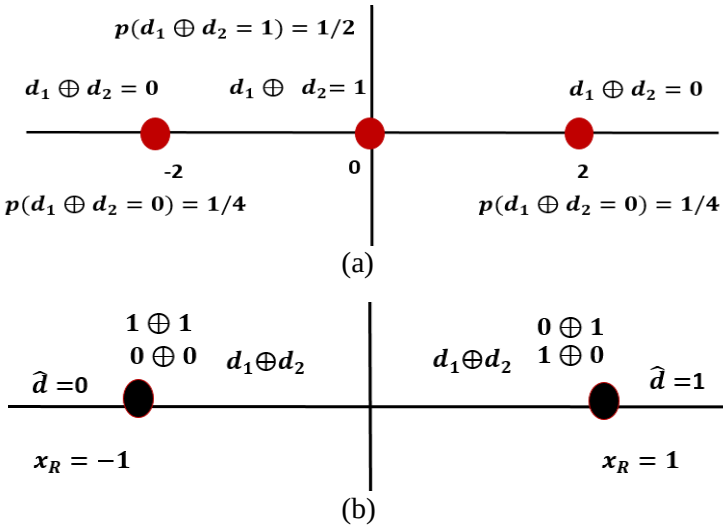

Figure 2.9 The constellation point:(a) of the PNC demapping at the RN, and (b) of the PNC mapping at the RN.

The demapping operates on a symbol-by-symbol basis, since d_1 and d_2 are the bits transmitted by two users, let $\hat{d}$ be the corresponding network-coded bit, then the log-likelihood ratio (LLR) of the demodulator at RN can be determined as:

$$L(\hat{d}) = log\frac{P_r(\hat{d}=1|y)}{P_r(\hat{d}=0|y)}, \tag{2.11a}$$

$$L(d_1 \oplus d_2) = log\frac{P_r(d_1 \oplus d_2 = 1|y)}{P_r(d_1 \oplus d_2 = 0|y)}, \tag{2.11b}$$

The term $d_1 \oplus d_2 = 1$ is represented when $x_1 + x_2 = 0$. In the same way, the term $d_1 \oplus d_2 = 0$ is represented when $x_1 + x_2 = 2$ or -2. Hence, the LLR can be expressed as:

$$L(d_1 \oplus d_2) = log\frac{P_r(x_1 + x_2 = 0|y)}{P_r(x_1 + x_2 = -2 \text{ or } 2|y)}, \tag{2.12a}$$

$$= log\frac{P_r(y, x_1 + x_2 = 0)}{P_r(y, x_1 + x_2 = 2) + P_r(y, x_1 + x_2 = -2)}, \tag{2.12b}$$

$$= log\frac{p(y|x_1 + x_2 = 0)P_r(x_1 + x_2 = 0)}{p(y|x + x_2 = 2)P_r(x_1 + x_2 = 2) + p(y|x_1 + x_2 = -2)P_r(x_1 + x_2 = -2)}, \tag{2.12c}$$

The maximum a posterior probability criterion (MAP) rule to minimize the probability that $\hat{d}$ is in error is given by:

$$\hat{d} = \arg\max_{i=0,1} \; p\,(y|d_1 \oplus d_2 = i) P_r(d_1 \oplus d_2 = i), \tag{2.13}$$

where $P_r(d_1 \oplus d_2 = i)$ is the priori distribution of $d_1 \oplus d_2$ and $p(y|d_1 \oplus d_2 = i)$ is the conditional probability distribution of the channel output given the modulo-2 sum, which can be characterized by Gaussian PDF as:

$$p(y|d_1 \oplus d_2 = 1) = \frac{1}{\sqrt{2\pi\,\sigma^2}} exp\left(\frac{-(y)^2}{2\sigma^2}\right), \tag{2.14a}$$

and

$$p(y|d_1 \oplus d_2 = 0) = \frac{1}{2\sqrt{2\pi\,\sigma^2}}\left(exp\left(\frac{-(y-2)^2}{2\sigma^2}\right) + exp\left(\frac{-(y+2)^2}{2\sigma^2}\right)\right). \tag{2.14b}$$

Therefore, the LLR for the received signal by the BPSK modulation is given by:

$$L\,(y|d_1 \oplus d_2 = 1) = \frac{exp\left(\frac{-(y)^2}{2\sigma^2}\right)}{2}\;, \tag{2.15a}$$

$$L\,(y|d_1 \oplus d_2 = 0) = \left(\frac{exp\left(\frac{-(y-2)^2}{2\sigma^2}\right) + exp\left(\frac{-(y+2)^2}{2\sigma^2}\right)}{4}\right), \tag{2.15b}$$

$$L\,(y|d_1 \oplus d_2) = \left(\frac{\frac{exp\left(\frac{-(y-2)^2}{2\sigma^2}\right) + exp\left(\frac{-(y+2)^2}{2\sigma^2}\right)}{4}}{\frac{exp\left(\frac{-(y)^2}{2\sigma^2}\right)}{2}}\right), \tag{2.15c}$$

Hence, the reliability for the received network-coded bits is expressed as:

$$L\left(y\middle|\hat{d}\right) = log\left(\frac{exp\left(\frac{-(2y+2)}{2\sigma^2}\right) + exp\left(\frac{(2y-2)}{2\sigma^2}\right)}{2}\right). \tag{2.16}$$

The RN for PNC detects the XOR version of the two received binary information, based on the original PNC design using XOR mapping, the common approach for the demapping and then mapping of synchronization algorithms embodies the application of

the maximum likelihood (ML) detection criterion. If the input symbols are equiprobable, it can be easily shown that the ML detection rule for the symbol x_R at RN is given by [104]:

$$[x_R = 1] = exp\left(-\frac{m(1,1)}{\sigma^2}\right) + exp\left(-\frac{m(-1,-1)}{\sigma^2}\right) ,$$
$$[x_R = -1] = exp\left(-\frac{m(1,-1)}{\sigma^2}\right) + exp\left(-\frac{m(-1,1)}{\sigma^2}\right) . \quad (2.17)$$

In the ML, the RN received the signal constellation closest to y and is determined from the minimum Euclidean distance (MED) and computed by [104]:

$$m(x_1, x_2) = |y - h_1 x_1 - h_2 x_2|^2. \quad (2.18)$$

2.5.4 The receiver structure

At the second time slot, the RN forwards the detected symbol x_R to the end users over BC phase, and the signal y_{sk} received by S_k is given by [47]:

$$y_{s1} = x_R\, h_1^*/|h_1|^2 + w_1. \quad (2.19a)$$
$$y_{s2} = x_R\, h_2^*/|h_2|^2 + w_2. \quad (2.19b)$$

The coherent BPSK detection computes each channel gain and can invert it. With perfect channel state information (CSI), S_1 and S_2 can multiply the received symbol x_R by $h_k^*/|h_k|^2$. The receiver consists from the soft demmapper to compute the LLRs of the soft information and provide the bit metric to the device decision. By applying the MED rule, S_k first detects x_R as follows [104]:

$$\widehat{d_1 \oplus d_2} = \arg \min_{x_R \in (\pm 1)} |y_{sk} - h_k x_R|^2. \quad (2.20)$$

Then, each user estimates the information for the other partner by applying the XOR operation. The process to obtain the LLRs bits to represents the modulo-2 sum of the estimated bit $\widehat{d_1 \oplus d_2}$ for S_1 as [105]:

$$d_1 \oplus (\widehat{d_1 \oplus d_2}) = (d_1 \oplus \hat{d}_1) \oplus \hat{d}_2$$
$$= (0) \oplus \hat{d}_2$$
$$= \hat{d}_2 \ . \tag{2.21}$$

Similarly, for S_2

$$d_2 \oplus (\widehat{d_1 \oplus d_2}) = (d_2 \oplus \hat{d}_2) \oplus \hat{d}_1$$
$$= (0) \oplus \hat{d}_1$$
$$= \hat{d}_1 \ . \tag{2.22}$$

2.6 Bit Error Rate Performance

In this section, the effect of fading is evaluated on BPSK and PNC modulation schemes. The bit error probability p_e often referred as BER is a better performance measure to evaluate a modulation scheme, which can be defined as:

$$BER = \frac{number\ of\ bits\ in\ error}{total\ number\ of\ bits\ sents} \ .$$

The BER expression is given by [24, 106, 107]

$$p_e = \int_0^\infty p_e(\psi) p(\psi) d\psi, \tag{2.23}$$

where $p_e(\psi)$ is the probability of error of a particular modulation scheme in AWGN channel at a specific value of ψ, where ψ is the SNR and can be expressed as $\psi = h^2 E_b/N_0$,where E_b is the bit energy and $p(\psi)$ is the PDF of ψ due to the fading channel.

The probability of error for BPSK modulation scheme over an AWGN channel for a given value of ψ is given by:

$$p_e = Q\left(\sqrt{2E_b/N_0}\right), \tag{2.24}$$

where $Q(.)$ is the complementary error function defined as:

$$Q(x) = \frac{1}{\sqrt{2\pi}} \int_{x}^{\infty} exp(-y^2/2)dy. \quad (2.25)$$

For Rayleigh fading channel, h is Rayleigh distributed, h^2 has chi-square distributed with two degrees of freedom and ψ is also chi-square distributed with PDF given by[106]:

$$p(\psi) = \frac{1}{E_b/N_0} \exp\left(\frac{-\psi}{E_b/N_0}\right) \quad \psi \geq 0 \quad . \quad (2.26)$$

Using (2.23) and (2.24), the probability of error for slowly Rayleigh fading channel with BPSK modulation can be expressed as:

$$p_{e,ray} = \frac{1}{2}\left(1 - \sqrt{E_b/N_0/(1 + E_b/N_0)}\right). \quad (2.27)$$

To analyses BER performance for the end-to-end PNC, we assumed that the received signal energy for one bit is unity, and the noise is Gaussian white with density $N_0/2$. In the consideration of noise over AWGN channel, the (2.10) becomes [44]:

$$y = x_1 + x_2 + w_r \, . \quad (2.28)$$

According to the Table 2.1, $\hat{d}$ is only mapped to two integral values: -1 when $x_1 + x_2 = 2$ or $x_1 + x_2 = -2$, and +1 when $x_1 + x_2 = 0$, which can be determined as follows. By applying MAP rule on (2.14), the optimal thresholds $\gamma_{th1}, \gamma_{th2}$ for the received signal y can be defined as [44, 106]:

$$\gamma_{th1} = -1 - \frac{N_0}{4} \ln\left(1 + \sqrt{1 - \exp(-8/N_0)}\right). \quad (2.29a)$$

$$\gamma_{th2} = +1 + \frac{N_0}{4} \ln\left(1 + \sqrt{1 - \exp(-8/N_0)}\right). \quad (2.29b)$$

When the received signal amplitude is less than γ_{th1} or greater than γ_{th2} , so the $x_1 + x_2$ will be -2 or 2, respectively, and $x_R = -1$. Similarly, if the received signal amplitude is greater than γ_{th1} and less than γ_{th2}, so the $x_1 + x_2$ will be zero and $x_R = +1$. Therefore, the average probability of error is calculated for all possible cases, and the BER of the PNC can be written as follows [108]:

$$p_e^{pnc} = Q\left[\sqrt{2E_b/N_0} + \frac{ln\left(1+\sqrt{1-e^{-8E_b/N_0}}\right)}{2\sqrt{N_0/2E_b}}\right] + \frac{1}{2}Q\left[\sqrt{2E_b/N_0} - \frac{ln\left(1+\sqrt{1-e^{-8E_b/N_0}}\right)}{2\sqrt{N_0/2E_b}}\right] - \frac{1}{2}Q\left[3\sqrt{2E_b/N_0} + \frac{ln\left(1+\sqrt{1-e^{-8E_b/N_0}}\right)}{2\sqrt{N_0/2E_b}}\right] . \quad (2.30)$$

2.7 Throughput of the PNC

The throughput is a key measure of the quality of the wireless data link. The PNC technique improves the system performance in terms of the throughput by reducing the number of transmissions required to successfully send packets between the source and destination. For one-hop transmission mode, the source node sends an infinite number of packets to the destination, which assumed to receive all the packets successfully. However, any erroneous packet is to be retransmitted again until it is correctly received. Therefore, the average number of required transmissions until a packet is successfully delivered is $1/p_c$, where p_c is the correct packet rate (average probability of correct decision of channel) [107]. Assuming that retransmission is being used, the throughput is defined as the number of information bits received correctly per unit time, which is given by [60]:

$$\mathcal{TH} = \mathcal{P}_{\mathcal{C}}/\mathcal{T}_p = (1-p_e)^{N_p}/\mathcal{T}_p \, , \quad (2.31)$$

where N_p is the length of the packet, $\mathcal{T}_p$ is the time to exchange data between the two nodes, $\mathcal{P}_{\mathcal{C}}$ is the probability to receive one correct packet, and p_e is the average probability of bit error and can be determined using (2.24). In order to avoid interference, under the traditional transmission mode, the destination node received one packet every four time

slots. Thus, the throughput for the traditional transmission (store-and-forward) can be expressed as [109]:

$$\mathcal{TH}_{ts} = \mathcal{P}_{\mathcal{C}}/4 = (1 - p_e)^{N_p}/4 \ . \tag{2.32}$$

In contrast to the NC transmission mode, where the data exchange between the two nodes takes three time slots, therefore the throughput can be defined as:

$$\mathcal{TH}_{nc} = \mathcal{P}_{\mathcal{C}}/3 = (1 - p_e^{NC})^{N_p}/3 \ , \tag{2.33}$$

where p_e^{NC} is the probability of error for NC and can be defined as [108]:

$$p_e^{NC} = 2Q\left(\sqrt{2E_b/N_0}\right)\left(1 - Q\left(\sqrt{2E_b/N_0}\right)\right). \tag{2.34}$$

Whilst PNC transmission technique outperforms that of the traditional and NC techniques, which arises from the fact that it involves fewer number of transmissions than what the other both techniques needed to deliver a packet successfully. Hence, the concurrent transmissions lead to receive one packet at the destination every two time slots, resulting a throughput [109]:

$$\mathcal{TH}_{pnc} = \mathcal{P}_{\mathcal{C}}/2 = (1 - p_e^{pnc})^{N_p}/2 \ , \tag{2.35}$$

where p_e^{pnc} is the probability of error for PNC and can be calculated using (2.30).

2.8 Simulation Results

The predicated probability of error for PNC system for two users using (2.30) along with the simulated BER performance against the value of SNR over AWGN is shown in Figure 2.10. The theoretical BER performance using (2.24) of the single user over AWGN for BPSK modulation is also shown here as a reference. Whereas the theoretical BER performance using (2.27) over Rayleigh flat-fading channel for BPSK modulation is depicted in Figure 2.11 together with the simulated and predicated BER performance of

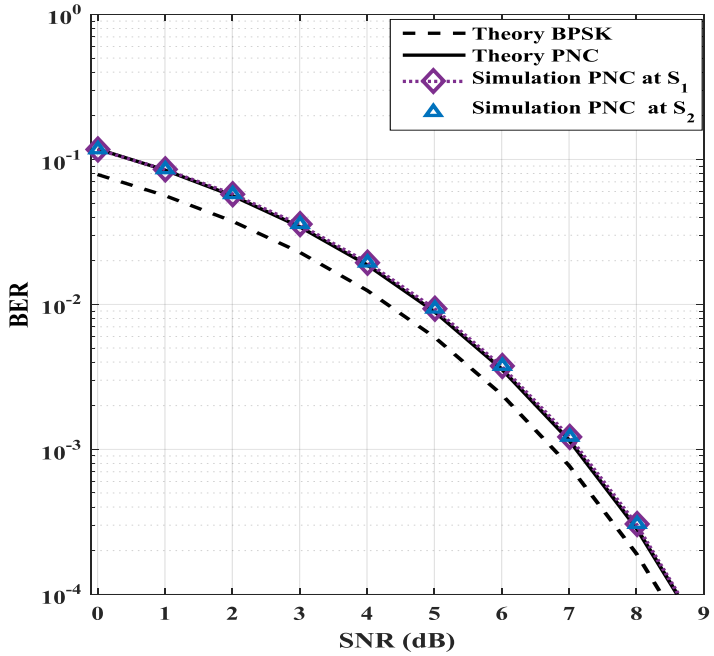

Figure 2.10 The predicated and simulated BER performance for PNC system against SNR alongside with predicated BPSK modulation over AWGN channel.

PNC system. It can be observed from the figures that while the error probability decreases exponentially with respect to SNR for AWGN channel, it decreases only inversely for the Rayleigh fading channel case. For instant, at a BER of 10^{-4}, SNR gains are 8.6, 8.8dB for

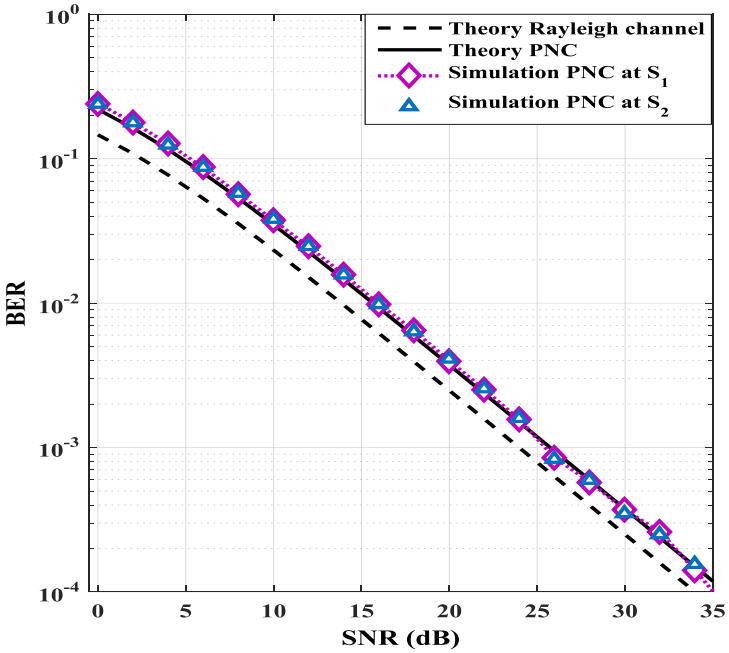

Figure 2.11 The predicated and simulated BER performance for PNC system against SNR alongside with predicated BPSK modulation over Rayleigh fading channel.

BPSK and PNC modulation over AWGN channel, respectively. The figures clarify that the BER of PNC system is slightly worse than that of the BPSK over AWGN as well as Rayleigh fading channels. However, even though the BER gets worse for PNC system, it will improve the performance of the system in terms of the overall throughput by reducing the number of transmissions time needed to successfully send packets along the end-to-end flow for TWRC. In Figure 2.12 the end-to-end simulation throughput for the store-and-forward, NC and PNC transmission mode techniques against the value of the SNR using (3.32), (3.33) and (3.35), respectively, are implemented. It can be observed from the figure that the throughput basically depends on the packet success rate, which in turn depends on BER performance. At the first glance to the figure, it is clear that the throughput increases for all the SNRs values for all the aforementioned transmission techniques. The lowest throughput of < 5 Mbps is observed for NC at 9.8dB of SNR, reaching the saturated level at 11.2dB of SNR. However, for the store-and-forward scheme, the lowest value for the throughput of < 1 Mbps at 9dB of SNR. Beyond this

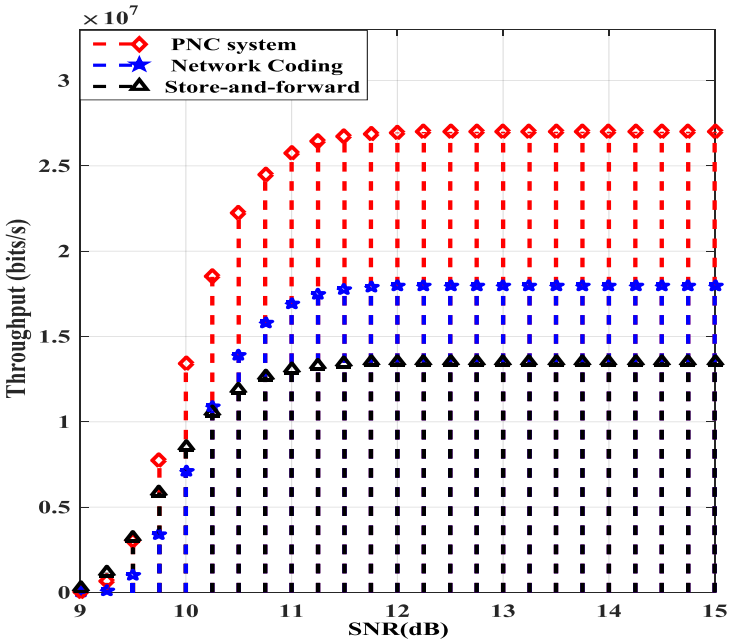

Figure 2.12 The throughput for the three type of the transmission mode (store-and-forward, NC and PNC) .

point, the throughput increases reaching the saturation level at 11dB of SNR. It can be noticed that under low SNR values, the throughput obtained under the store-and-forward transmission technique is slightly higher than that obtainable under the PNC technique. Conversely, under medium to high values of SNR, PNC shows much better throughput than the other two schemes, which achieving a throughput of more 10 Mbps at 10.5dB of SNR and reaching the saturation level of 27 Mbps at 11.5dB of SNR.

2.9 Summary

A brief description of cooperative communication system, TWRC system, and relaying strategies were discussed. This chapter presented an overview of fundamental concepts of the FSO technology, which used throughout the remainder of the thesis. The features of FSO technology that make it more viable compared with other existing RF was explained. The basic concept of FSO communication using the block diagram was illustrated. Different blocks of optical transmitter and receiver and its functions was detailed. Furthermore, the various noise sources were also outlined. In this chapter, the relationship between the TWRC and PNC was emphasized. Once a foundation of the transmitter and channel model concepts were presented, a relay of PNC system was introduced. It was shown how AWGN and Rayleigh fading channels could be applied on the PNC system of the two phases. A brief performance investigation of a PNC system with its throughput was existed. However, a comparative study between the PNC technique with store-and-forward and NC schemes in terms of the system throughput was carried out. It was shown that PNC technique had a better throughput than the other two schemes.

Chapter 3

PHYSICAL LAYER NETWORK CODING OVER FREE SPACE OPTICAL COMMUNICATION

Physical layer network coding is a promising technique used to improve the network throughput in a wireless TWRC. However, this technique has been widely investigated in the context of RF owing to its ability to accommodate the complete communication between two nodes in a minimum number of time slots. Therefore, in this chapter, the PNC technique is embraced for TWR-FSO communication link for the full utilization of network resources. This is done by employing a special demodulation-and-forward strategy to map the signal at the intermediate node rather than using traditional relay strategies. Such a scheme is particularly useful in situations where two FSO communication nodes wish to exchange their information but there is no direct link between them, thus, the intermediate node is essential. Compared with a traditional relay-assisted FSO link, the new scheme uses two phases in a round loop for a TWR transmissions link. The contribution of this chapter is to study the design of the TWR-

FSO communication system that employing PNC mapping at the intermediate node. The new model is referred to as TWR-FSO PNC. The software implementation of the new system is investigated and compared with P2P FSO link based on IM/DD with BPSK modulation. The performance results in terms of the BER show the effect of both path loss and atmospheric turbulence for the log-normal and gamma-gamma distributions combined with the pointing errors taking into account some parameters that can affect the system performance such as link distant, beam width and optical wavelength.

The rest of the chapter is organized as follow: Section 3.1 briefly describes the most popular mitigation techniques used in FSO system to alleviate the effects of the fading channels. Relay-assisted FSO transmission scheme based on network coding technique is demonstrated in Section 3.2. The role of the TWR-FSO link to combat turbulence-induced fading is highlighted in Section 3.3. Emphasis is placed on the explanation of the system model for TWR-FSO link based on PNC technique alongside with its channel characteristic in Section 3.4. Mathematical expressions for the error performance of log-normal distribution for FSO links is defined in Section 3.5, whereas the average bit error rate analysis over gamma-gamma model is outlined in Section 3.6. Our simulation results and discussion are presented in Section 3.7. Finally, the summary of this chapter is drawn in Section 3.8.

3.1 Mitigation Techniques in FSO Communications

RF communications are generally reliable and well understood, but cannot support emerging very high data rates unless they use a large portion of the precious radio spectrum. On the other hand, FSO communications offer enormous data rates, immunity to the electromagnetic interference, and provide a significant degree of secrecy, but

operate much more at the mercy of the environment [110]. Therefore, for many applications demanding higher data rates requires the FSO communication link to be more robust and seamless in order to provide a high QoS under all weather conditions. Despite the major advantage of FSO, its widespread deployment is hindered by the combined effects from numerous factors in which the greatest challenges are directly attributable to the turbulence and fog. The atmospheric channel is unpredictable and vulnerable to different weather conditions, such as scattering and absorption, hence, the requirement for FSO links to offer link availability under such environments. Additionally, FSO networks may also experience from pointing errors [94, 111, 112]. However, FSO links severely suffers from strong turbulence and is far away from satisfying the typical BER targets for FSO applications within the practical ranges of SNR. In order to maximize the overall system throughput and link availability, the FSO communication terminals must dynamically react to the changes taking place within the atmospheric environment. Therefore, various techniques have been investigated and proposed to combat the deterioration of signal quality as a result of the atmospheric conditions and the link misalignment, which are outlined in the following sections.

3.1.1 Coding techniques

Coding technique has been successfully implemented in wireless communications to provide error-free transmission. The forward error correction (FEC) schemes, which are used in RF communications technology, can be utilized in FSO systems to improve the reliability of communications system and to achieve the predetermined BER.

FEC is an effective channel coding technique to dispose the effect of FSO channel coming from the attenuation and the strong turbulence [113, 114]. These schemes realize error correction by adding redundant check bits into the input bits prior to transmission in order

to ensure that the transmitted bits can be automatically corrected and recovered those input and check bits at the receiver side [85]. H. G. Sandalidis investigated the error performance for FSO system with OOK using CC schemes [115]. The author considered various combinations of channels modelled assuming the existence of strong turbulence and pointing error effects. It was shown that, by using coding, lower BER and SNR values was obtained. For instant, to achieve a BER of 10^{-6}, 60dB of SNR was required. LDPC code was also prevalently utilized in FSO system and was performed reasonably well. A considerable amount of relevant research works in LDPC-FSO system were conducted by Ivan B. Djordjevic *et al.* [116-118]. In their work, they pointed out that coding was capable of enhancing the overall performance of the FSO and mitigation the channel effects. Likewise, they observed that the uncoded channel became practically useless as the turbulence strength and/or the propagation length increased.

However, FEC introduced a redundancy in the transmitted data stream, which imposes a requirement on the increased data rate, thus, accounting for increase in the bandwidth requirement. Moreover, there is a computational complexity and power consumption in implementing FEC for higher data rates in the design of a FSO system. Therefore, a trade-off in power efficiency and spectral efficiency needs to take into account when the error control coding is used [85].

3.1.2 Spatial diversity techniques

As FSO system operates at a rate of several gigabits per second, turbulence-induced fading can result in the loss of the large number of consecutive bits. Thus, the spatial diversity techniques provide an attractive alternative approach for fading compensation with their inherent redundancy. This technique has been well investigated in wireless RF communications and can be easily implemented in FSO systems, which was firstly

introduced in [119]. This method depends on multiple identical transmissions with uncorrelated paths from multiple transmitters and receivers [120], thus, allowing independently faded versions of the signal at the receiver, so that the effective level of scintillation and probability of fade can be reduced. Additionally, the possibility for temporal link blockage of the laser beams by obstructions (such as birds or other small object) is further decreased, therefore, it can support longer link distances through harsh weather conditions [121]. To mitigate the turbulence fading by exploiting the advantage of spatial diversity, multiple transmitters and receivers can be placed at the both ends of the FSO communications link. Consequently, spatial diversity includes single-input multiple-output (SIMO) systems, if a single transmit antenna is used, multiple-input single-output (MISO) systems, if only a single antenna is deployed at the receiver side, finally multiple-input multiple-output (MIMO) configurations when multiple transmit antennas and receive antennas are utilized [122-124]. With such a configuration, the transmitted information can go through different channels to arrive at the receiver. As long as one of the channels was strong enough, the receiver should be able to recover the transmitted information. In MIMO systems multiple sources and detectors are physically situated so that the channel fading experienced between source-detector pairs is statistically independent, and thus the diversity benefits can accrue from MIMO channel. Therefore, MIMO systems are a well-established technology, known for improved capacity, better diversity gain, and increased coverage area as compared to P2P FSO systems [125]. On other hand, SIMO and MISO FSO links have proposed as another approach with less complexity than MIMO. In [126], the performance of a SIMO link using OOK was investigated. It was shown that over longer link distances, where beam divergence was greater, multiple-receivers provide an improved performance over a

single detector. In [127], the error rate performance of SIMO, MISO and MIMO FSO systems were studied by employing IM/DD with OOK over independent and not necessarily identically distributed double generalized gamma turbulence channels. The numerical results demonstrated that spatial diversity schemes were significantly improved the system performance and bring impressive performance gains over P2P systems. For instance, at a BER of 10^{-5}, an improvement about 47.2dB of SNR was observed for SIMO FSO links with respect to the P2P transmission. However, diversity systems can get very complex because of issues such as optics alignment between the sources and the sink, signal synchronization and interference effects [17].

3.1.3 Cooperative diversity

The performance of FSO system depends strongly on the atmospheric conditions between the transmitter and the receiver, which can degrade the performance of the communications system mainly over link distances from a few meter to longer than 1 km [128]. Thus, the concept of cooperative diversity, where the mobile nodes cooperate with each other in order to exploit the benefits of spatial diversity without the need for using physical antenna arrays, was attracted a great interest. Additionally, this technique offers an efficient and low cost-effective compared to the MIMO systems in which it does not need to add an additional transmitter and receiver apertures.

In RF wireless communications, this method takes advantage of the broadcasting nature of RF transmissions, where a message transmitted from a source to a destination can be overheard by neighbouring nodes, which retransmit the same message to the destination. This redundancy messages allows the ultimate receivers to essentially average channel variations resulting from fading, shadowing, and other forms of interference, thus enhancing the quality of signal reception. The source nodes along with the neighbouring

nodes, which are willing to share their resources, create a virtual antenna array. An advantage of this virtual multiple-aperture system is that multiple paths are spatially separated from each other, thus ensuring independence of the corresponding fading channels.

Recently, research studies in FSO field illuminate on the performance evaluation of multihop communication systems under the atmospheric turbulence condition, where the source node communicates with the destination node via a number of relay nodes in a serial configuration [129]. Multihop transmission is a promising technique to achieve broader coverage, mitigate wireless channels impairment and have a number of advantages in terms of the capacity, deployment, and connectivity, while minimizing the need for a fixed infrastructure [129]. The cooperative FSO transmission was first proposed by A. S. Acampora and S. V. Krishnamurthy in [130]. Their work, however, has a networking perspective and did not address the physical layer aspects. J. Akella *et al*. analyzed the performance of the multihop FSO transmission in terms of the BER and compared their results with a single hop FSO system [131]. For instant, at a BER of 10^{-5}, there was a degradation about 35dB of SNR for a single hop FSO system when the weather condition changing from light fog - moderate to heavy fog. Their results showed that the decrease in the error rate was not significant after 8 hops for the given visibility distribution and the end-to-end link length. Thus, the error rate could be improved when the numbers of hops were increased at a cost of increased delay at each hop. However, both multihop transmission and cooperative diversity with AF and DF strategies were studied by M. Safari and M. Uysal [132].

3.1.4 One-way relay-assisted FSO scheme

Relay-assisted FSO communications consisted from three-node relaying network; one source, one relay, and one destination. It has been originally introduced for RF wireless systems by V. D. Meulen and C. Edward [28]. The concept of cooperative relay was considered in the context of FSO communications by C. Abou-Rjeily and A. Slim [133]. Their work presented numerical results for the symbol-error probability (SEP) performance of the FSO links with and without the cooperation relay. It was shown that the cooperative diversity was useful in enhancing the performance of FSO links. For instance, at a SEP of 10^{-3}, a SNR gain of 8dB was observed relative to non-cooperative systems when the source was far away from the relay and destination. Whereas M. Karimi and M. Nasiri-Kenari considered a relay-assisted FSO communication system that used optical AF strategy, which means that the relay passes the received signal through an optical amplifier and forwards it to the destination node [134]. They pointed out that the performance of the relay-assisted system was much better than that of the multihop transmitter especially when the source-destination link was long, or the attenuation factor was high. Whereas, M. R. Bhatnagar studied the differential in DF relay-assisted FSO over gamma-gamma channels. In his work, the simulated and analytical BER performance for relay-assisted FSO system with non-cooperative direct transmission for different propagation length was compared. The numerical result showed that the cooperative differential FSO system achieved significantly better performance and diversity gain than the direct transmission based FSO system. For example, at a BER of 10^{-5}, there was an improvement about 18dB of SNR compared to that of a direct FSO link [135]. R. Boluda-Ruiz *et al.* studied the impact of MISO relay-assisted FSO systems by using transmit laser selection scheme in source-relay link as well as relay-destination link

on the diversity order and derive novel approximate closed-form BER expressions over gamma-gamma fading channels with pointing errors [136]. However, cooperative communication based on DF and AF protocols can significantly improve the performance in FSO systems and was considered as a promising technique to mitigate the effect of fading.

3.2 Network Coding in FSO Communications

As optical networks operate at very high data rates, thus, any failure in the link may cause a severe loss of data, hence, providing resilient service against failures is a crucial issue for the wireless network. Recently, as a new form of cooperative relay technology, NC was introduced in wireless network because of its capability to increase the system throughput and combat link failures. This technique allows the intermediate nodes to perform arbitrary mathematical operations to combine the data received from different links and as a result of this calculation it may create one or more new packets to be forwarded to the adjoining nodes. The NC node at the recipient's location may then need to gather the data streams from multiple adjoining nodes, and calculate a linear combination of these streams, to recover the data intended for the recipient, thus, offering numerous advantages over the traditional routing schemes [43]. A. E. Kamal conducted the first research into applying NC to optical unicast protection [137]. He delivered some sufficient conditions for which static NC was provided in the multisource unicast case and showed that this basic approach offered many benefits over traditional protection schemes. Later, O. M. Al-Kofahi and A. E. Kamal also characterised networks admitting static network codes for multiple sources with a common sink and applied it to protection of wireless flows [138]. While most NC solutions assumed that the coding operations were performed at all nodes, it was often possible to achieve the NC advantage for

multicast by coding only at a subset of nodes. Therefore, R. C. Menendez and J. W. Gannet proposed a photonic bitwise XOR NC technique for fault-tolerant all-optical multicast networks [139]. They demonstrated that NC could lead to significant saving in the back-up resources for the multicast scenario protected against link failure by live back-up, which provided extremely fast recovery as only the receiver nodes needed to react after failures. The analysis presented that performance and efficiency of all-optical multicast networks could be very beneficial by using the basic XOR functionality and the information spreading could be achieved. Also, E. D. Manley *et al.* investigated the algorithmic problem for protected optical-layer multicast connections and corresponding infrastructural designs with all-optical network coding [140]. Compared with the existing techniques for multicast protection, they found a remarkable improvement when applying NC that found valid solutions even for large multicast group. Z. Xiaolin *et al.* designed a MISO relay-assisted FSO transmission scheme based on NC with IM/DD OOK modulation over gamma-gamma turbulence channels [141]. It was shown that the new scheme achieved a significant BER performance compared with non-cooperative direct transmission scheme. For instant, at a BER of 10^{-4}, there was an improvement about 16dB of SNR compared to that of direct FSO link.

3.3 Two-Way Relay FSO Link

There has been a growing interest in FSO communications as an alternate and more effective approach for transmitting data to the users due to the limitations of the RF spectrum and the ever increasing demand for high-speed communication. As the only essential requirement for an FSO system is the need for the LOS path between the transmitter and the receiver, the TWR-FSO solutions can be effectively used to establish communications between FSO nodes located over long link distances. The concept was

adopted from the well-known cooperative RF systems that were extensively investigated for more than a decade [142].

Recently, this technology has been adopted as a widely accepted solution for combatting turbulence-induced fading in FSO systems [143-145]. Y. Tang *et al.* proposed a TWR-FSO based on NC to establish the communication between the source-destination pair through multi-relay. The authors used NC technique to improve the robustness and persistence for data transmission in TWR optical system [143]. Compared with the traditional relay-assisted FSO, three transmission phases were enough to complete the data transmission in TWR-FSO. They investigated the impact of the turbulence level on their model over gamma-gamma distribution channels. The results outlined that the proposed scheme offered a significant BER performance improvement compared with that of the direct link transmission. For a BER of 10^{-3}, the SNR gain was 4dB compared with direct link. Whereas P. Parul *et al.* investigated the performance of a TWR-FSO system over weak turbulence regime in two transmission phases, where the signals received at the relay were decoded and XOR before being retransmitted to the destination [144]. They examined the performance and reliability of a TWR-FSO system in terms of the outage probability. The results established that the TWR-FSO scheme outperformed the direct FSO scheme and offered an improved performance even in harsh weather conditions. For example, the TWR-FSO link achieved a SNR gain of 3dB at an outage probability of 10^{-1} compared to a direct FSO link. This scheme was extended in [145] for TWR-FSO with coherent heterodyne detection, whereby the authors evaluated the performance of the system over an optical channel affected by both moderate-to-strong atmospheric turbulence induced scintillation and the pointing errors. It was observed from the results that a remarkable improvement in the outage performance was obtained for a

TWR-FSO link in comparison to the direct link. For instance, the TWR-FSO link achieved a SNR gain of 14dB at an outage probability of 10^{-3} in comparison to a direct FSO link.

3.4 TWR-FSO Link Based on PNC Technique

Hence, the TWR-FSO is a viable solution for establishing communications between two nodes that cannot have a direct link due to the larger link distances. Additionally, this scheme is spectrally efficient as it is only need two transmission time to complete data exchange. Through the observation of the relevant literatures, it is evident that a substantial number of analytical and simulation studies for TWR-FSO system have considered only the AF and DF schemes or applied the linear NC at RNs. The configuration of the FSO link generally is based on the LOS to point-to-point high speed transmission. Therefore, this research work considers the PNC technique at RN for TWR-FSO communication system when the path between the two communication nodes is unavailable. The communication between the two nodes is achieved with the aid of the RN, and therefore is referred to as the TWR-FSO PNC system for increased link

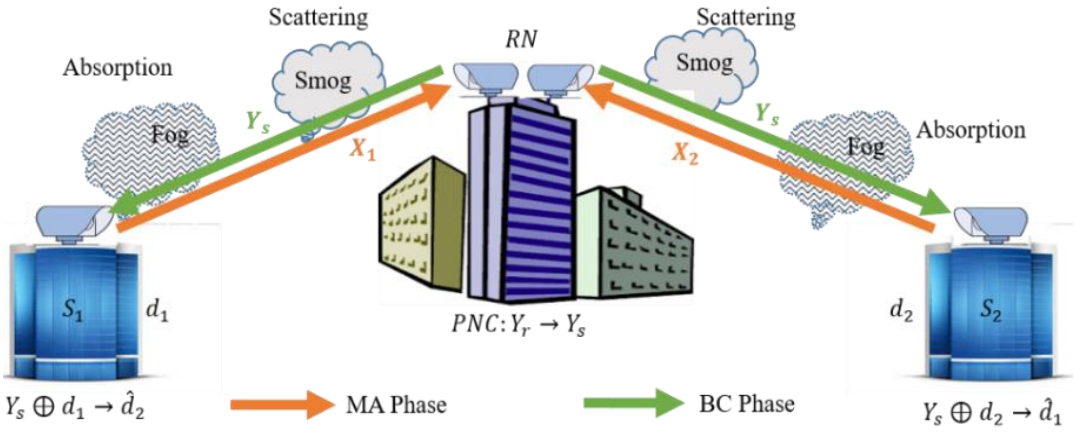

Figure 3.1 The block diagram of the proposed model TWR-FSO PNC, which consist from two transmission phases when there is no direct path between the two nodes transmitted during FSO channel.

reliability and the system throughput as shown in Figure 3.1. Similar to RF communication systems, the basic concept of TWR-FSO PNC communications is essentially comprised of an optical transmitter (data generation), a channel (media of transmission) and an optical receiver (processing of data). In the proposed system, the two nodes (S_1, S_2) swap their information with the help of the RN during only two transmission phases, MA and BC phases as depicted in Figure 3.1.

The following sub- sections introduce the full structure of the transmitter, RN and the receiver for the proposed model.

3.4.1 The transmitter model

The basic transmitter structure for the proposed model is shown in Figure 3.2. The main functionality of this block is to convert the electrical signal into the optical signal using LDs, which is then, propagates through the atmosphere channel to the receiver. The transmitter side consists of modulator, LD drive and transmit optics (lens, telescope) for each source node (S_1, S_2). The Modulator's purpose is to convert the information into the electrical signals with the required choice of modulation scheme.

In [146], the effect of the atmospheric turbulence using OOK and BPSK in FSO communications was investigated showing that the BER performance of BPSK outperformed the performance of the system employing OOK over turbulence-induced fading. Therefore, in our proposed scheme, the modulation scheme adopted is BPSK in which the information is encoded in the phase of the RF carrier, which offers higher immunity to the intensity fluctuation and requires no adaptive threshold [146]. Prior to modulating the laser irradiance, the input data $d_k(t)$ is modulated onto the RF signal using BPSK modulator. The k^{th}modulated signal can be presented as [146]:

$$m_k(t) = \sum_j g(t - jT_b)\cos\left(w_c(t) - \emptyset_j\right), \tag{3.1}$$

where $g(t)$ is a rectangular shaping pulse function, w_c is a carrier angular frequency, and $\emptyset$ is phase angular and equal to 0 or π depending on the binary one or zero being transmitted. Since the signal $m_k(t)$ is sinusoidal having both positive and negative values, a direct current (D.C.) bias level b_o is added to the electrical signal to ensure positive signal prior to the IM of the optical source. The IM optical signal can be expressed as [146]:

$$x_k(t) = P_t[1 + \zeta m_k(t)], \tag{3.2}$$

where P_t is the average transmitted optical power and ζ is the modulation index satisfying the condition $-1 \leq \zeta m_k \leq 1$ in order to avoid clipping due to the over-modulation [146]. An optical telescope is used to collimate and direct the optical beam into the channel for reception at the receiver in order to minimize the beam divergence [94, 111, 112]. Due to the atmospheric effects, the channel state of the FSO link is modelled as a stochastic process denoted by h as explained in detail in the next sub-section .

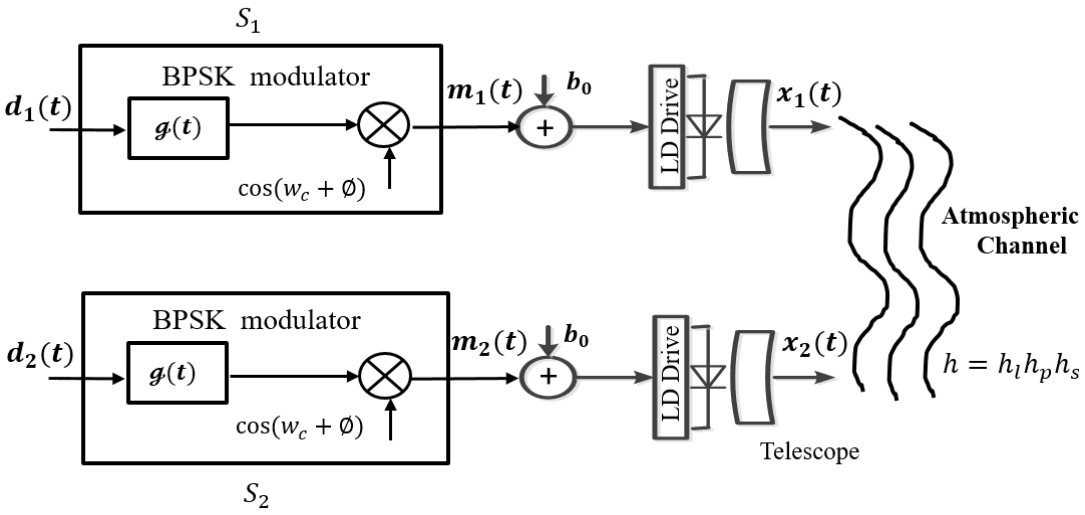

Figure 3.2 The transmitter structure for the proposed TWR-FSO PNC model.
The $d_k(t)$ and $x_k(t)$ denote the data information and the transmitted optical signal for the MA phase, respectively, through atmospheric channels indicate by h.

3.4.2 The channel characteristics

The optical beam traversing the turbulent atmosphere experiences random fading in its irradiance and phase. The state of atmospheric channel can be described as [147]:

$$h = h_l h_s h_p \,, \tag{3.3}$$

where h_l is the channel loss coefficient, h_s is a random variable representing the intensity fluctuation due to atmospheric turbulence, and h_p is the misalignment fading due to the pointing error loss. In the following sub-sections, the effect of each channel state with its mathematical expression is presented.

3.4.2.1 Atmospheric loss

The intensity of a propagating optical laser beam in FSO is limited by the attenuation (or extinction) of the optical beam wave, mainly due to the interaction with aerosol particles of different type composition within the earth's atmosphere, which include: carbon dioxide (CO_2), oxygen (O_2), nitrogen (N_2), Methane (CH_4), ozone (O_3), water vapour (H_2O), and other small particles generated by combustion, dust, debris and soil [148]. The atmospheric molecular concentration depends on the pressure and temperature that vary with weather, altitude, and geographical locations. In particular, the absorption process occurs as a result of heating of the atmosphere when some of the photons energies are converted into the kinetic energy of the particle's molecules, which are responsible for the heating of the earth atmosphere. Absorption varies as a function of the wavelength. On other hand, scattering results through photons collided with molecules, thus resulting in angular re-distribution of the optical field with and without wavelength modification. The types of scattering (i.e., Rayleigh scattering, Mie scattering, and geometric scattering) are determined by the size of the particular atmospheric particle with respect to the transmission wavelength [79, 110]. However, the atmospheric loss (or transmittance) is

considered as a fixed scaling factor over multiple fading states of the FSO channel and results from the combined deterministic effects of absorption and scattering. For a terrestrial FSO link transmitting an optical signal through the atmosphere, the received irradiance at a link distance L from the transmitter is related to the transmitted irradiance by Beer-Lambert's law as [92]:

$$\sigma = \frac{P_o}{P_t} = exp[-\delta(\lambda)L]\,, \tag{3.4}$$

where σ is the transmittance, $\delta(\lambda)$ represents the total attenuation/extinction coefficient of the atmosphere at wavelength λ and P_o is the received optical power. For clear and foggy weather conditions, the attenuation coefficient can be determined from the visibility data through Kim's model as [12, 149]:

$$\delta = \frac{3.91}{V}\left(\frac{\lambda}{550}\right)^{-q}, \tag{3.5}$$

where V is the visibility, and q being the particle size distribution coefficient, which is defined as [94]:

$$q = \begin{cases} 1.6 & V > 50\,\text{km} \\ 1.3 & 6\,\text{km} < V < 50\,\text{km} \\ 0.16V + 0.34 & 1\,\text{km} < V < 6\,\text{km} \\ V - 0.5 & 0.5\,\text{km} < V < 1\,\text{km} \\ 0 & V < 0.5\,\text{km} \end{cases}, \tag{3.6}$$

Absorption and scattering due to particulate matter may significantly attenuate the transmitted optical signal, while the wave-front quality of a signal-carrying laser beam transmitted through the atmosphere can be severely degraded, thus, causing intensity fading, increased BER, and random signal losses at the receiver.

3.4.2.2 Geometric loss

One of feature of FSO systems is the security resulting from the ability to transmit a very narrow optical beam. On the other hand, due to diffraction, the beam spreads out, thus, causing a beam divergence loss because the receiver aperture is only able to collect a fraction of the beam. Therefore, the geometrical spreading loss is simply the ratio of the surface area of the receive aperture to the surface area of the transmit beam at the receiver. Note that the transmit beams spread constantly with increasing range at a rate determined by the divergence angle θ_s (in milliradian (mrad)). Hence, the geometrical spreading loss depends primarily on the divergence angle, the path link, and the area of the receiver aperture and can be given by [97]:

$$G_{loss} = -20\ log\left[\frac{d_R}{d_T + \theta_s L}\right], \tag{3.7}$$

where d_T and d_R are the transmitter and the receiver aperture diameters, respectively. This loss is a fixed value for a specific FSO deployment scenario; it does not vary with time, unlike the loss due to rain attenuation, fog, haze or scintillation. Thus, the channel loss can be determined by combining the exponential Beer-Lambert law and the geometric loss formula as given by [150]:

$$h_l = \frac{{d_R}^2}{(d_T + \theta_s L)^2} exp(-\delta L)\ . \tag{3.8}$$

The simulated BER performance of P2P FSO system due to the different optical wavelengths using (3.5), which influence the optical signal propagation, is shown in Figure 3.3 (a and b) for weak and strong turbulence regimes, respectively, for $L = 1$ km under a clear weather condition at $V = 10$ km. It can be concluded from the figure that for a given link distance the total attenuation at a wavelength of 1550 nm is less than that at wavelengths of 650 and 850 nm, thus resulting improved BER performance. For

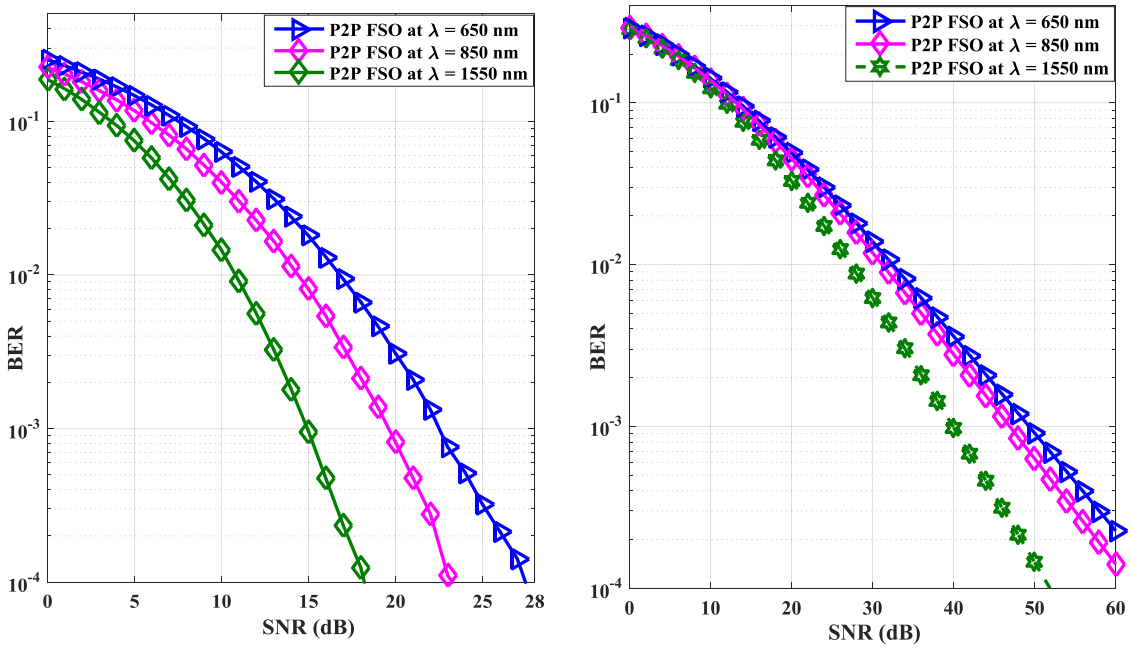

Figure 3.3 The simulated BER performance against the SNR for the P2P FSO system for a range of wavelengths over: (a) weak turbulence, and (b) strong turbulence for $L = 1$ km under clear weather condition at $V = 10$ km.

example, at a BER of 10^{-4}, the SNR gains are 11 and 6dB for the 1550 nm compared with 650 nm and 850 nm, respectively, for weak turbulence-induced fading. Whereas Figure 3.4 (a and b) shows the simulated BER performance for the P2P FSO system for a range of transmission spans for weak and strong turbulence regimes at $V = 10$ km and $\lambda = 1550$ nm, respectively. The results show that the BER performance for P2P FSO system deteriorates at $L = 3$ and 6 km compared with FSO system at $L = 1$ km. For instance, at a BER of 10^{-4} for $L = 1$ km, the SNR gains are 2 and 4dB compared to that of $L = 3$ and 6, respectively, over weak turbulence. Similarity, for the strong turbulence where the lower BER performance can be obtained at shorter link distance. For example, at a BER of 10^{-4} for $L = 1$ km, the SNR gains are gains are 5 and 10dB compared to that of $L = 3$ and 6, respectively. This is mainly because the absorption and scattering effects, due to the presence of atmospheric particles, attenuates the optical beams propagating at longer link distances.

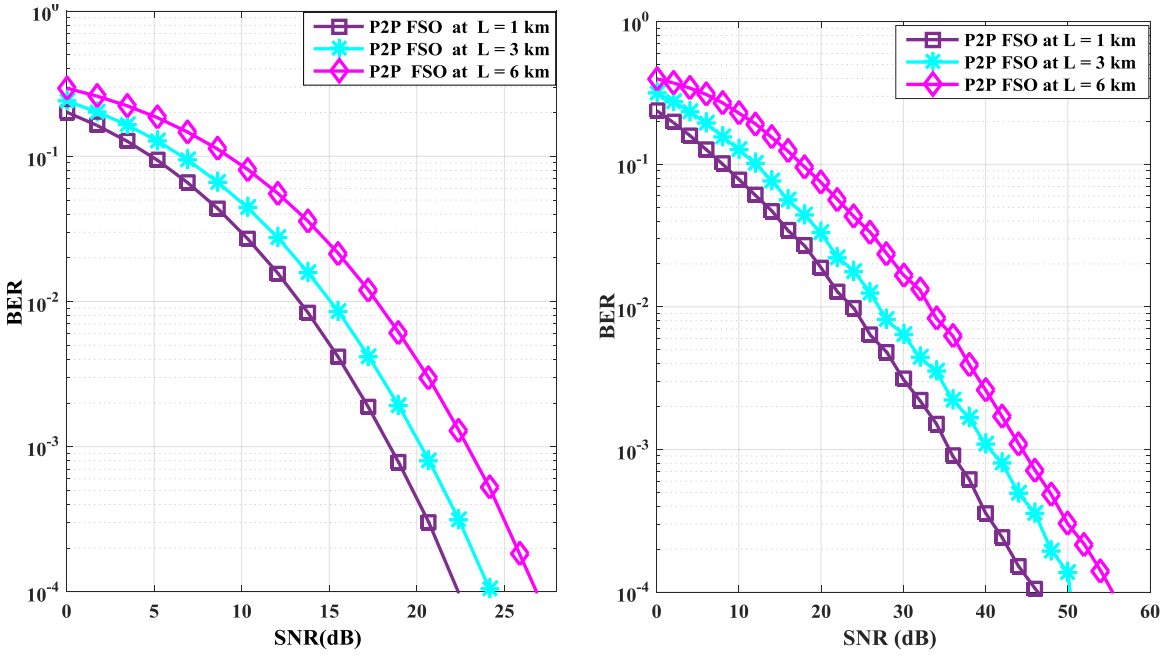

(a) (b)

Figure 3.4 The simulated BER performance against SNR for P2P FSO system for different propagation path over: (a) weak turbulence, and (b) strong turbulence under clear weather condition at $V = 10$ km and $\lambda = 1550$ nm.

3.4.2.3 Turbulent atmospheric channel

When a laser beam propagates through the atmosphere, the direction of an optical beam could be altered due to interaction with randomly varying distribution of the refractive index due to temperature, pressure, and wind variations along the optical propagation path. This is result in fluctuation of the received optical signal intensity variations referred to as the scintillation or turbulence-induced fading. Turbulence-induced fading is one of the main impairments affecting the operation of FSO communication systems [151, 152]. The scintillation index σ_I^2 can be defined as the normalized variance of irradiance fluctuations given by [95]:

$$\sigma_I^2 = \frac{\langle \mathbb{I}^2(r) \rangle}{\langle \mathbb{I}(r) \rangle^2} - 1 \,, \tag{3.9}$$

where $\mathbb{I}$ is the signal light intensity of the optical beam, r is the radial distance from the optical axis and $\langle . \rangle$ denotes ensemble averaging. Andrews and Phillips define the plane

wave scintillation index for a constant reflection index as Rytov variance σ_R^2, which can be described as [111]:

$$\sigma_R^2 = 1.23\, C_n^2 (2\pi/\lambda)^{7/6} L^{11/6}, \tag{3.10}$$

where C_n^2 is the reflection index, which its value varies with altitude. Typically, C_n^2 ranges from 10^{-12} (in m $^{-2/3}$) for strong turbulence to 10^{-17} (in $m^{-2/3}$) for weak turbulence [153]. The theoretical studies of the optical wave propagation are traditionally classified as belonging to either weak or strong fluctuation theories based on the value of the Rytov variance. Under weak fluctuation conditions, the scintillation index is approximately equal to Rytov variance [154]. Fundamentally, weak fluctuation conditions correspond to the scintillation index for the beam profile of less than unity $\sigma_R^2 \ll 1$. Strong fluctuations correspond to Rytov variance $\sigma_R^2 \gg 1$, whereas moderate fluctuations are designated as $\sigma_R^2 \sim 1$. To describe the atmospheric turbulence-induced irradiance and its effects on the optical beam propagation, theoretical and experimental studies have been carried out within the research community in order to develop tractable and reliable mathematical models for the irradiance PDF. As the observable atmospheric channel quantities such as aerosols, pressure, wind velocity and temperature are mixed and behave in a nonlinear fashion, the evaluation of the turbulence based on theory becomes rather complex [18]. Therefore, the atmospheric turbulence can be simply expressed and characterized based on the statistical distributions of PDF of the received irradiance and its related properties.

3.4.2.3.1 Log-normal turbulence model

When the optical beam propagates through the atmosphere, the phase aberrations cause intensity variations at the receiver. These effects are particularly important in laser communication systems, since these variations can cause fades and bit errors. Therefore, the turbulence effect can be characterized by the variance σ_x^2, often referred to as Rytov

parameter. For horizontal propagation with uniform C_n^2 profile, σ_x^2 can be calculated as [155]:

$$\sigma_x^2 = 0.30545\ C_n^2\ (2\pi/\lambda)^{7/6} L^{11/6}\ . \tag{3.11}$$

The fading channel coefficient, which models the channel from the transmitter aperture to the receiver aperture, is given by [155]:

$$h_s = \frac{\mathbb{I}}{\mathbb{I}_o} = exp(2\chi), \tag{3.12}$$

in which $\mathbb{I}$ is the signal light intensity at the receiver with turbulence, $\mathbb{I}_o$ is the signal light intensity at the transmitter with no turbulence, and χ denotes the Gaussian distributed log-amplitude fluctuation [125].

By the central limit theorem, the marginal distribution of the log-amplitude χ is Gaussian with mean μ_x and variance σ_x^2 given by [156]:

$$p(\chi) = \frac{1}{\sqrt{2\pi\sigma_x^2}}\ exp\left[\frac{(\chi - \mu_x)^2}{\sigma_x^2}\right], \tag{3.13}$$

After performing a transformation of random variable, $p(\mathbb{I}) = p(\chi)\left|\frac{d\chi}{d\mathbb{I}}\right|$, (3.13) takes on the familiar log-normal PDF described by [125]:

$$p(\mathbb{I}) = \frac{1}{\mathbb{I}\sqrt{2\pi\sigma_x^2}}\ exp\left[\frac{(\ln(\mathbb{I}/\mathbb{I}_o) - \mu_x)^2}{\sigma_x^2}\right]. \tag{3.14}$$

The probability of the mean μ_x is obtained by invoking the standard relation (3.15), which is valid for any real valued Gaussian random variable as [153]:

$$\mathbb{E}[\exp(az)] = exp\left(a\mathbb{E}[z] + \frac{a^2\sigma_z^2}{2}\right). \tag{3.15}$$

Substituting (3.15) into (3.12), result in:

$$\mathbb{E}[\mathbb{I}] = \mathbb{I}_o\ exp\left(\mu_x + \frac{\sigma_x^2}{2}\right). \tag{3.16}$$

Note that $\mathbb{E}[\mathbb{I}] = \mathbb{I}_o$, therefore:

$$exp\left(\mu_x + \frac{\sigma_x^2}{2}\right) = 1\,. \tag{3.17}$$

So that the mean μ_x is found as:

$$\mu_x = -\sigma_x^2/2\,. \tag{3.18}$$

Rytov variance follows directly from the variance, which depends upon the strength of the optical turbulence along the path. Therefore, for uniform horizontal path, the Rytov variance can be considered as $\sigma_R^2 = 4\sigma_x^2$. So that, the distribution of the light intensity fading induced by turbulence can be described as log-normal distribution as:

$$p(h_s) = \frac{1}{h_s\sqrt{2\pi\sigma_R^2}}\, exp\left[-\frac{(\ln(h_s) + \sigma_R^2/2)^2}{2\sigma_R^2}\right]. \tag{3.19}$$

Figure 3.5 demonstrates the log-normal PDF for different values of Rytov variance using (3.10). Note that, as the value of σ_R^2 increases, the distribution becomes more skewed with longer tails towards the infinity. This describes the extent of intensity fluctuations as the channel heterogeneity increases due to the atmospheric turbulence.

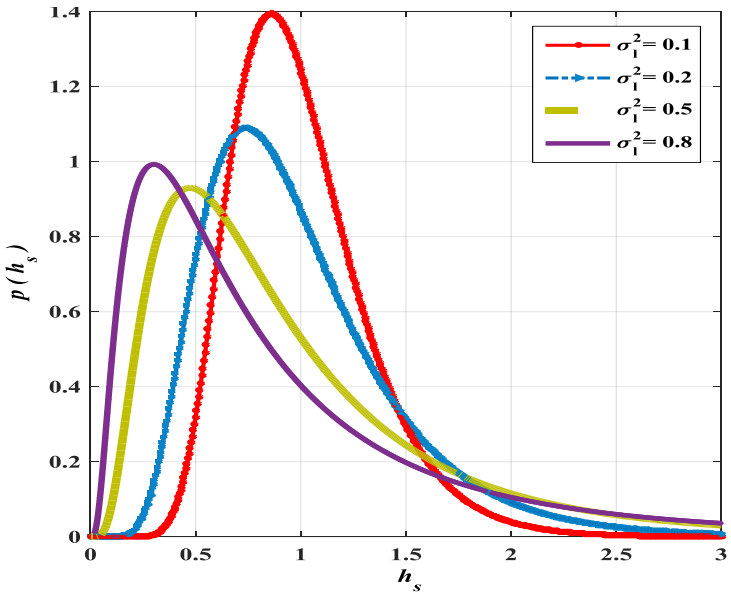

Figure 3.5 Log-normal PDF against turbulence channel state for different values of Rytov variance.

3.4.2.3.2 Gamma-gamma turbulence model

The gamma-gamma model was proposed in [154, 157], which has evolved from an assumed modulation process, whereby the fluctuation of light radiation traversing a turbulent atmosphere is comprised of small scale (scattering) and large scale (refraction) effects. The heuristic model treats the irradiance $\mathbb{I}$ of the received optical wave as a product of statistically independent random processes (h_x, h_y) [95]:

$$\mathbb{I} = h_x h_y \,, \tag{3.20}$$

where h_x and h_y arise from the large-scale and small-scale turbulent eddies, respectively, and it is suggested that both obey the gamma distribution [157]. Their PDFs are given by[95]:

$$p(h_x) = \frac{\alpha\ (\alpha h_x)^{\alpha-1}}{\Gamma(\alpha)} exp(-\alpha h_x) \qquad h_x > 0\ ;\ \alpha > 0\ . \tag{3.21}$$

$$p(h_y) = \frac{\beta\ (\beta h_y)^{\beta-1}}{\Gamma(\beta)} exp(-\beta h_y) \qquad h_y > 0\ ;\ \beta > 0\ . \tag{3.22}$$

By fixing h_x and using the change of variable $h_y = \mathbb{I}/h_x$, the conditional PDF given by (3.23) is obtain in which h_x is the (conditional) mean value of the $\mathbb{I}$ as [18]:

$$p(\mathbb{I}/h_x) = \frac{\beta\ (\beta\ \mathbb{I}/h_x)^{\beta-1}}{h_x \Gamma(\beta)} exp(-\beta\ \mathbb{I}/h_x) \qquad \mathbb{I} > 0\ . \tag{3.23}$$

To obtain the unconditional irradiance distribution, the conditional probability $p(\mathbb{I}/h_x)$, is averaged over the statistical distribution of h_x given by (3.21) as [18]:

$$\begin{aligned} p(\mathbb{I}) &= \int_0^\infty p(\mathbb{I}/h_x) p(h_x) dh_x \\ &= \frac{2(\alpha\beta)^{(\alpha+\beta)/2}}{\Gamma(\alpha)\Gamma(\beta)} \mathbb{I}^{((\alpha+\beta)/2)-1} K_{\alpha-\beta}\left(2\sqrt{\alpha\beta\mathbb{I}}\right) . \end{aligned} \tag{3.24a}$$

Relating the normalized intensity $\mathbb{I}$ of the optical laser beam to the instantaneous turbulent channel state h_s , the gamma-gamma distribution is given by [18, 95]:

$$p(h_s) = \frac{2(\alpha\beta)^{(\alpha+\beta)/2}}{\Gamma(\alpha)\Gamma(\beta)} h_s^{((\alpha+\beta)/2)-1} K_{\alpha-\beta}\left(2\sqrt{\alpha\beta h_s}\right), \quad (3.24b)$$

where α and β respectively represent the effective number of large and small scale eddies of the scattering process. $K_n(.)$ is the modified Bessel function of the 2nd kind of order n and $\Gamma(.)$represents the Gamma function. If the optical radiation at the receiver is assumed to be a plane wave, then the two parameters α and β that characterise the irradiance fluctuation PDF are related to the atmospheric conditions by [125]:

$$\alpha = \left\{ exp\left[\frac{0.49\,\sigma_R^2}{\left(1 + 1.11\,\sigma_R^{12/5}\right)^{7/6}} \right] - 1 \right\}^{-1}. \quad (3.25a)$$

$$\beta = \left\{ exp\left[\frac{0.51\,\sigma_R^2}{\left(1 + 0.69\,\sigma_R^{12/5}\right)^{5/6}} \right] - 1 \right\}^{-1}. \quad (3.25b)$$

Provided (3.24b) and (3.25), the gamma-gamma PDF is plotted against the irradiance for various value of α and β corresponding to the weak, moderate, and strong turbulence regimes shown in Figure 3.6. As the turbulence level increases from weak to strong, the distribution spreads out more and the tail becomes longer, which raises the extent of irradiance.

3.4.2.4 Pointing error

The misalignment fading model derived in [112] offers a tractable PDF for describing the behavior of the pointing error loss, which considers detector size, beam width and jitter variance. The model assumes a circular detection aperture of radius *r*, and a Gaussian spatial intensity profile of beam waist radius w_L on the receiver plane. In addition, both the vertical and horizontal displacement (sway) is considered independent and identically Gaussian distributed with variance σ_s^2. Pointing errors play an important role in channels

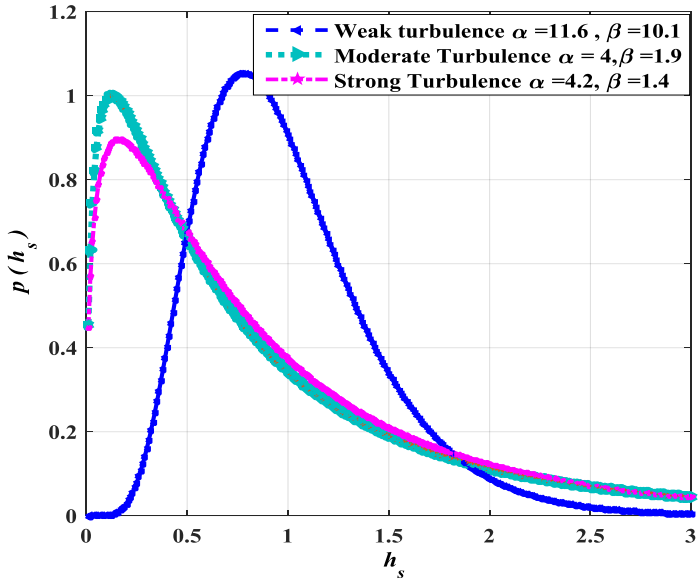

Figure 3.6 Gamma-gamma PDF across all of turbulence regimes, namely weak, moderate and strong for different value of α and β.

fading characteristics. Hence, the presence of the pointing error impairments is assumed for which the PDF of the irradiance h_p is given by [149, 158]:

$$p(h_p) = \frac{\xi^2}{A_o^{\xi^2}} h_p^{\xi^2-1}, \qquad 0 \le h_p \le A_o \tag{3.26}$$

where

$$\xi = \frac{w_{Leq}}{2\sigma_s}, \tag{3.27}$$

is the ratio between the equivalent beam radius w_{Leq} at the receiver and the pointing error displacement (jitter) standard deviation at the receiver; and

$$A_o = [\mathrm{erf}(v)]^2, \tag{3.28}$$

is the fraction of the collected power at a radial distance $r = 0$, where

$$w_{Leq}^2 = w_L^2 \frac{\sqrt{\pi}\mathrm{erf}(v)}{2v\exp(-v^2)}, \tag{3.29}$$

and

$$v = \sqrt{\pi/2}\, r/w_L, \tag{3.30}$$

where erf(.) denotes the error function and w_L/r identifies the beam width normalized by the radius of the receiver aperture. According to the result in [112], the pointing loss is given as:

$$h_p = A_o exp\left(-2\,\mathrm{r}^2/w_{Leq}^2\right), \qquad 0 \le h_p \le A_o \tag{3.31}$$

where the radial displacement r at the receiver is determined by a Rayleigh distribution and the PDF of the Rayleigh distribution can be described as:

$$p_{ra}(\mathrm{r}) = \frac{\mathrm{r}^2}{\sigma_s^2}\exp(-\mathrm{r}^2/2\sigma_s^2). \qquad \mathrm{r} > 0 \tag{3.32}$$

Figure 3.7 demonstrates the PDF of the Rayleigh distribution for different values of the jitter variance σ_s . It can be noticed that as the value of standard deviation increases, the distribution becomes more diffusion with longer tails towards the infinity.

Figure 3.8 (a and b) depicts the simulated BER performance against the SNR for a P2P FSO normalized beam width and a fixed normalized jitter for $L = 1$ km , $\lambda = 1550$ nm under clear weather condition at $V = 10$ km. The figure demonstrates that in P2P FSO, widen the beam width can mitigate the effects of pointing errors. Meanwhile, narrowing

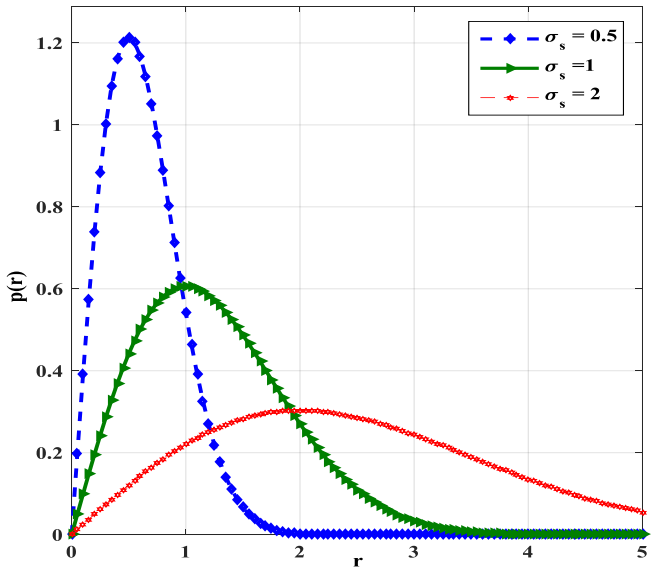

Figure 3.7 The PDF of the Rayleigh distribution with normalized r for different value of jitter variance.

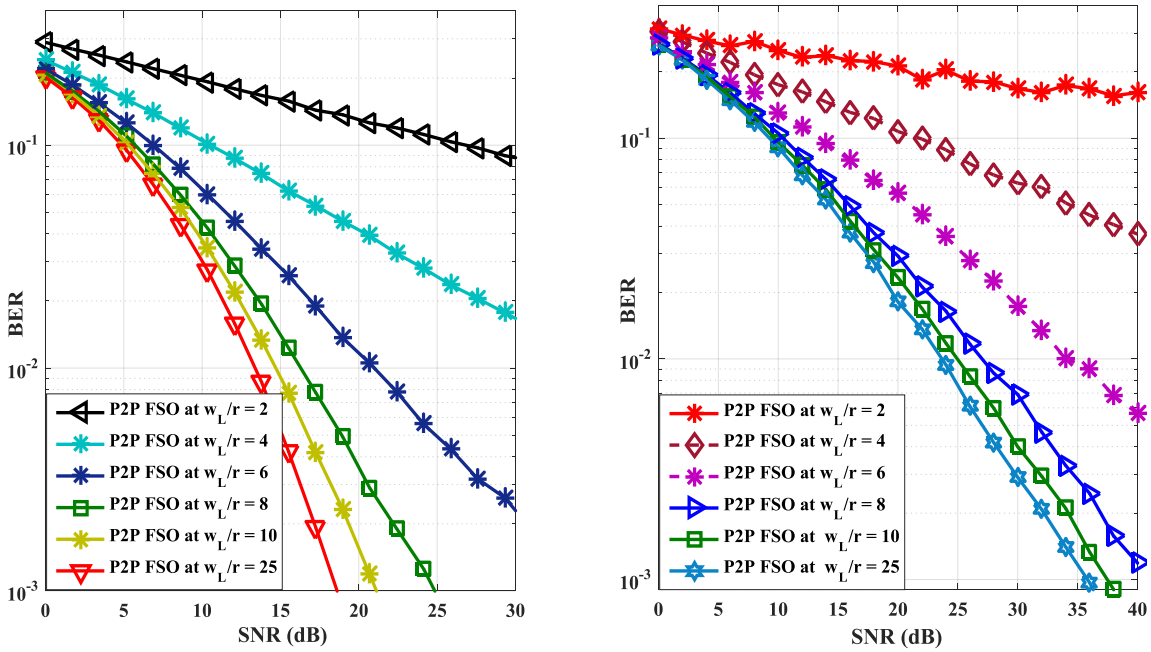

(a) (b)

Figure 3.8 The simulated BER performance against the SNR for P2P FSO system with a range of normalized beam width and a fixed normalized jitter of 3 under: (a) log-normal distribution, and (b) gamma-gamma distribution for $L = 1$ km, $\lambda = 1550$ nm under clear weather condition at $V = 10$ km.

the beam width will be contributing to the problem of misalignment and beam wandering. Therefore, the transceiver should be designed with optimum values of beam width to increase the robustness of the link in the presence of pointing errors. For instant, at a BER of 10^{-3}, about 22dB of SNR is achieved for $w_L/r = 10$. For the same BER, 18dB of SNR is required for $w_L/r = 25$ over weak turbulence.

3.4.2.5 Turbulence and misalignment fading combined model

The combined channel fading model of $h = h_l h_s h_p$ can be expressed as [112, 158]:

$$p_h(h) = \int p_{h|h_s}(h|h_s) p_{h_s}(h_s) dh_s \,, \tag{3.33}$$

where $p_{h|h_s}(h|h_s)$ is the conditional probability given a turbulence state h_s and can be expressed as [158]:

$$p_{h|h_s}(h|h_s) = \frac{1}{h_s h_l} p_{h_p}\left(\frac{h}{h_s h_l}\right)$$
$$= \frac{\xi^2}{A_o^{\xi^2}} \left(\frac{h}{h_s h_l}\right)^{\xi^2 - 1} . \qquad 0 \le h \le A_o h_s h_l \quad (3.34)$$

Substituting (3.34) into (3.33) gives as [95]:

$$p_h(h) = \frac{\xi^2}{(A_o h_l)^{\xi^2}} h^{\xi^2} \int_{h|A_o h_l}^{\infty} h_s^{-\xi^2} p_{h_s}(h_s) dh_s . \quad (3.35)$$

By combining (3.19) and (3.24b) in (3.35), the channel state distribution for the weak and strong turbulence regime are given by (3.36) and (3.37), respectively, [147]:

$$p(h_s)$$
$$= \frac{2\xi^2}{(A_o h_l)^{\xi^2}} h^{\xi^2 - 1} \int_{h|A_o h_s}^{\infty} \frac{1}{\sqrt{2\pi\sigma_R^2}} \frac{1}{h_s^{\xi^2+1}} exp\left[-\frac{(\ln(h_s) + \sigma_R^2/2)^2}{2\sigma_R^2}\right] dh_s . \quad (3.36)$$

and

$$p(h_s)$$
$$= \frac{2\xi^2(\alpha\beta)^{(\alpha+\beta)/2}}{(A_o h_l)^{\xi^2}\Gamma(\alpha)\Gamma(\beta)} h^{\xi^2 - 1} \int_{h|A_o h_s}^{\infty} h_s^{((\alpha+\beta)/2)-1-\xi^2} K_{\alpha-\beta}\left(2\sqrt{\alpha\beta h_s}\right) dh_s . \quad (3.37)$$

3.4.3 The relay model

The receiving side of the TWR-FSO PNC system at the RN, which essentially helps recover the transmitted data from the incident optical field, is composed from a two directional antennas each having one optical receiver directed to the corresponding user's nodes, a PD, and an amplifier followed by a PNC demodulator as it shown in Figure 3.9. The main advantage of the receiver telescope is to collect and focus the received optical beam towards the PD, which converts the optical energy into the electrical energy before the signal is amplified using a TIA. Following amplification, the original signal is recovered using a PNC demodulation process. This research work is based upon that both

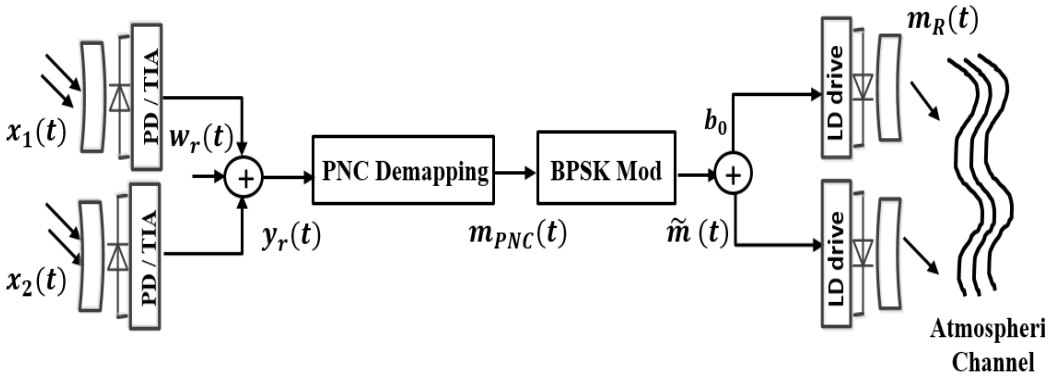

Figure 3.9 The structure of the RN for the TWR-FSO PNC system.
PNC mapping is performed on the superimposed received signal and the transmitted signal for the BC phase denotes by $m_R(t)$.

phase and amplitude synchronization of the signal from the two sources is achieved at the RN. The received electrical signal to the RN for the MA phase can be expressed as:

$$y_r(t) = P_t R \sum_{k=1}^{K} h_k x_k(t) + w_r(t), \tag{3.38}$$

where R is the detector responsivity (in Amper/Watt (A/W)), and w_r the noise arises from various sources, which include the shot noise caused by the signal itself or ambient light, the dark current noise, and the electrical thermal noise, and can be conveniently modelled as AWGN with zero mean and variance σ^2. For a slow-fading channel with BPSK signalling, the received electrical SNR is defined as [95]:

$$SNR(h_k) = \frac{(P_t R\, h_k)^2}{\sigma^2}. \tag{3.39}$$

SNR is fluctuating (i.e., an instantaneous value) due to the influence of h, which is chosen from the random ensemble according to the distribution. After down conversion, the PNC mapping is then employed on the superimposed electrical symbols to map them to the bits associated to the three-point constellation as it demonstrated in Chapter 2. However, PNC technique can avoid the effects of the interference by performing network coding arithmetic at the physical layer on the received signal. Through PNC mapping at RN, the

received electrical signal can be mapped to module-2 addition of the digital bit stream so that the interference becomes part of the arithmetic operation, which can be expressed as [104, 159]:

$$m_{PNC}(t) = \arg \min_{x_1 x_2 \in (1,-1)} |y_r(t) - (x_1 + x_2)| \,. \tag{3.40}$$

After PNC mapping the signal, BPSK modulation is carried out on the superimposed electrical signal, $\tilde{m}(t)$. Following that, a D.C bias level will be added to ensure the positive signal and then passes through LD to convert the signal from electrical to optical. Afterward, the optical signals are collected, collimated and directed by the transmitter telescope to propagate the signal over the atmospheric channel. The output optical signal at the LD transmitter of the RN can be expressed as [146]:

$$m_R(t) = P_t[1 + \zeta \tilde{m}(t)] \,. \tag{3.41}$$

The signal $m_R(t)$ in the BC phase contains the XOR received signal from the two sources and the target of the destination node to decode the desired signal from the broadcast signal with the help of the self-information provided.

3.4.4 The receiver model

The primary aim of optical detection in communication engineering is to recover the information embedded on the intensity, phase or frequency of the incoming optical radiation. The receiving side of the TWR-FSO PNC system is made up from a receiver telescope, a PD, and an amplifier followed by a suitable demodulator to recover the transmitted data from the incident optical field as it shown in Figure 3.10. As in RN, the telescope collects the incoming light and focuses it onto the PD, which then converts it to the electric current. The electrical signal amplified and is processed. Using DD at each receiver, the incoming optical signal for the BC phase convert into an electrical signal as:

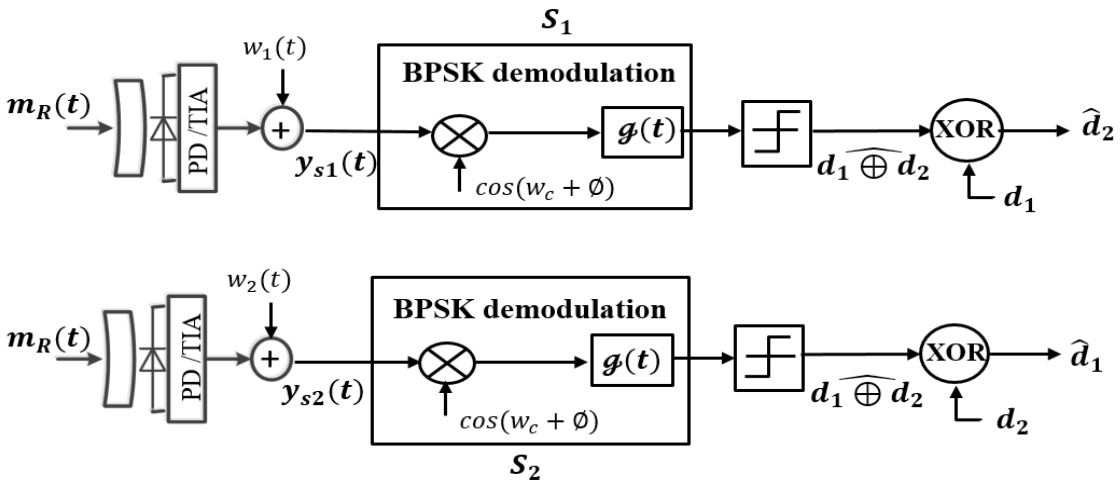

Figure 3.10 The receiver structure for the TWR-FSO PNC model.
The received signal from the BC phase represents by $y_{sk}(t)$ in which each node can get the desired information by performing XOR operation.

$$y_{sk}(t) = Rh_k m_R(t) + w_k(t), \tag{3.42}$$

where w_k and h_k are the AWGN and the channel state from the relay to the destination, respectively. The component of the signal is down converted by the reference signal. This is followed by a standard BPSK coherent detector to recover the transmitted symbol. The matched filters, which are part of the standard RF receiver, remove any out of unwanted signals from the demodulated signal and then pass it onto the decision circuit, which estimates the phase of the received signal and decides which symbol has been received. A decision device determines the nature of the signal according to its amplitude and arrival time. The quality of reception is measured by the probability of error, expressed in terms of BER. Thereafter, for our proposed system working under the PNC technique, the desired information at each destination node will be decoded from the estimated transmitted data with the help of its self-information by employing XOR operation, as shown in Figure 3.10, and can be modelled as:

$$\hat{d}_2 = d_1 \oplus (d_1 \widehat{\oplus} d_2) \ , \ \hat{d}_1 = d_2 \oplus (d_1 \widehat{\oplus} d_2) \, . \tag{3.43}$$

3.5 Average Bit Error Rate Over Log-normal Model

In this section, the BER analysis is presented in a clear but turbulent atmospheric channel. The turbulence-induced irradiance fluctuation considered in this section is based on the log-normal model. By employing a coherent demodulation, the symbol-by-symbol detection is carried out by multiplying the received signal by a locally generated RF signal of the same frequency and phase. Therefore, the coherent demodulator output $y_d(t)$ can be expressed as $y_d(t) = R\mathbb{I}\zeta g(t)[1 + \cos(2w_c(t))]/2$. For an IM/DD FSO communication link using BPSK modulation, the BER can be expressed as [96, 158]:

$$p_e = p(0)p(e|0) + p(1)p(e|1), \tag{3.44}$$

where $p(0)$ and $p(1)$ represent the probabilities of transmitting 0 and 1 bits, respectively, and $p(e|0)$ and $p(e|1)$ resemble the conditional bit error probabilities when the transmitted bit is 0 or 1, respectively. Assuming that the transmitter is sending 1's and 0's with equal probability, each has a probability equaled to 1/2, so that the probability of error conditioned on the received irradiance becomes:

$$p_e = 0.5p(e|0) + 0.5p(e|1) = 0.5\,[p(e|0) + p(e|1)]\,. \tag{3.45}$$

The marginal probabilities are given by [125]:

$$p(e|0) = \frac{1}{\sqrt{2\pi\sigma^2}} \int_0^\infty exp\left[\frac{(y_d(t) + R\mathbb{I}\zeta/2)^2}{\sigma^2}\right] dy_d(t)\,. \tag{3.46a}$$

$$p(e|1) = \frac{1}{\sqrt{2\pi\sigma^2}} \int_0^\infty exp\left[\frac{(y_d(t) - R\mathbb{I}\zeta/2)^2}{\sigma^2}\right] dy_d(t)\,. \tag{3.46b}$$

For BPSK signalling technique both binary symbols 1 and 0 are affected by the irradiance fluctuation, since the optical source is ON during the transmission of both symbols and the decision threshold level can hence be fixed at the zero mark [111]. Thus, this zero level cannot be affected by the irradiance fluctuation caused by the atmospheric

turbulence. Therefore, the BER conditioned on the received irradiance can be written as [125]:

$$p_e = \frac{1}{\sqrt{2\pi\sigma^2}} \int_0^{\infty} exp\left[\frac{-(y_d(t) + R\mathbb{I}\zeta/2)^2}{\sigma^2}\right] dy_d(t)$$
$$= 0.5\, erfc\left(\sqrt{\psi(\mathbb{I})}\right) = Q\left(\sqrt{\psi(\mathbb{I})}\right). \quad (3.47)$$

The unconditional probability, P_{uncon}, is obtained by averaging BER over the PDF of h_s for log-normal to obtain the following [125, 160]:

$$P_{uncon} = \int_0^{\infty} p_e\, p(h_s) dh_s$$
$$= \int_0^{\infty} Q\left(\sqrt{\psi(h_s)}\right) \frac{1}{h_s\sqrt{2\pi\sigma_R^2}} exp\left[-\frac{(\ln(h_s) + \sigma_R^2/2)^2}{2\sigma_R^2}\right] dh_s . \quad (3.48)$$

According to [160], this integral cannot be evaluated in terms of elementary functions where it can be constructed using only a finite combination of constant functions, exponential, and logarithmic operations. Hence, using the numerical integration could result in truncating its upper limit. In addition, the evaluation of this equation is difficult because of the presence of Q-function in the lower limit of the Gaussian Q-function integral [160]. Consequently, a closed form solution of (3.48) does not exist, which is defined in [161] that's an equation said to be a closed-form solution if it solves a given problem in terms of elementary functions. Therefore, an alternative form of the Q-function will be used, which is given by [125]:

$$Q(x) = \frac{1}{\pi} \int_0^{\pi/2} exp\left(\frac{-\varepsilon^2 x}{2\sin^2\theta}\right) d\theta , \qquad x > 0 \quad (3.49)$$

where ε is a constant. By making a change of variable, $x = \frac{\ln(h)+\sigma_R^2}{\sqrt{2}\sigma_R}$ in (3.48) and substitution (3.49) in (3.48) will result in:

$$P_{uncon} = \frac{1}{\pi} \int_0^{\pi/2} \left\{\frac{1}{\sqrt{\pi}} \int_{-\infty}^{\infty} exp\left[\frac{-\varepsilon^2\left(\exp(\sqrt{2}\sigma_R x_i - \sigma_R^2/2)\right)}{2\sin^2\theta}\right] e^{-x^2} dx\right\} d\theta . \quad (3.50)$$

The inner integral can be efficiently computed using a Gauss–Hermit quadrature integration that is [160]:

$$\int_{-\infty}^{\infty} f(x)\, e^{-x^2} dx \cong \sum_{i=1}^{\mathrm{z}} \mathbb{w}_i\, f(\mathbb{x}_i)\,, \tag{3.51}$$

where $(\mathbb{w}_i)_{i=1}^{\mathrm{z}}$ and $(\mathbb{x}_i)_{i=1}^{\mathrm{z}}$ are weight factors and the zeros of an z^{th} order Hermit polynomial, $H_{e\mathrm{z}}(\mathbb{x})$[162]. By combining (3.50) and (3.51), the unconditional PDF given by (3.48) can be reduced to the following [163]:

$$\begin{aligned} P_{uncon} &= \frac{1}{\pi}\int_0^{\pi/2} \frac{1}{\sqrt{\pi}} \sum_{i=0}^{\mathrm{z}} \mathbb{w}_i exp\left[\frac{-\varepsilon^2\left(\exp(\sqrt{2}\sigma_R \mathbb{x}_i - \sigma_R^2/2)\right)}{2\sin^2\theta}\right] d\theta \\ &= \frac{1}{\sqrt{\pi}} \sum_{i=0}^{\mathrm{z}} \mathbb{w}_i Q\left[\varepsilon \exp(\sqrt{2}\sigma_R \mathbb{x}_i - \sigma_R^2/2)\right]. \end{aligned} \tag{3.52}$$

In [163], it was shown that the BER performance against SNR was excellent agreement between (3.48) and (3.52), however, the Gauss–Hermit quadrature integration is preferred for its compactness and relative simplicity. Figure 3.11 presents the simulation result for the error probability of the P2P FSO link in terms of the SNR under the clear weather

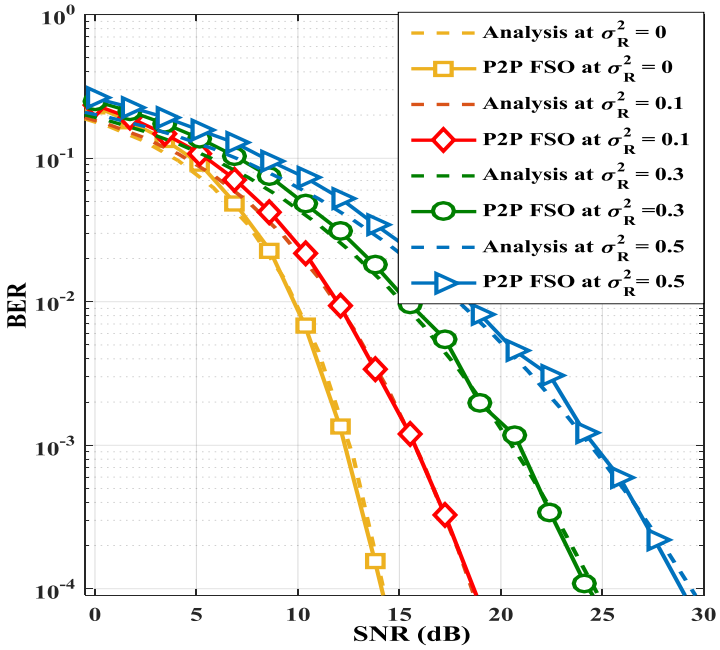

Figure 3.11 The analysis and simulated BER performance against SNR for P2P FSO communication system and Gauss-hermit approach for $\mathrm{z} = 20$ in a weak turbulence channel for different value of Rytov variance.

condition $V = 10$ km at $L = 1$ km for a variety of log variance irradiance. The analysis error performance of FSO in a log-normal channel, obtained from (3.52), is shown as a function of the SNR. This analysis achieved for 20th order Hermit polynomial [125]. It can be noticed that the performance of the FSO system is increased as the strength of the fading increased from 0 to 0.5. For instant, at a BER of 10^{-4}, the SNR gain is 18dB for scintillation strength $\sigma_R^2 = 0.1$, which increases to 29dB of SNR for scintillation strength $\sigma_R^2 = 0.5$. This denotes the extent of fluctuation of the irradiance as the channel inhomogeneity increases.

3.6 Average Bit Error Rate over Gamma-Gamma

For BPSK signaled commination system, the conditional BER probability depends on the fluctuation intensity and can be expressed as in (3.47). However, in order to provide a closed-form solution for (3.37), $K_\alpha(.)$ can be written in terms of the Meijer's G-function as [162]:

$$K_\alpha\left(2\sqrt{x}\right) = \frac{1}{2} G_{0,2}^{2,0}\left(x\middle|\frac{\alpha}{2}, \frac{-\alpha}{2}\right). \tag{3.53}$$

So (3.37) can be simplified as[164]:

$$p_h(h) = \frac{(\alpha\beta)\xi^2}{A_o h_l \Gamma(\alpha)\Gamma(\beta)} G_{1,3}^{3,0}\left(\frac{\alpha\beta h}{A_o h_l}\middle|_{\xi^2 - 1, \alpha - 1, \beta - 1}^{\xi^2}\right). \tag{3.54}$$

For gamma-gamma channel with the pointing error, the average BER can be realized by averaging (3.54) over the PDF of h. Therefore, the unconditional probability is obtained as:

$$P_{uncon} = \frac{(\alpha\beta)\xi^2}{A_o h_l \Gamma(\alpha)\Gamma(\beta)} \int_0^\infty p_e \; G_{1,3}^{3,0}\left(\frac{\alpha\beta h_s}{A_o h_l}\middle|_{\xi^2 - 1, \alpha - 1, \beta - 1}^{\xi^2}\right) dh_s. \tag{3.55}$$

By using the expression the erfc (.) as Meijer G function [160]:

$$erfc(\sqrt{x}) = \frac{1}{\sqrt{x}} G_{1,2}^{2,0}\left(x \middle| \begin{matrix} 1 \\ 0, \frac{1}{2} \end{matrix}\right). \tag{3.56}$$

The unconditional PDF in terms of ψ for (3.55) can be expressed as [164]:

$$P_{uncon} = \frac{2^{(\alpha+\beta-4)}\xi^2}{\sqrt{\pi^3}\Gamma(\alpha)\Gamma(\beta)} G_{7,4}^{2,6}\left(\frac{\psi(A_o h_l)^2}{(\alpha\beta\sigma)^2} \middle| \begin{matrix} \frac{1-\xi^2}{2}, \frac{2-\xi^2}{2}, \frac{1-\alpha}{2}, \frac{2-\alpha}{2}, \frac{1-\beta}{2}, \frac{2-\beta}{2}, 1 \\ 0, \frac{1}{2}, \frac{-\xi^2}{2}, \frac{1-\xi^2}{2} \end{matrix}\right). \tag{3.57}$$

Figure 3.12 presents the simulated BER for P2P FSO link under gamma-gamma turbulence model given by (3.24b). This model is valid for all turbulence scenarios from weak to strong regimes with the values of α and β at any given regime, which can be obtained from (3.25). While the analysis BER is achieved by using (3.57). The simulated BER performance is obtained under clear weather condition at $L = 1$ km with the pointing error characterized by a normalized beam width $w_L/r = 25$ and a normalized

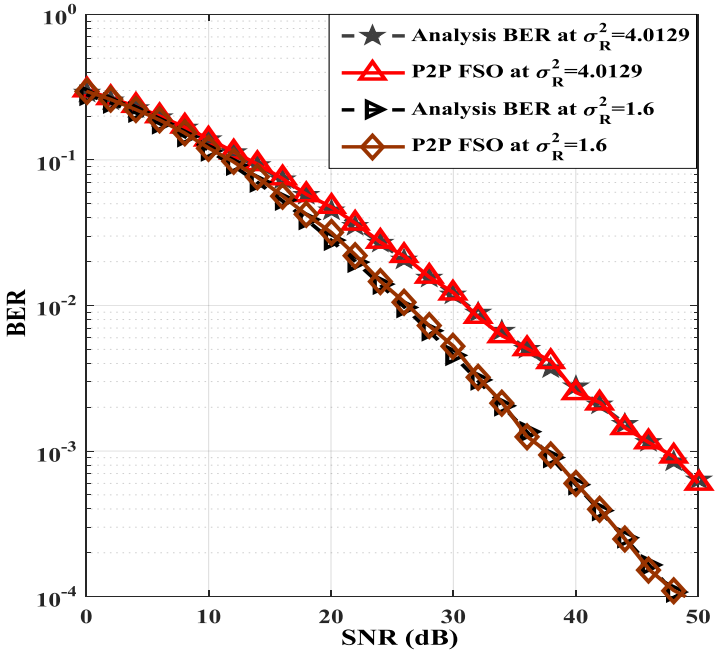

Figure 3.12 The analysis and simulated BER performance against SNR for P2P FSO across all of turbulence regimes (moderate to strong) with pointing error for $L = 1$ km under clear weather conditions at $V = 10$ km.

jitter value of $\sigma_s/r = 3$ under clear weather conditions $V = 10$ km. It can be noticed that the simulated BER performance degrades as the strength of the turbulence growth.

For example, at a BER of 10^{-3}, the SNR gains are 38dB and 48dB for P2P FSO when the strength of turbulence in creases from 1.6 to 4.0129, respectively.

3.7 Simulation Results

The link performance of the TWR-FSO PNC wireless optical communication is affected by the channel condition. Therefore, this section presents some case studies for the design of the proposed system under clear weather environments that contribute to the overall link performance such as link distance, pointing error effects, turbulence and laser wavelength. Thereafter, a comparison between the performances of the proposed system and the P2P FSO system is carried out. We consider the proposed system under log-normal and gamma-gamma channel models in which the strength of the irradiance fluctuation is characterized by σ_R^2. However, the simulation parameters considered in the BER analysis are defined in Table 3.1 [95, 112, 125]. The choice of the operating wavelength in FSO communication is important design parameter as it affects link

Table 3.1 Simulation parameters of the TWR-FSO PNC and P2P FSO systems.

Parameter	**Typical value**
Laser wavelength	$\lambda = 650,850,1550$ nm
Average transmitted optical power	$P_t = 14$ mW
Photodetector responsivity	$R = 0.5$ A/W
Receiver diameter	$d_R = 8$ cm
Transmitter diameter	$d_T = 2.5$ cm
Beam divergence	$\theta_s = 1.2$ mrad
Normalized beam width	$w_L/r = 2,4,6,8,10,20$
Pointing error jitter standard deviation	$\sigma_s = 30$ cm
Reflection index for weak	$C_n^2 = 0.75 \times 10^{-14}$ m$^{-2/3}$
Reflection index for strong	$C_n^2 = 1 \times 10^{-13}$ m$^{-2/3}$
Visibility (clear weather condition)	V =10 km
Rytov variance for weak	$\sigma_R^2 = 0.1,0.2,0.3,0.5$
Rytov variance for moderate to strong	σ_R^2 =1.6,4.0129
Link distance	$L = 1,2,3,6,12$ km

performance and detector sensitivity of the FSO system. Since it is not possible to change the physics of the atmosphere, the wavelengths used in the system are basically chosen to coincide with the atmospheric transmission windows. Figure 3.13 (a and b) demonstrates the impact of wavelength on the performance of the proposed system. It illustrates the simulated BER performance of the system in terms of the SNR under the clear weather condition for L = 2 km and three different values of wavelengths 650, 850, and 1550 nm. It is observed that TWR-FSO PNC links operating at $\lambda = 1550$ nm can achieve lower BER performance for the same value of σ_R^2 compared to lower wavelengths. For instance, for log-normal model and at a BER of 10^{-4}, an achievable SNR of 29dB is attainable at λ of 650 nm, while a much lower SNR values of 27.9 and 25dB are achieved at λ of 850 and 1550 nm, respectively. Similarity, for the gamma-gamma model where the lower BER performance can be obtained for $\lambda = 1550$ nm. Thus, the assertion that operation at 1550 nm is considerably more robust. Therefore, this implies that the adopted

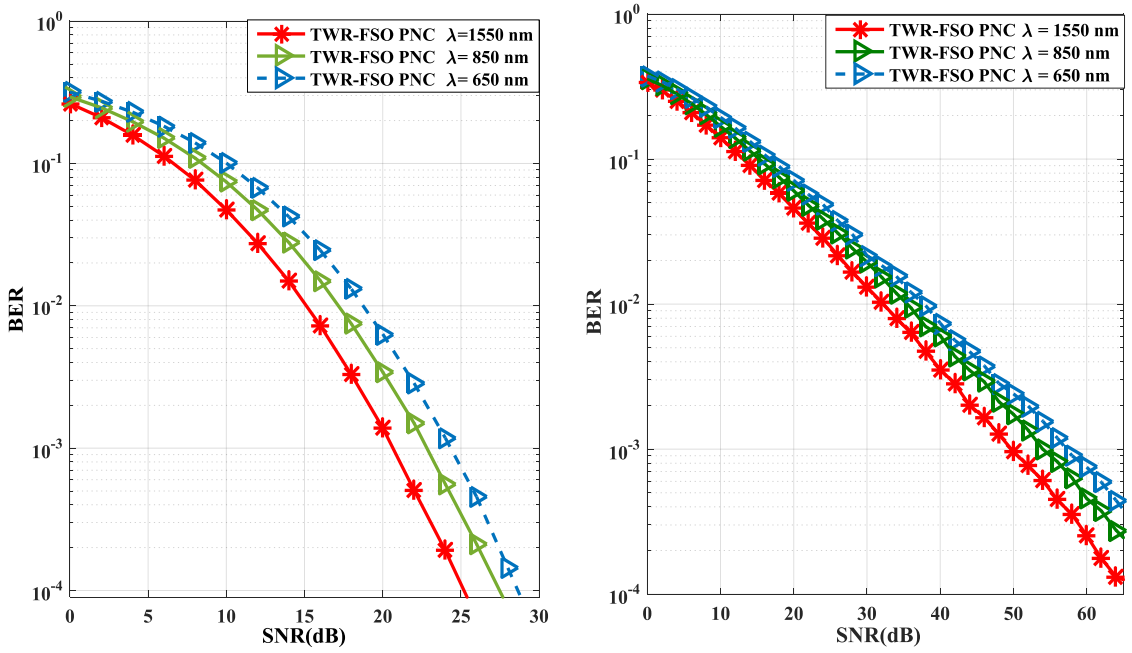

(a) (b)

Figure 3.13 The simulated BER performance against SNR for TWR-FSO PNC for different value of wavelength over: (a) weak turbulence, and (b) moderate turbulence channel with pointing error for $L = 2$ km under clear weather conditions at $V = 10$ km.

wavelength is an important link design criterion for maximizing the transmission rate with low error probability. On other hand, the link distance L, which represents the distance between the two sources and relay, is another parameter that affects the performance of the proposed system. The impact of link distance is depicted in Figure 3.14 (a and b). It shows the simulated BER performance against the SNR for TWR-FSO PNC system for $L = 2, 3, 6, \text{and } 12$ km under high visibility for the weak and moderate turbulence scenarios. At $L = 12$ km, it is observed that higher SNR values of 34 dB and 57 dB for λ of 1550 nm are desirable at a BER of 10^{-4} over weak and moderate turbulence fading, respectively. While for $L = 6$ km lower values of SNR of 27 and 52dB are attained for the weak and moderate turbulence regimes at the same BER, respectively, as shown in Figure 3.14 (a and b). This is expected, since the optical beams are less susceptible to the attenuation caused by absorption and scattering for a shorter propagation link, which is indicated by a higher value of $h_l = 0.8160$. Whereas, the

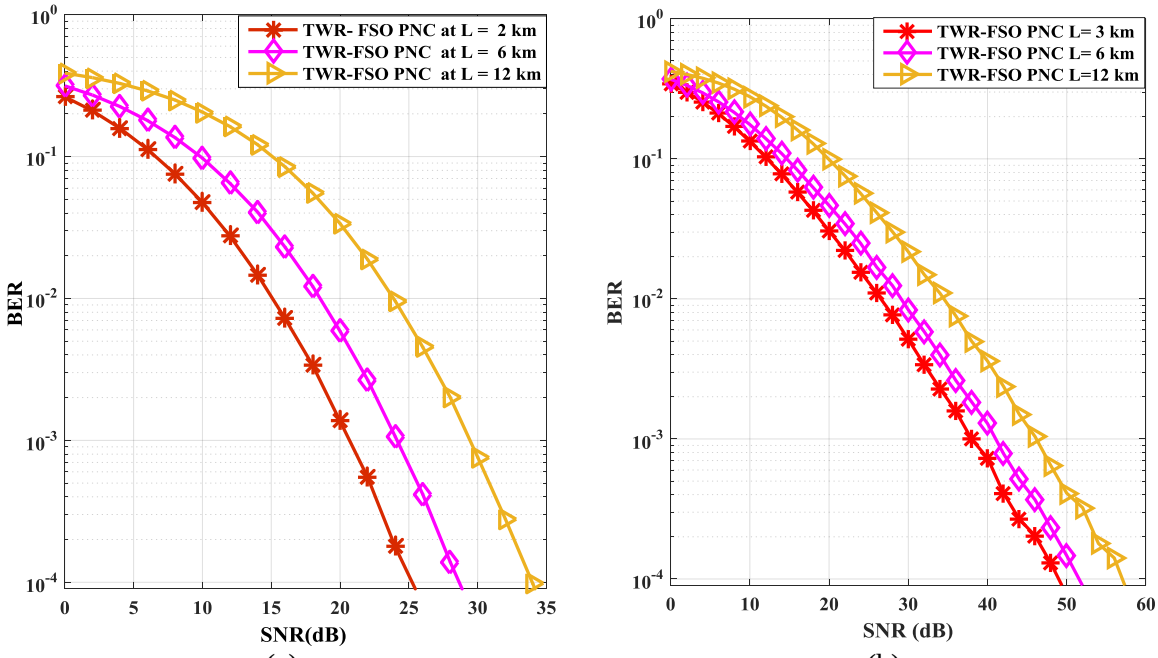

(a) (b)

Figure 3.14 The simulated BER performance against SNR for TWR-FSO PNC for different link range (2, 3, 6, 12) km under: (a) weak, and (b) moderate atmosphere channel with pointing error under clear weather condition at $V = 10$ km.

optical beams propagating over longer link distances can be attenuated and absorbed due to the presence of atmospheric particles. Next, the impact of the normalized beam width on the BER performance for the TWR-FSO PNC in the presence of the atmospheric turbulence and the pointing error is investigated. The weak and moderate turbulence regimes denotes by $\sigma_R^2 = 0.3$ and 1.6, respectively, are also considered for $V = 10$ km as shown in Figure 3.15. To achieve a BER of 10^{-2} with a normalized beam width $w_L/r = 8$, about 18dB of SNR is required, while with a normalized beam width $w_L/r = 25$, about 25dB of SNR is needed to achieve a BER of 10^{-4}, as shown in Figure 3.15 (a). Similarity, the performance degradation is observed with decreasing the value of the normalized beam width for $\sigma_R^2 = 1.6$ at $L = 2$ km under clear weather condition, as shown in Figure 3.15 (b). For instead, at a BER of 10^{-4}, the SNR gains is 48dB for $w_L/r = 25$, while at BER of 10^{-3} an achievable SNR of 54dB is attainable at $w_L/r = 10$. It is obvious that the FSO channel performance in terms of the BER is susceptible to the

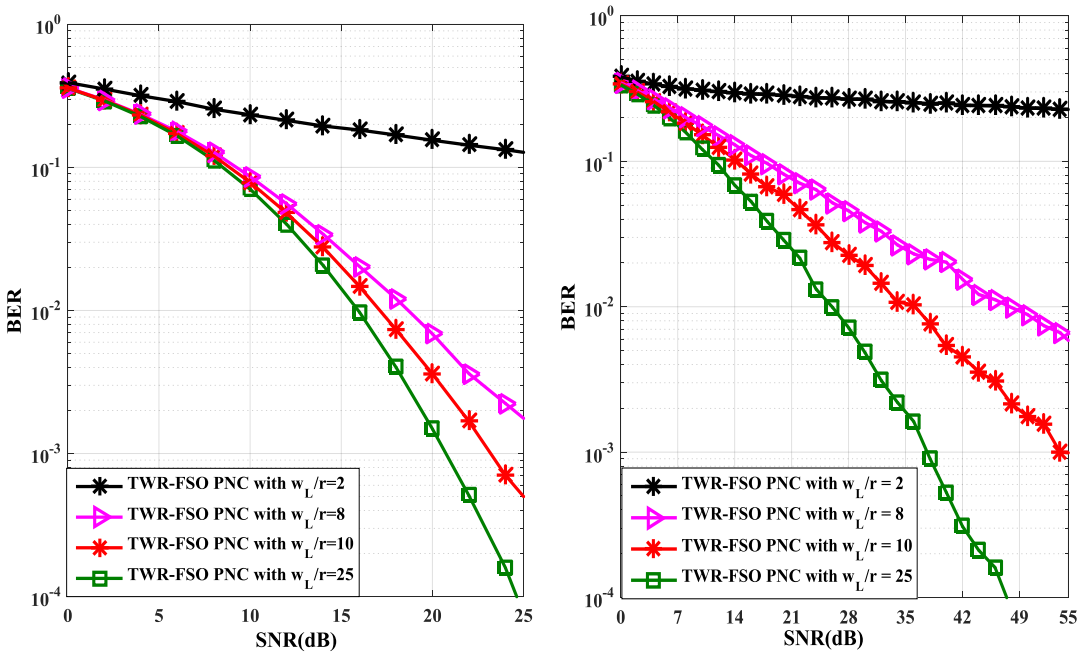

(a) (b)

Figure 3.15 The simulated BER performance against the SNR for the TWR-FSO PNC system for different normalized beam width (2, 8, 10, 25) and fixed jitter value for clear weather condition and $L = 2$ km over: (a) weak turbulence, and (b) moderate turbulence.

adverse effects of turbulence-induced scintillations and pointing error, in which this phenomenon is particularly prevalent in the moderate turbulence case. This observation can be explained by the fact that the optical channel fading characteristics have altered the propagation properties of the laser beam, thereby concluding that a better BER can be achieved through proper selection beam width for a known wavelength. However, by taking the above observations into our consideration, the BER performance of the TWR-FSO PNC and the P2P FSO system is investigated. Figure 3.16 (a and b) presents the simulated BER as a function of the SNR for different levels of atmospheric turbulence based on the log-normal and gamma-gamma distribution models showing the performance of the TWR-FSO PNC with P2P FSO system. As an example, to achieve a BER of 10^{-4} with a fading strength of $\sigma_R^2 = 0.3$, a SNR gains about 25.5 dB is required for TWR-FSO PNC system. This value increases to 30dB of SNR as the fading strength increases to $\sigma_R^2 = 0.5$. While for P2P FSO system, the SNR values vary from 24.5dB to

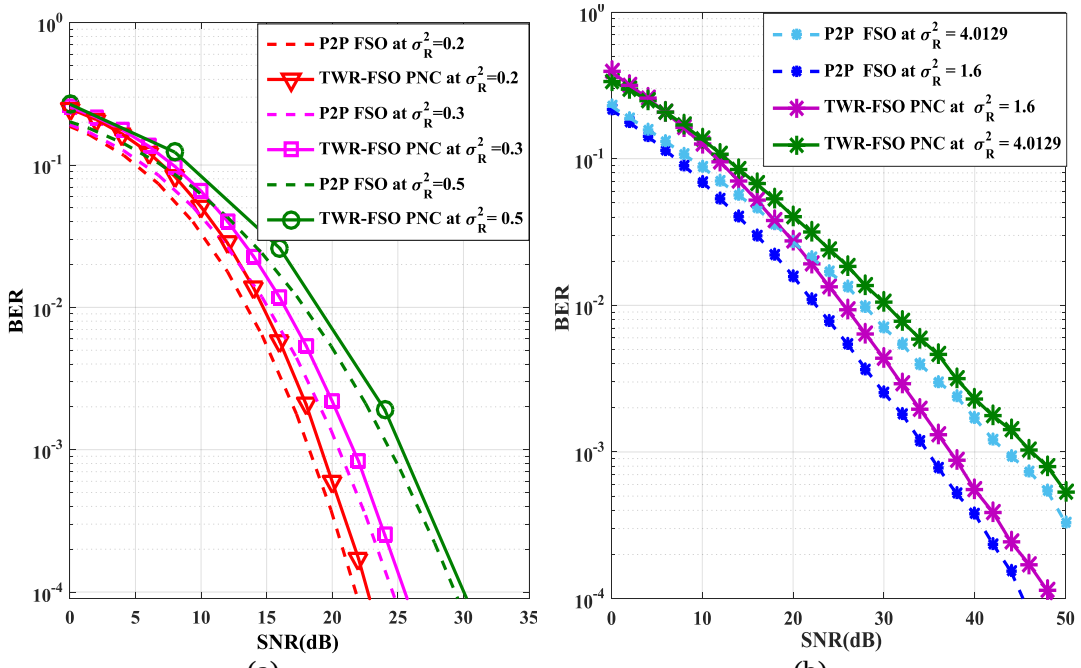

(a) (b)

Figure 3.16 The simulated BER performance against the SNR for TWR-FSO PNC and FSO P2P systems for different values of Rytov variance for $V = 10$ km, $L = 2$ km and $\lambda = 1550$ nm over: (a) weak turbulence, and (b) moderate-to-strong turbulence.

29dB at a BER of 10^{-4}. Whereas, Figure 3.16 (b) demonstrates the performance of the TWR-FSO PNC under moderate-to-strong turbulence with pointing error under the same condition parameters for the P2P FSO system.

3.8 Summary

This chapter outlined in details the mitigation techniques to overcome the atmospheric channel effects. The role of the NC in P2P FSO alongside its relevant features in TWR assisted FSO system was clarified in this chapter. The TWR-FSO PNC communication system was proposed with NLOS path between the two FSO nodes. Emphasis was placed on examination the performance of TWR-FSO PNC communication links from the information theory perspective, taking into account the adverse effects of atmospheric loss, turbulence-induced scintillations and pointing errors. The new scheme takes the advantage of the PNC technique to overcome the deterioration of signal quality. Furthermore, it used NC technique to provide protection against link failures in network and to increase the robustness and persistence for data transmission in TWR optical system under different atmospheric conditions. This chapter presented the relevant components of the transmitter, relay and receiver pertaining to the TWR-FSO PNC system model together with the important characteristics of the atmospheric channel by considering absorption, scattering and turbulence posed by the channel on the transmitted optical beam. We evaluated the link performance of the TWR-FSO PNC system together with P2P FSO in terms of BER and investigated the impact of some parameters that affect the system performance such as link distant, beam width and optical wavelength. It has been demonstrated that an improved BER was achieved with the introduction of a larger wavelength, shorter distance and wider beam width, which effectively alleviated the scintillations and pointing error loss. With the introduction of an enlarged beam width, a

notable BER improvement was achieved. For instance, at a BER of 10^{-3}, the SNR gain of 18dB for normalized beam with of 25 was attained with respect to the normalized beam with of 10 under strong turbulence regime. Nevertheless, it was observed from the preliminary results that the performance of the proposed system had a slightly worse BER compared to that of P2P FSO system. it is worth stating that an end-to-end BER of TWR-FSO PNC was evaluated for two transmission phases in which the system will experience channel fading. This is caused by fluctuation of the signal strength while propagating over a communication channel that had a significant effect on the performance of the system, while the LOS FSO system consists of a single hop transmission phase. For example, to achieve a BER of 10^{-4} with a fading strength of $\sigma_R^2 = 1.6$, a SNR gain of about 48dB was required for P2P FSO system. This value increased to ~50dB of SNR to achieve the same BER for TWR-FSO PNC system. Conversely, the proposed system reduced the complexity at the RN in constructing a large wireless network by performing a specialist detected-and-forward method to map the signal at the relay. In contrast to other traditional relay-assisted FSO system that employ the AF and DF strategies to process the signal at the intermediate node. Moreover, it increased the network throughput by reducing the transmission time slot needing to complete data exchange. A different atmospheric turbulence models covering short to very long range TWR-FSO PNC links were also hosted in this chapter. The log-normal model was mathematically tractable but was only valid for the weak turbulence regime. Beyond the weak turbulence regime, the gamma-gamma model was more suitable, which indeed covered all turbulence regimes. These models used in the simulation to characterize the behavior of the TWR-FSO PNC system and in deriving expressions for the error performance of short to very long TWR-FSO PNC links.

Chapter 4

ITERATIVE DECODING FOR TWR-FSO PNC SYSTEM

Over the years, there has been a tremendous growth in the wireless communications demand and usage, which require innovative schemes and techniques that increase the information rate and improve the robustness of a communication system under the harsh conditions of the wireless circumference. The communication channel is considered as a source for much impairment to a digital communication system due to some factors such as the mobility of transmitter and receiver, multipath propagation, interference from other users of the frequency spectrum and time-variation. Therefore, errors may be introduced during transmission from the source to the receiver. For correcting and detecting the errors, channel coding is often used in digital communication systems to enable reliable delivery of data over unreliable communication channels, which reduces the number of bit error to an acceptable level to ensure the quality of data transmission. Channel coding is mostly accomplished by selectively introducing redundant bits into the transmitted information stream. These additional bits will allow detection and correction of bit errors in the received data stream and provide more reliable information transmission. However,

the cost of using channel coding to protect the information is a reduction in data rate or an expansion in bandwidth. This chapter will focus on the state of the art FEC coding, which provided reliable communications by iterative turbo-decoding, namely, bit-interleaved coded modulation with iterative decoding (BICM-ID). This scheme combines the concept of iterative decoding, soft-in-soft-out (SISO) decoding, non-recursive systematic (NRS) convolutional encoding, and non-uniform random interleaving. The key contribution of this chapter is to evaluate the performance of TWR-FSO PNC system with iterative receiver decoding technique. The implementation of TWR-FSO PNC with the BICM-ID coding schemes is investigated in terms of BER taking into account the link impairments imposed by the atmospheric attenuation as a result of beam extinction, and channel fading due to the strong turbulence for BPSK modulation. This scheme provides a significant BER performance compare to the non-iterative CC and uncoded system.

The rest of the chapter is organized as follow: Section 4.1 gives a brief introduction about channel coding, while Sections 4.2 demonstrate the general structure of the encoder and the decoder for the CC with its mathematical expression for the algorithm that are used to decode the data encoded. Convolutional channel coding with TWR-FSO PNC is presented in Section 4.3. An overview of the coded modulation (CM) is given in Section 4.4 with describing the two major CMs, namely, trellis-coded modulation (TCM) and bit interleaved coded modulation (BICM). Section 4.5 focuses on the BICM-ID over P2P FSO link. Section 4.6 devotes on BICM-ID code with TWR-FSO PNC link by identifying the system model and the iterative processing between the demodulator and the channel decoder. Next, the simulation results and discussions are presented in Section 4.7. Finally, conclusions are drawn in Section 4.8.

4.1 Channel Coding

In digital communication, it must be providing a cost-effective facility for transmitting information from one end of the system at a rate and a level of reliability and quality that are acceptable to user at the other end. The source information, which is taken binary form, is sent to the destination by the transmission scheme through a noisy communication channels. Therefore, a string of data bits is subject to fading or other harsh impairments such us noise and interfering resulting in several consecutive bits arriving at the receiver in error. In communication system, the three crucial system parameters accessible to the designer are the channel bandwidth, the PSD of receiver noise and transmitted signal power, which are determined the SNR [107]. A general objective in the context of the digital communications is often to achieve maximum data transfer in a minimum bandwidth, while maintaining an acceptable quality of transmission. Accordingly, for a fixed SNR, the practical option available for changing data quality from problematic to acceptable is to ECC.

The approach to ECC taken by modern digital communication systems started in the late 1940's with the ground breaking work of C. Shannon [46], R. Hamming [165], and M. Golay [166]. Shannon's noisy channel coding theorem showed that by properly encoding of the information, errors induced by the noisy channel could be reduced to any desired level, which was less than the channel capacity [46]. Since that, a great deal of effort was expanded on the problem of developing efficient encoding and decoding methods for error control in noisy channel [167]. On other hand, the use of channel coding will add complexity to the system by the implementation of the decoding operation at the receiver side and enlarge the channel bandwidth by add redundancy in the coded message. Thus, in any communication system there is trade-off in the use of the ECC to achieve reliable

information with acceptable error performance and the consideration of bandwidth and the system complexity. However, truly random codes are impractical, as the codes should possess some structure in order to have computationally tractable encoding and decoding algorithms. Therefore, the code design and decoding for a group of ECC is achieved for reliable communication by employing algebraic methods in the form of convolution or block coding. All these algorithms have common features of adding extra redundancy to the original information during the transmission, which in turns are removed by the decoder at the receiver. There are two types of ECC techniques used for the reliable and efficient data transmission, namely, automatic repeat request (ARQ) and FEC techniques. In the former, it demands a feedback channel to request the source encoder to retransmit the data. The latter technique helps correcting errors at the receiver and prevents re-transmission of corrupted signals [167].

However, the channel encoder works as follow. In digital communication system, the channel encoder is a very important part at the transmitter, which is used to add a redundancy in the binary information sequence. Then, it translates the information bits to symbol signals to be ready to propagate over the channel. This redundant information can be used to overcome the effects of noise and interference encountered during the transmission of the signal through the channel. At the receiving end of the system, the decoder tries to decode the received signals as correctly as possible and reconstructs the original information sequence from the knowledge of the code word used by the channel encoder and the redundancy contained in the received data.

4.2 Convolutional Codes

Channel coding can be indicated by means of FEC and it has been developed to combat against the noise, which is assumed to be statistically independent. In 1955, the use of the CC was firstly proposed by Elias for discrete memoryless channel as an alternative to block codes [168]. After the development of the VA [169], CC began to see extensive applications in communication systems. All the 2G and 3G digital mobile cellular standards incorporate CC such as global system for mobile communication (GSM), united states digital cellular (USDC), IS-95 and Iridium communication using different rate [24]. Unlike block code, where the code words are generated on block-by-block data basis, a CC accepts a continuous stream of data bits and map them into an output data stream adding redundancies in the convolutional process. Nevertheless, its computations depend not only on the current state of input bits but also on some of the previous input state. Moreover, the most algebraic-based decoders for block codes work with hard-bit decision, rather than soft-decision decoding [165]. However, in order to achieve the performance bounds predicted by Shannon, a soft-decision channel output is required. Though, CCs are now widely used in wireless communications and are highly structured, allowing simple implementation and good performance, but they are still far away from reaching the capacity limit predicted by C. Shannon. The following sub-sections describe the encoder and the decoder for the CC alongside with its algorithms.

4.2.1 Encoding structure

One of the modules that plays an essential role in reducing the negative effects of errors caused by the noisy channel during the transmission using limited spectrum is the channel encoding. The fundamental working principle of a convolutional encoder is that the

encoder adds redundancy to a continuous sequence of binary input vectors by using a linear shift register circuit. The encoding process consists of braking up the data input d into streams, and then performing a one-to-one mapping of each d_i to produce output streams c_i called code word. So, each set of encoder binary output bits is a linear combination of the current set of encoder binary input bits and the bits stored in the shift register. The output streams are multiplexed to form the code word $C = \left(c_0^{(0)} c_0^{(1)}, c_1^{(0)} c_1^{(1)}, \ldots\right)$. The maximum number of bits that each output depends on are defined as the constraint length K_c and it is one of the two characteristic parameters of CCs. A more tangible definition of the constraint length is $K_c = M_p + 1$, where M_p is the length of the shift register associated [170]. The second parameter is the code rate R_c of the convolutional encoder, which represents the number of the inputs bits taken in by the encoder in one coding interval divided by the number of code bits output during the same interval. In any linear system, time-domain operations involving convolution can be replaced by more convenient transform-domain operation involving polynomial multiplication. Since a convolutional encoder is a linear system, each sequence in encoding equations can be replaced by a corresponding polynomial, and the convolution operation replaced by polynomial multiplication [167]. In the polynomial representation of binary sequence, the sequence itself is represented by the coefficient of the polynomial. Therefore, the input bits can be expressed as information polynomial $d(D) = d_0 + d_1(D) + d_2(D^2) + \cdots + d_n(D^n)$, and the encoded sequence $c(D) = c_0 + c_1(D) + c_2(D^2) + \cdots + c_n(D^n)$. The CCs specified by a set of generator polynomials, which can be expressed as $g(D) = g_0 + g_1(D) + g_2(D^2) \ldots + g_n(D^n)$, then the encoding equation become $c(D) = d(D)G(D)$, where the indeterminate D can be interpreted as a delay operator, the power of D denoting the number of time units a bit is delayed with respect

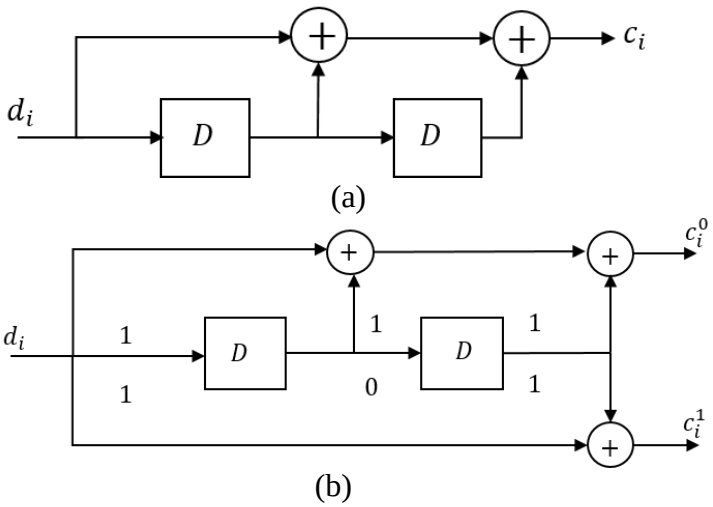

Figure 4.1 The convolutional encoder with NRS: (a) generator polynomial $g(D) = 1 + D + D^2$, and (b) with $R_c = 1/2, K_c = 3$ and generator polynomials $(7,5)_8$.

to the initial bits in the sequence, as shown in Figure 4.1(a). Then, the encoding proceeds by firstly convolving the coefficients of each generator polynomial with the corresponding input bits. An example of rate $R_c = 1/2$ with generator polynomials $g^{(0)} = 1 + D + D^2$ and $g^{(1)} = 1 + D^2$ is shown in Figure 4.1(b). The coefficients of each generator polynomials are often concatenated into a signal binary word, which is then represented as an octal number as $(7,5)_8$. There are two types of convolutional encoders, namely, non-recursive systematic (NRS) CC, which is usually implemented by feedforward shift register circuits shown in Figure 4.1(b). Another one is called recursive systematic (RSC) CC, where the shift register circuits with feedback are commonly used to implement the encoders' algorithm. A code is said to be systematic if the data input is contained within the code word.

4.2.2 Representation of encoder

The convolutional encoder can be observed in many dissimilar ways. From one perspective, they can be considered as a sequence of input and output finite impulse response (FIR) filters with operations performed over $GF(2)$. Alternatively, they can be

represented by state diagrams, graphs, and trellises. The state of a convolutional encoder is determined by the contents of its shift registers. For a convolutional encoder with memory M_c, there are a finite number 2^{M_c} states and each state is represented by a node $\mathbb{S}$, whereas the branches connect nodes at time i to nodes at time $i+1$ and labelled with the notation d/c, which specifies the input bit d required to make the transition and the corresponding code bits c, which indicated the output during the state transition. Once the encoder receives a new input binary bit, it can only make a transition to one of two other states depending on whether the input bit is 0 or 1. Afterward, a particular sequence of binary bits will be the output of the encoder as shown in Figure 4.2(a). The state diagram can be extended into a trellis diagram method, which shows how each possible input to the encoder influences both the output and the state transitions of the encoder as depicted in Figure 4.2(b). For CCs, every code word is associated with a unique path through the trellis. The trellis diagram is drawn by lining up all the possible states and next states in the vertical axis denoted by $(\mathbb{S}_i, \mathbb{S}_{i+1}, \ldots\ldots)$. Each state in a column is connected to two states in the next column with allowable code words for that state. There are only two choices possible at each state. These are determined by the arrival of either a 0 or a 1 bits. The top link from each state in a column of the trellis shows what gets transmitted on a 0,

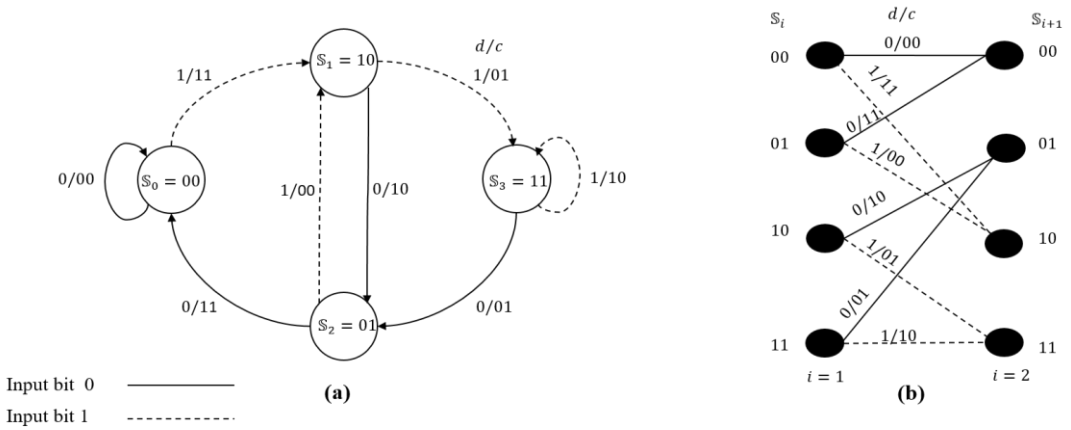

Figure 4.2 Convolutional encoder with code rate $R_c = 1/2, K_c = 5$ and generator polynomials $(7,5)_8$ represent by : (a) the state diagram, and (b) the trellis diagram.

while the bottom shows what gets transmitted on a 1. Figure 4.2(b) presents the trellis diagram for the convolutional encoder depicts in Figure 4.1(b).

4.2.3 Decoding algorithm

After the development of the VA, convolutional coding began to see extensive application in communication systems [24]. Furthermore, the decoding algorithms can make full use of soft-decision information from the demodulator. The problem of estimating the state sequence $\mathbb{s}$ of Markov process observed through noise has two well-known trellis based solution; the VA and the symbol-by-symbol MAP algorithm referred to as BCJR algorithm, after Bahl, Cock, Jelenik, and Raviv who proposed it originally in [171]. These two algorithms differ in their criterion in which the VA finds the most probable state sequence $\mathbb{s}$ given the received sequence y as [167]:

$$\hat{\mathbb{s}} = \arg\left(\max_{\mathbb{S}} \quad P_r(\mathbb{s}|y)\right). \tag{4.1}$$

While the BCJR algorithm attempts to find the most likely individual state $\mathbb{s}_i$, given y as [106]:

$$\hat{\mathbb{s}_i} = \arg\left(\max_{\mathbb{S}_i} \quad P_r(\mathbb{s}_i|y)\right). \tag{4.2}$$

When applied to the digital transmission systems, the VA minimises the probability of a code word error, whereas BCJR algorithm tries to minimize the bit error probability. The BCJR algorithm calculate the a posteriori probability (APP) of each state transition, information bit, and/or code symbol produced by a Markov process, given the noisy channel output y.

Once the APPs are calculated for all possible values of the desired quantity, a hard decision is made by taking the quantity with highest probability. When used for turbo

process, the BCJR algorithm calculates the APPs of the information bits, $P_r[d_i = 0|y]$ and $P_r[d_i = 1|y]$, which are then represented as LLR of the form [106]:

$$L(d_i) = log\frac{P_r[d_i = 1|y]}{P_r[d_i = 0|y]}, \tag{4.3}$$

where $L(.)$ is typically represented the soft-bit decision. A decoding algorithms that accepted a prior information at its inputs and produces a posteriori information at its output is called a soft-input-soft-output (SISO) decoding algorithm [172]. The SISO algorithm based on the BCJR algorithm is generally more computationally intensive and perform better than the algorithms based on VA.

Before finding the APPs for the information bits, the MAP algorithm first finds the probability $P_r[\mathbb{s}_i \longrightarrow \mathbb{s}_{i+1}|y]$ of each valid state transition given the noisy channel observation y**.** From the definition of the probability as [106, 170]:

$$P_r[\mathbb{s}_i \longrightarrow \mathbb{s}_{i+1}|y] = \frac{P_r[\mathbb{s}_i \longrightarrow \mathbb{s}_{i+1}|y]}{P_r[y]}. \tag{4.4}$$

The properties of the Markov process can be used to partition the numerator as:

$$P_r[\mathbb{s}_i \longrightarrow \mathbb{s}_{i+1}|y] = \mathcal{o}(\mathbb{s}_i)\mathfrak{B}(\mathbb{s}_{i+1})\gamma(\mathbb{s}_i \longrightarrow \mathbb{s}_{i+1}), \tag{4.5}$$

where

$$\mathcal{o}(\mathbb{s}_i) = P_r[\mathbb{s}_i, (y_0, \ldots\ldots, y_{i-1})], \tag{4.6a}$$

$$\gamma(\mathbb{s}_i \longrightarrow \mathbb{s}_{i+1}) = P_r[\mathbb{s}_{i+1}, y_i|\mathbb{s}_i], \tag{4.6b}$$

$$\mathfrak{B}(\mathbb{s}_{i+1}) = P_r\left[\left(y_{i+1}, \ldots y_{L_\tau - 1}\right)|\mathbb{s}_{i+1}\right]. \tag{4.6c}$$

The term $\gamma(\mathbb{s}_i \longrightarrow \mathbb{s}_{i+1})$ is the branch metric associated with the transition $\mathbb{s}_i \longrightarrow \mathbb{s}_{i+1}$, which can be expressed as [106]:

$$\begin{aligned}\gamma(\mathbb{s}_i \longrightarrow \mathbb{s}_{i+1}) &= P_r(\mathbb{s}_{i+1} \longrightarrow \mathbb{s}_i)P_r(y_i|\mathbb{s}_i \longrightarrow \mathbb{s}_{i+1}) \\ &= P_r(d_i)P_r(y_i|c_i),\end{aligned} \tag{4.7}$$

where c_i is the encoder output associated with the state transition $\mathbb{s}_i \longrightarrow \mathbb{s}_{i+1}$. In (4.7), the term $P_r(d_i)$ is the a priori probability of the input bit, while the term $P_r(y_i|c_i)$ is a function of the modulation and channel model. If the states $\mathbb{s}_i$ and $\mathbb{s}_{i+1}$ are not connected in the trellis diagram, then the probability in (4.7) is zero.

The probability $\sigma(\mathbb{s}_i)$ can be found according to the feedforward recursion as [173]:

$$\sigma(\mathbb{s}_i) = \sum_{\forall \mathbb{s}_{i-1}} \sigma(\mathbb{s}_{i-1})\, \gamma(\mathbb{s}_{i-1} \longrightarrow \mathbb{s}_i), \tag{4.8}$$

where $\mathbb{s}_{i-1}$ represents the set of previous state that are connected to state $\mathbb{s}_i$. Similarly, $\mathfrak{B}(\mathbb{s}_i)$ can be found according to the feedback recursion as[173]:

$$\mathfrak{B}(\mathbb{s}_i) = \sum_{\forall \mathbb{s}_{i+1}} \mathfrak{B}(\mathbb{s}_{i+1})\, \gamma(\mathbb{s}_i \longrightarrow \mathbb{s}_{i+1}), \tag{4.9}$$

where $\mathbb{s}_{i+1}$ represents the set of future state that are connected to state $\mathbb{s}_i$. Once the APP of each state transition $P_r(\mathbb{s}_i \longrightarrow \mathbb{s}_{i+1}|y)$ is found, the information bit probabilities can be determined according to:

$$\begin{aligned} P_r(d = 1|y) &= \sum_{\mathbb{S}_1} P_r(\mathbb{s}_i \longrightarrow \mathbb{s}_{i+1}|y) \\ &= \sum_{\mathbb{S}_1} \sigma(\mathbb{s}_i)\mathfrak{B}(\mathbb{s}_{i+1})\gamma(\mathbb{s}_i \longrightarrow \mathbb{s}_{i+1}). \end{aligned} \tag{4.10}$$

and

$$\begin{aligned} P_r(d = 0|y) &= \sum_{\mathbb{S}_0} P_r(\mathbb{s}_i \longrightarrow \mathbb{s}_{i+1}|y) \\ &= \sum_{\mathbb{S}_0} \sigma(\mathbb{s}_i)\mathfrak{B}(\mathbb{s}_{i+1})\gamma(\mathbb{s}_i \longrightarrow \mathbb{s}_{i+1}), \end{aligned} \tag{4.11}$$

where $\mathbb{S}_1 = (\mathbb{s}_i \longrightarrow \mathbb{s}_{i+1}: d = 1)$ and $\mathbb{S}_0 = (\mathbb{s}_i \longrightarrow \mathbb{s}_{i+1}: d = 0)$ are the set of all the state transitions associated with the information bit of 1 and 0, respectively.

4.2.4 BCJR algorithm in logarithm domain

The BCJR algorithm is optimal for estimating the information sequence on a bit-by-bit basis. However, due to high computational cost, the BCJR algorithm was considered too complex for implementation in real systems [171]. Additionally, the values of $\mathscr{o}$, $\mathfrak{B}$ and γ, which represent probabilities in the range of [0….1] arises another problem in the BCJR algorithm. Therefore, the main benefit of executing the BCJR algorithm in the logarithm domain was that multiplication becomes addition to reduce its complexity. There are two versions of BCJR algorithms that work in the Log domain; Max-Log-MAP [174] and Log-MAP [175], both algorithms perform multiplication in the Log domain as addition. The Max-Log-MAP algorithm propagates approximations to logarithms of the $\mathscr{o}$, and $\mathfrak{B}$ probabilities, which significantly reduces the complexity at the expense of some performance degradation. This was solved in [175] which suggested the Log-MAP algorithm, that corrected the approximation used in the Max-Log-MAP algorithm.

4.2.4.1 The Max-Log-MAP algorithm

For the Max-log-MAP algorithm, let $\tilde{\gamma}(\mathbb{s}_i \longrightarrow \mathbb{s}_{i+1})$ denotes the natural logarithm of $\gamma(\mathbb{s}_i \longrightarrow \mathbb{s}_{i+1})$ as[106, 170]:

$$\begin{aligned}\tilde{\gamma}(\mathbb{s}_i \longrightarrow \mathbb{s}_{i+1}) &= \ln \gamma(\mathbb{s}_i \longrightarrow \mathbb{s}_{i+1}) \\ &= \ln P_r[d_i] + \ln P_r[y_i|c_i]. \end{aligned} \tag{4.12}$$

and $\tilde{\mathscr{o}}(\mathbb{s}_i)$ to be the logarithm of $\mathscr{o}(\mathbb{s}_i)$ as:

$$\begin{aligned}\tilde{\mathscr{o}}(\mathbb{S}_i) &= \ln \mathscr{o}(\mathbb{s}_i) \\ &= \ln\Big(\sum exp[\tilde{\mathscr{o}}(\mathbb{s}_{i-1}) + \tilde{\gamma}(\mathbb{s}_{i-1} \longrightarrow \mathbb{s}_i)]\Big). \end{aligned} \tag{4.13}$$

At this point, an approximation was made in the interest of developing a fast algorithm [170]:

$$\ln\left(\sum_i exp(x_i)\right) \approx \max_i(x_i). \tag{4.14}$$

Then, (4.13) will become:

$$\tilde{\sigma}(\mathbb{s}_i) = \max_{\mathbb{S}_i}{}^{*}\left[\tilde{\sigma}(\mathbb{s}_{i-1}) + \tilde{\gamma}(\mathbb{s}_{i-1} \longrightarrow \mathbb{s}_i)\right]. \tag{4.15}$$

Likewise, $\tilde{\mathfrak{B}}(\mathbb{s}_i)$ denotes the logarithm of $\mathfrak{B}(\mathbb{s}_i)$ as:

$$\begin{aligned}\tilde{\mathfrak{B}}(\mathbb{s}_i) &= \ln(\mathfrak{B}(\mathbb{s}_i)) \\ &= \max_{\mathbb{S}_i}{}^{*}\left[\tilde{\mathfrak{B}}(\mathbb{s}_{i+1}) + \tilde{\gamma}(\mathbb{s}_i \longrightarrow \mathbb{s}_{i+1})\right].\end{aligned} \tag{4.16}$$

Once $\tilde{\sigma}(\mathbb{s}_i)$ and $\tilde{\mathfrak{B}}(\mathbb{s}_i)$ have been found for all the states in the trellis, the LLR in (4.10) and (4.11) can be found as [106]:

$$\begin{aligned}L(d_i) &= \ln\frac{\sum_{\mathbb{S}_1} exp\left[\tilde{\sigma}(\mathbb{s}_i) + \tilde{\mathfrak{B}}(\mathbb{s}_{i+1}) + \tilde{\gamma}(\mathbb{s}_i \longrightarrow \mathbb{s}_{i+1})\right]}{\sum_{\mathbb{S}_0} exp\left[\tilde{\sigma}(\mathbb{s}_i) + \tilde{\mathfrak{B}}(\mathbb{s}_{i+1}) + \tilde{\gamma}(\mathbb{s}_i \longrightarrow \mathbb{s}_{i+1})\right]} \\ &= \ln\sum_{\mathbb{S}_1} exp\left[\tilde{\sigma}(\mathbb{s}_i) + \tilde{\mathfrak{B}}(\mathbb{s}_{i+1}) + \tilde{\gamma}(\mathbb{s}_i \longrightarrow \mathbb{s}_{i+1})\right] \\ &\quad - \ln\sum_{\mathbb{S}_0} exp\left[\tilde{\sigma}(\mathbb{s}_i) + \tilde{\mathfrak{B}}(\mathbb{s}_{i+1}) + \tilde{\gamma}(\mathbb{s}_i \longrightarrow \mathbb{s}_{i+1})\right] \\ &= \max_{\mathbb{S}_1}{}^{*} exp\left[\tilde{\sigma}(\mathbb{s}_i) + \tilde{\mathfrak{B}}(\mathbb{s}_{i+1}) + \tilde{\gamma}(\mathbb{s}_i \longrightarrow \mathbb{s}_{i+1})\right] \\ &\quad - \max_{\mathbb{S}_0}{}^{*} exp\left[\tilde{\sigma}(\mathbb{s}_i) + \tilde{\mathfrak{B}}(\mathbb{s}_{i+1}) + \tilde{\gamma}(\mathbb{s}_i \longrightarrow \mathbb{s}_{i+1})\right].\end{aligned} \tag{4.17}$$

4.2.4.2 The modification to the Max-Log-MAP algorithm

The Max-Log-MAP algorithm degrades the performance compared to the BCJR algorithm due to the approximation of (4.14). Another algorithm can be made exact by using the Jacobian logarithm as [170]:

$$\begin{aligned}\ln(exp(d_1) + exp(d_2)) &= \max(d_1, d_2) + \ln(1 + exp(-|d_1 - d_2|)) \\ &= \max(d_1, d_2) + f_c\,(|d_1 - d_2|).\end{aligned} \tag{4.18}$$

This shows that addition, when preformed in the log-domain, becomes a maximization operation followed by a correction function $f_c(.)$. Moreover, it is noted that when d_1 and

d_2 are different, the correction function is close to zero. Thus, a reasonable approximation to equation (4.18) is:

$$\ln(exp(d_1) + exp(d_2)) = \max(d_1, d_2). \quad (4.19)$$

Similarly to the Max-Log-MAP algorithm, values for $\tilde{\sigma}(\mathbb{s}_i)$ and $\mathfrak{B}(\mathrm{s}_i)$ are calculated using forward and backward recursions. However, the maximization in (4.15) and (4.16) is complemented by the correction term in (4.19) leading to exact values of $\tilde{\sigma}(\mathbb{s}_i)$ and $\mathfrak{B}(\mathbb{s}_i)$. The Log-MAP algorithm is only slightly more complex than the Max-Log-MAP algorithm, but it gives exactly the same performance as the BCJR algorithm. Therefore, it is a very attractive algorithm to use in the component decoders of an iterative turbo decoder.

4.3 Channel Coding with TWR-FSO PNC System

In wireless networks, because of the various interference and noise in channel links, there would be inevitable transmission errors. Therefore, channel coding must be considered to combat the deleterious effect of the wireless channels by save the message being transmitted so increasing the reliability of the information. Consequently, PNC system should be integrated with channel coding to further improve the reliability of the system and there are two ways to apply channel coding in such system. However, the difference between the two methods state in how the relay treatments the received signal. The first approach states that channel coding could be used on an end-to-end basis, in which only the end nodes but not the RN execute channel encoding and decoding [47]. Hence, the RN does not need to decode the exact information of two source packets, but instead directly map the received symbols to the network-coded symbols and forwards the superimposed signal. At the end nodes, they will extract the information needed from the received signals, in which its own transmitted signal can be canceled beforehand. The

channel decoding operation at the end node in PNC was designed to be similar to that for a point-to-point channel, which disregards the potential error caused by PNC mapping, thus results in high performance loss.

The second approach occurs when the channel coding could be performed as a link-by-link basis, where the end node and the RN implement channel encoding and decoding [48]. In this method, the RN tries to perform the channel decoding and network-encoded packets from the received superimposed signal, and then propagates the coded symbol to the end nodes after channel encoding. Therefore, the RN makes use of the correlations among successive symbols to recover the desired network-coded symbols with more accuracy. Compared with the link-by-link approach, the end-to-end approach is simpler because the RN does not make use of the correlations among symbols. Subsequently, the performance of the FSO systems are limited by the effect of the atmospheric turbulence as a result of random changes in atmospheric temperature, pressure and wind speed. In order to improve the P2P FSO system performance, channel coding was adopted for minimizing degradation effects and used to increase the robustness of a communication system against noise and interference. However, channel coding is not sufficient to mitigate the fading in the case of the moderate to strong turbulence conditions, so that diversity techniques were proposed to enhance system performance. In [176], a combination of channel coding and interleaving was considered with time diversity to evaluate the performance improvement in weak, moderate, and strong turbulence regimes for OOK modulation. The authors pointed out that the improvement in the receiver performance did not depend only on time diversity, but also on the coding rate and the interleaver design. For instance, at BER of 10^{-5}, the SNR gain about 3.4dB was obtained for a TC compare to the uncoded system. In [177], a combination of the CC with the

existing diversity technique called selection combining (SC) was proposed over strong turbulence and pointing errors. The numerical results were obtained in terms of the BER against the average transmitted optical power. It was showed that the system had improved performance. For instance, a coding gain of 5dB was achieved for BER of 10^{-4} at the influence of pointing errors with respect to the uncoded one. LDPC codes have recently become very popular due its strong error correction capability. In [114], punctured LDPC with interleaver was proposed to exploit time diversity in digital video broadcast satellite standard (DVB-S2). The results provided performance improvements in terms of BER. For example, the code with rate of 2/3 with time diversity achieved a coding gain of 16.74dB at BER of 10^{-5} under moderate turbulence conditions. Therefore, to enhance the performance of the proposed system (TWR-FSO PNC), a CC as a channel coding is proposed in the following section.

4.3.1 Convolutional code for TWR-FSO PNC system

The full structure of the transmitter, RN and the receiver for the coded TWR-FSO PNC system is depicted in Figure 4.3, in which the two nodes (S_1, S_2) exchange their information with the help of the RN. BPSK modulation is adopted and all nodes work in half-duplex mode. The whole transmission is divided into two phases, where 1st phase correspond to the MA phase, while 2nd phase corresponding to BC phase. The input data sequence $d_k \in (0,1)$, where $k \in (1,2)$, is encoded by NRS convolutional encoder (ENC) with generator polynomial $(23,35)_8$ and constraint length $K_c = 5$ with code rate $R_c = 0.5$ to produce code bits sequence $c_k \in (0,1)$ before being modulated to $x_k \in (-1,1)$. To ensure that the modulated signals are all positive, a D.C. bias level b_o is introduced prior to IM of the light source. Thus, the received signal at RN after optical/electrical conversion is given by:

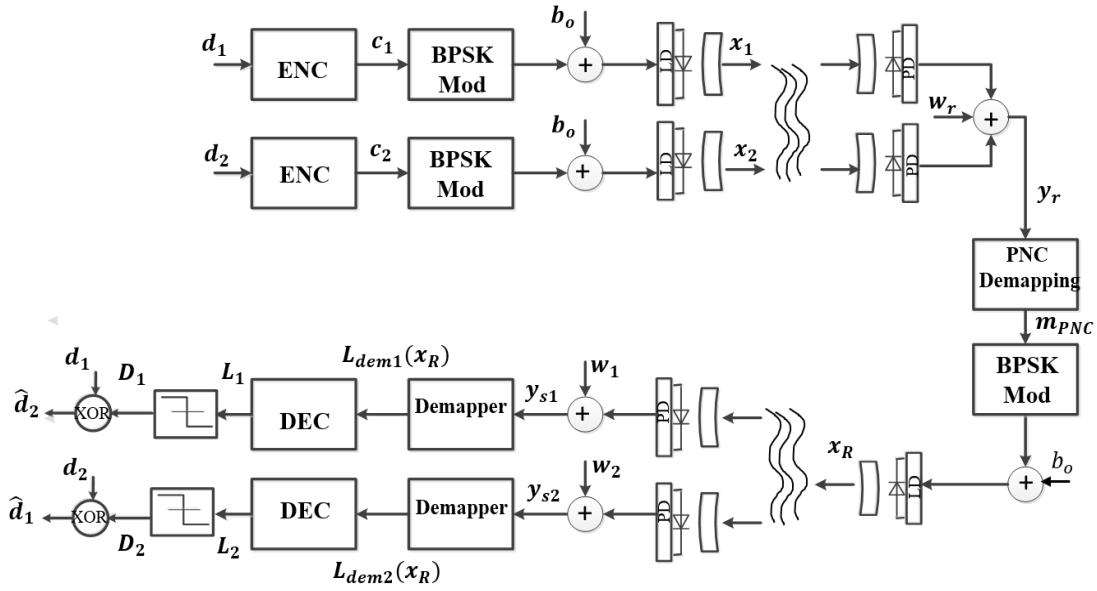

Figure 4.3 The block diagram of the coded TWR-FSO PNC with CC at $R_c = 1/2$ with generator polynomial$(23,35)_8$ and $K_c = 5$.

$$y_r = P_t R \sum_{k=1}^{K} h_k x_k + w_r. \tag{4.20}$$

The RN performs PNC demapping, where the LLR of the XOR coded bit of both source code word is estimated as [56]:

$$L(\hat{c} = (x_1 \oplus x_2)) = log\left(\frac{P_r(\hat{c} = 0|y_r)}{P_r(\hat{c} = 1|y_r)}\right). \tag{4.21}$$

Based on the BCJR criterion rule to minimize the probability that $\hat{c}$ is in error is given by [176]:

$$\hat{c} = \arg\max_{i=0,1} p(y_r|\hat{c} = i)P_r(\hat{c} = i), \tag{4.22}$$

where $P_r(\hat{c} = i)$ is the priori distribution of $\hat{c}$ and $p(y_r|\hat{c} = i)$ denotes the conditional probability distribution of the channel output. Then, the network-coded bits are obtained according to the mapping rule of PNC technique, which can be demonstrated as [48]:

$$m_{PNC} = \begin{cases} 1, & L(\hat{c}) \geq 0 \\ 0, & L(\hat{c}) < 0 \end{cases}. \tag{4.23}$$

Afterward, the network-coded bit is modulated prior broadcast it towards both nodes $x_R \in (-1,1)$. Thus, the received signal at each node after optical/electrical conversion can be modelled:

$$y_{sk} = R\ P_t h_k x_R + w. \tag{4.24}$$

The LLR of the demapper can be expressed as:

$$L_{dem(k)}(x_R) = log\left(\frac{P_r(x_R = 0|y_{sk})}{P_r(x_R = 1|y_{sk})}\right). \tag{4.25}$$

The demapper provides at its output LLR on the transmitted symbols instead of hard values as it performs SISO channel decoding, because as it is well known, soft decoding provides a better performance, compared to hard-decoding [178]. In such a case, the LLRs at the output of the demapper can be calculated as:

$$L_{dem(k)}(x_R) = 2Rh_k y_{sk}/\sigma^2. \tag{4.26}$$

This LLR at the output of the demapper are fed to the channel decoder, which in turn, performs the standard APP decoding for further eliminating from error. Finally, the channel decoder computes the a posteriori LLR on the information data bits at its output L_k, which is used to make a hard decision to obtain the estimation bits D_k. As TWR-FSO system based on the concept of the PNC technique, each node can acquire the estimation of the other node's information by performing XOR operation on the output of the hard decision with a copy of the original information and can be described as:

$$\hat{d}_2 = D_1 \oplus d_1, \qquad \hat{d}_1 = D_2 \oplus d_2 \tag{4.27}$$

Figure 4.4 (a and b) shows the simulated BER performance against SNR for uncoded and CC for P2P FSO and TWR-FSO PNC systems under weak and moderate turbulence fading channels. The simulation parameters considered in the BER analysis are defined in Table 4.1. The simulation results show a significant BER improvement of the coded

Table 4.1 Simulation parameters of the coded TWR-FSO PNC and P2P FSO systems.

Parameter	**Typical value**
Code rate	$R_c = 0.5$
Constraint length	$K_c = 5$
Generator polynomial	$(23,35)_8$
Laser wavelength	$\lambda = 1550$ nm
Photodetector responsivity	$R = 0.5$ A/W
Visibility (clear weather condition)	$V = 10$ km
Link distance	$L = 1, 2$ km
Rytov variance	$\sigma_R^2 = 0.3, 1.6$

systems compared to that of uncoded one in both figures. For instance, at a BER of 10^{-4}, there is an improvement about ~9dB of SNR for CC P2P FSO compared to uncoded one over weak turbulence as shown in Figure 4.4 (a). Meanwhile, to achieve a BER of 10^{-4}, the required coding gain is 9dB of SNR for CC P2P FSO compared to that of uncoded system for moderate turbulence as depicted in Figure 4.4 (b). Similarly, the simulation results show that by using ECC, lower BER and SNR values can be also obtained for our proposed coded system. Figure 4.4 (a and b) shows that there are improvements of SNR

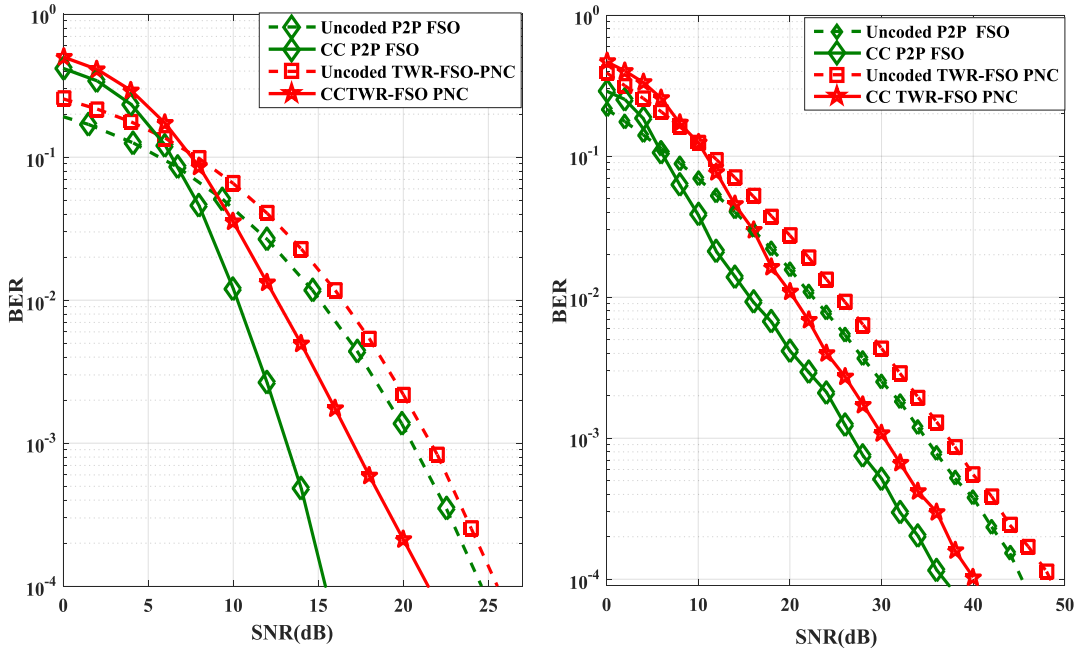

(a) (b)

Figure 4.4 The simulated BER performance against SNR for uncoded and CC P2P FSO and TWR-FSO PNC systems with $R_c = 1/2$, $K_c = 5$, $L = 1$ km, $\lambda = 1550$ nm under clear weather condition at $V = 10$ km over : (a) weak turbulence, and (b) moderate turbulence.

gains are 5 and 9dB to achieve a BER of 10^{-4} for CC TWR- FSO PNC system compare to that of uncoded one under weak to moderate turbulence conditions, respectively.

4.4 Coded Modulation

Bandwidth is a limited resource for most communication systems, therefore, the most important benchmark for the design of a communication systems is the efficient usage of the available frequency spectrum. Additionally, the other important criterion is how to achieve a reliable transmission. Hence, the commonly way of building reliable application relies on the introduction of FEC, which have added redundancy by increasing the number of coded symbols. However, the existing channel coding such as convolutional and block codes were found incapable of achieving performance close to the Shannon' capacity. This was still true even when powerful combination of block and CC, called concatenated code, was introduced in 1966 by D. Forney [179]. He showed that concatenated codes could be used to achieve exponentially decreasing error probabilities at all data rates less than capacity. While the decoding complexity increased only polynomial with the code block length. Thereafter, the breakthrough came when TCs were first invented by Berrou *et al*.[180]. The advantages of the TCs are its efficiency and the near Shannon capacity performance with relatively simple code structure and decoding algorithm.

However, in a conventional communication system incorporating with channel coding, the encoder and mapping function of the modulator are designed independently. In such system, the power efficiency can be increased by adding extra bits to the transmitted symbol sequence. On other hand, in a bandwidth-limited environment, the use of higher order modulation schemes can increase efficiency in frequency utilization, which caused a higher signal power to get the same error probability. In order to achieve improved

reliability of a digital transmission system without increasing transmitted power or expanding the signal bandwidth, the encoder is combined with higher order modulator, where more than one bit per symbol can be transmitted, to build a new system referred to as coded modulation (CM) system. In 1974, Massey founded the field of the CM to jointly design coding and modulation [181]. Early examples of CM systems are the trellis-coded modulation (TCM), where a binary convolutional encoder is combined with a memoryless modulator. Nowadays, more advanced CM systems usually insert a bit interleaver between the encoder and the modulator, so called bit interleaved coded modulation (BICM). There are two options for interleaving in CM, first is to interleave the bits and then map them to modulated symbols. This technique is called bit-interleaved. Alternative option, the modulation and coding can be done jointly and the resulting symbols interleaved prior to transmission. This is called symbol interleaved. The interleaved bits can be reordered into the original position by performing the inverse permutation of interleaving (deinterleaving). The following sub-sections give a brief description about the most popular of the CM.

4.4.1 Trellis coded modulation

The spectrally efficient coding breakthrough came when Ungerboeck introduced TCM [182], based on CCs, to jointly optimize both channel coding and modulation for digital transmission over band-limited channels. Accordingly, TCM concept is to accommodate the code redundancy by doubling the number of constellation points, while keeping the bandwidth fixed. Thus, the bandwidth efficiency of the system relative to the uncoded system is unchanged. While the block and CC can enhance the performances of the system by expanding the bandwidth and keeping the signal constellation fixed. The design of a good code strives to maximize its minimum Hamming distance (MHD) [167]. On

other hand, TCM relies upon the primary parameter that determines the code's performance is to increase the free Euclidean distance (FED) between the sequence of the coded symbol, rather than MHD of the code[182]. The TCM schemes described by Ungerboeck were optimized for AWGN channels and referred to as Ungerboeck codes. TCM achieved significant coding gains on AWGN channels, relative to uncoded systems, without sacrificing data rate or requiring bandwidth expansion. Ungerboeck proposed mapping by set partitioning well suited for this application [182], as opposed to the conventional Gray mapping used in uncoded systems, turned out to be the key to achieving performance gains with TCM compared to uncoded modulation. The basic idea was to divide the signal constellation recursively into subsets of signal points such that the MED between two signal points within a subset was maximized at each stage. Thus, minimizing the probability of short, one-branch error event, due to the uncoded bits. Accordingly, Ungerboeck encoding involves the convolutional encoding of source symbols $M = 2^d$ followed by the mapping of coded symbols onto an expanded signal set $M = 2^{d+1}$ using mapping by set partitioning to maximize the FED of the code. At the receiver, the decoder uses a VA decoder, which found the most likely coded sequence. Compared to the performance of TCM in AWGN, direct application of TCM to wireless fading channels did not result in the same performance improvements [183]. It was well known that over fading channels the so-called diversity order, which was defined as the spreading out of information across time or space of any coded systems, was the key parameter in determining its error performance not the Euclidean measure used in the design of TCM.

4.4.2 Bit interleaved coded modulation

Practically, the enhancement in the performance for a powerful communication system should be either over the AWGN or a fading channel. Many FEC and CM schemes were designed for good performance in AWGN channels. Accordingly, in fading channels the errors occur in bursts relating to the period of the channel was in a deep fade. Hence, most of ECC schemes were intended to correct random errors but fail to correct the long bursts of errors. In this case, to improve the system performance working under fading channels, the combination of the channel code with interleaving to mitigate the effect of burst errors was implemented. The approach of coding and interleaving was to transform error bursts over the received code word, which corrected by the code. The task of the interleaver at the transmitter side was to convert the burst error into random errors. Coding and interleaving could be considered as a form of diversity, whose performance could be characterized by the diversity order. Traditionally, the symbol interleaver was used to break the fading correlation and the diversity order was measured at the symbol level. With a symbol interleaver, the diversity order was typically a function of the MHD between any two code words. Thus, design for coding and interleaving on fading channels constraints on maximizing the diversity order rather than on MED, which was used in TCM over AWGN channels. However, attempts to design a new codes, which employed a high degree of time diversity was made by Zehavi [184]. In his approach, he pointed out that by making the diversity equal to the number of bits rather than the number of the symbols, a further improvement in the system performance could be achieved. This was introduced another powerful coded modulation referred to as BICM [184]. BICM was a technique that combines coding, modulation, and interleaving in a clever way such that the diversity of a communications system was increased. Later, Zehavi showed that

BICM achieved large coding gain over fading channels with coherent detection and perfect knowledge of the channel response. Thus, the performance of BICM was better than that of TCM over uncorrelated fading channels. On the AWGN, the performance of BICM worse than TCM, which significantly reduced the Euclidean distance imposed by the random modulation involved in a bit-interleaver based scheme.

In the context of the FSO system, Ben He *et al.* proposed a novel architecture for hybrid RF/FSO wireless with CC using BICM of the bit steams transmitted over the RF and FSO sub-channels [185]. They showed that new scheme robust to the various weather impairments and outperformed hybrid systems that employ simple repetition code and selection diversity. However, BICM is now the dominant technique for improving the performance of CM in fading channels.

4.5 BICM with Iterative Decoding

After introduction of TCs, the interleaving and iterative decoding were applied to the CM systems. L. Xiaodong and J. A. Ritcey proposed a scheme referred to as BICM with iterative decoding (BICM-ID) to overcome the drawback of conventional BICM due to random modulation caused by the bit-interleaver [186]. BCIM-ID utilizes iterative decoding in combination with hard-decision or soft decision feedback. They showed that this technique provided up to 1dB improvement over BICM in both AWGN and Rayleigh environments. The purpose of BICM-ID was to increase the Euclidean distance of the BICM code and to exploit maximum advantage of bit interleaving by an iterative decoding. BICM-ID was shown to be better than TCM and BICM in both Gaussian and uncorrelated Rayleigh fading channels [187]. The fundamental role for designing a good interleaver for a BICM-ID system is to make the interleaved coded bits in the same

channel symbol as far apart as possible. This is lead to increase MED between any two coded sequences and to mitigate the error propagation during the iterative decoding. Moreover, it was well known for many iterative decoding schemes that the longer the interleaver, the better the error performance becomes, which could be adopted to design a system with BICM-ID systems. In spite of the channel coding was an efficient solution for improving the link performance for FSO link under weak turbulence, its performance could be further improved by using efficient modulation techniques such as pulse position modulation (PPM) and multipulse PPM (MPPM) with iterative decoding. Accordingly, M. A. Khalighi *et al.* proposed the use of a simple binary CC to the case of Q-ary PPM or MPPM for channel coding with iterative soft demodulation and decoding scheme, called binary convolutional encoding with iterative detection (BCID) to improve the terrestrial FSO system performance [188]. The results showed that the gain obtained by the iterative detector was significant for higher modulation scheme. For instant, for 16 PPM at BER of 10^{-5}, the SNR gain was about 2.25dB compared to the same modulation without iterative decoding. Whereas K. Kumar *et al.* proposed for the first time a novel hybrid symbols for parallel FSO/RF links using BICM-ID detection, where the coded bits from the channel encoder were mapped to joint hybrid symbols instead of separate FSO and RF symbols [189]. The proposed symbol mapping achieved gain of 3dB of SNR over conventional mappings at a BER of 10^{-4}. This work was developed in [190] by using BICM-ID with asymmetric data rates between the FSO and the RF links. The authors designed hybrid symbols that required multiple uses of the FSO channel for each use of the RF link to exploit the much higher bandwidth available with FSO link. Results showed that hybrid symbol mappings obtained significant performance improvement in FSO/RF channels even with high data rate asymmetry between the two links. For instant, at BER

of 10^{-5}, there was a gain about ~8dB of SNR compared to the conventional mapping. Additionally, K. Kumar investigated PPM and MPPM for FSO channels using BICM-ID [191]. The simulation results showed that an improvement in the error performance achieved by using optimized mapping and iterative decoding at the receiver.

The following sub-sections describe the functionality of the encoder and decoder for BICM-ID code for P2P FSO communication link. The performance of the system is evaluated in terms of BER against SNR by taking into account link impairments imposed by the atmospheric attenuation as a result of beam extinction and channel fading caused by turbulence (ranging from weak to strong).

4.5.1 BICM encoder structure

The encoder structure of the BICM code for the P2P FSO system is a serial concatenation of the information source, convolutional encoder, bit interleaver, and BPSK modulator, as shown in Figure 4.5. The information bits d_k , where $k = 1$, of length L_d are encoded by NRS ENC with code rate R_c to produce a code word c_k with length $N_c = L_d/R_c$. These coded bits are passed through a bit-interleaver (Π) to produce interleave sequence I_k with length N_c , where the size of the interleaver would be equal to the length of the code word. Once interleaved, the coded and interleaved bits are mapped to the appropriate constellation points according to mapping scheme $M = 2^n$. CC is chosen to

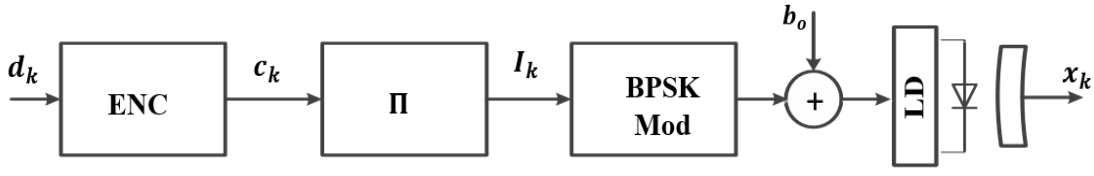

Figure 4.5 The block diagram of the transmitter structure of P2P FSO system with BICM-ID for NRS convolutional encoder at generator polynomial$(23,35)_8$, $R_c = 1/2$ and $K_c = 5$. Whereas Π is used to break the fading correlation so that the errors within a code word appear to be independent.

produce the largest Hamming distance for the given code rate and constraint length. The random interleaver permutes coded bits in order to position adjacent bits as far as possible. The interleaver is used to break the fading correlation and increase the diversity order to the MHD of the CC. Then, the interleave sequence is used for modulating of an RF signal using BPSK modulation. To ensure that the modulated signals are all positive, a D.C. bias level is introduced prior to IM of the light source as described in Chapter 3. The received optical beam is detected by a PD with optical/electrical efficiency and can be written as:

$$y_{sk} = RP_t h x_k + w_k. \tag{4.28}$$

4.5.2 Iterative demapper and decoder structure

The essential concept of the turbo or iterative receiver is to exchange the soft information between the demapper and the decoder. Therefore, the design of soft output algorithm was encouraged by the need to provide soft input to the next processing stage. Thus, in an iterative decoding process, the decoder was a soft information at the input and output ports for each constituent code. By doing a number of such iterations the performance of the system got closer to the performance of the optimal decoder for the overall code. The channel decoder then not only provided APPs of the information bits but also delivered APPs of the encoded bits. These APPs, known as extrinsic information, could be used after interleaving as prior probabilities, also known as intrinsic information, for the next iteration. The receiver structure of the BICM-ID code is shown in Figure 4.6. At the receiver side, the soft demapper computes extrinsic soft information LLRs on the coded bits $L_{dem}(x_k)$ based on the received signal and the received a priori LLR from the decoder $L_{dec}(c_k)$ and can be expressed as:

$$LLR = \underbrace{L_{dem}(x_k)}_{extrinsic\ LLR} + \underbrace{L_{dec}(c_k),}_{a\ priori\ LLR} \tag{4.29}$$

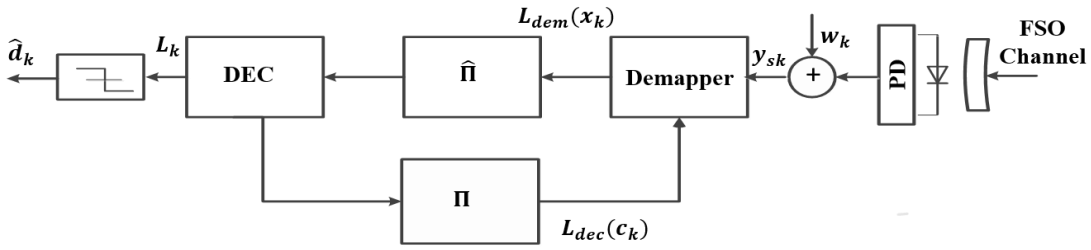

Figure 4.6 The block diagram of the receiver structure of P2P FSO system with BICM-ID for NRS convolutional encoder at generator polynomial$(23,35)_8$, $R_c = 1/2$ and $K_c = 5$.

where a priori $L_{dec}(c_k)$ of the coded bits is computed as:

$$L_{dec}(c_k) = log\frac{P_r[c_k = 1]}{P_r[c_k = 0]}. \tag{4.30}$$

and the extrinsic $L_{dem}(x_k)$ can be written as:

$$L_{dem}(x_k) = log\frac{P_r[x_k = 1|y, L_{dec}(c_k)]}{P_r[x_k = 0|y, L_{dec}(c_k)]} - L_{dec}(c_k)\,. \tag{4.31}$$

Using Bayes' rule and taking the expectation of $p(y|x_k)$ over $P_r[x_k|c_k = d]$, where the value of $d \in (0,1)$, yield:

$$L_{dem}(x_k) = log\frac{\sum_{x\in 1}\, p(y|x_k)P_r[x_k|c_k = 1]}{\sum_{x\in 0}\, p(y|x_k)P_r[x_k|c_k = 0]}. \tag{4.32}$$

The first term $p(y|x_k)$ is computed according to the channel model assuming a Gaussian distribution as:

$$p(y|x_k) = \frac{1}{2\pi\sigma^2}exp\frac{|y - x_k|^2}{2\sigma^2}. \tag{4.33}$$

The second term $P_r[x_k|c_k = d]$ is computed from the a priori information of the individual bits as:

$$P_r[x_k|c_k = d] = tanh\left(\frac{L_{dem}(x_k)}{2}\right). \tag{4.34}$$

The extrinsic information $L_{dem}(x_k)$ is deinterleaved by a distinct interleaver ($\hat{\Pi}$) and applied to the Log-MAP channel decoder. Performing iterative decoding, extrinsic

information about the coded bits $L_{dec}(c_k)$ from the decoder and after proper interleaver is fed back and regarded as a priori information to the demapper. During the initial demapping step, the a priori LLRs are set to zero. Finally, a hard decision is made on the LLR of the information bits L_k at the last iteration as:

$$\hat{d} = sign\ (L_k). \tag{4.35}$$

Figure 4.7(a and b) shows the performance of the BICM-ID for P2P FSO link over weak and strong turbulence, respectively, for different value of Rytov variance employing NRS convolutional encoder. The simulation BER performance evaluates against SNR by taking into account link impairments imposed by the atmospheric attenuation as a result of beam extinction and channel fading caused by turbulence (ranging from weak to strong) for L = 1 km , $\lambda = 1550$ nm at clear weather condition at V = 10 km. The simulation results show that an improvement in the BER performance achieved by using the iterative decoding at the receiver. For instance, at a BER of 10^{-4} for Rytov variance

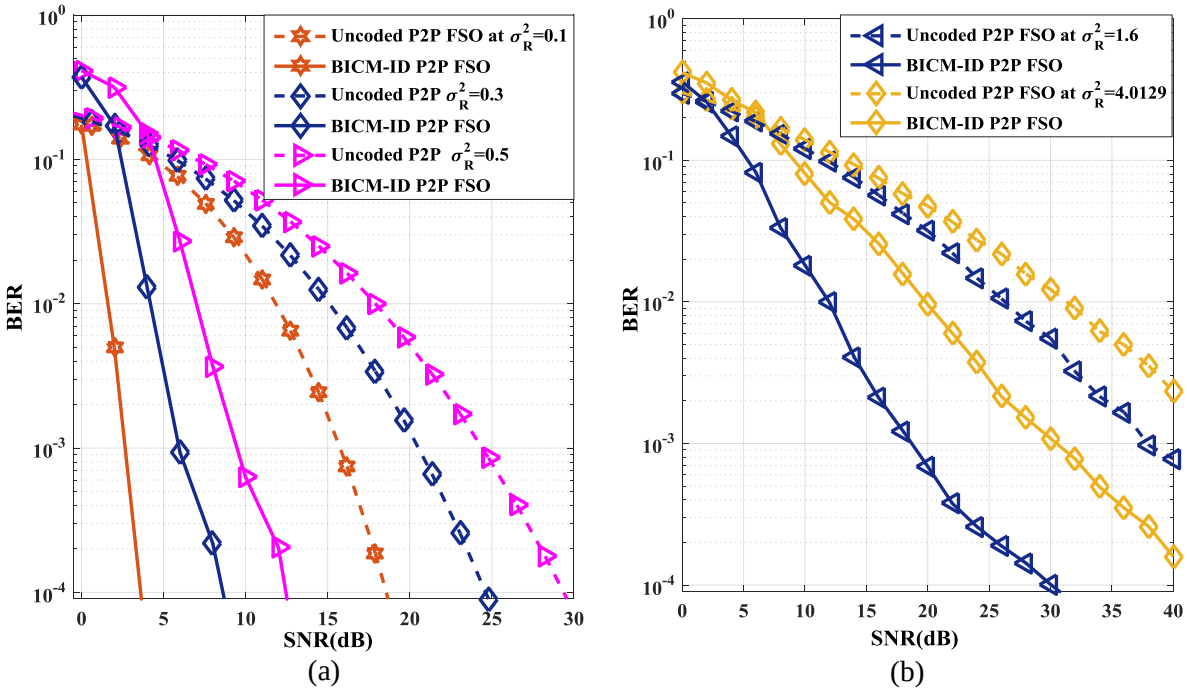

Figure 4.7 The simulated BER performance against SNR of the uncoded and coded P2P FSO with BICM-ID for different value of Rytov variance over : (a) weak turbulence, and (b) strong turbulence.

of 0.5, the coding gain is 5dB for BICM-ID P2P FSO compared to that of uncoded P2P FSO as shown in Figure 4.7(a). Similarly, under moderate turbulence of 1.6, at a BER of 10^{-3}, there is an enhancement performance about 12dB of SNR compared to that of uncoded P2P FSO system as shown in Figure 4.7(b).

4.6 TWR-FSO PNC System using BICM-ID Code

FSO systems are affected by a number of atmospheric phenomena, such as rain, haze, fog, snow, scintillation and pointing errors. Interestingly, the severity of such random degradations is highly related to the transmission range, thus resulting in link deterioration and ultimately complete link failure. Therefore, TWR-FSO system has been proposed to combat these impairments. Although PNC can increase throughput, it is at the expense of performance degradation due to the errors resulting from the demapping of the interference signal without any detection at the RN. A number of papers in the literature have investigated coded PNC with an iterative channel coding scheme in order to improve performance. An improved decoding algorithm for joint turbo decoding and PNC was presented in [192]. Interleaving operation was also introduced in [186] by performing in each user prior to transmission to the channel. Simulation results showed that a substantially improved error performance was obtained by this operation. For instance, the improvement of up to 4.5dB of SNR for a BER of 10^{-4} was observed for decoding XOR signal at relay instead of individually decoding signal for each user. In [193] joint PNC with channel coding using non-coherent orthogonal FSK modulation was proposed. At relay an iterative channel decoding with information feedback from decoder to demodulator with BICM-ID was used. The performance of the receiver was investigated in fading channels through BER, simulations and results showed an energy efficiency improvement of 0.5-0.9dB over similar systems, which used on BICM. However, to

enhance the performance of the proposed system, the end-to-end coded TWR-FSO PNC based on iterative decoding using BICM-ID system is carried out. The full structure of the transmitter, RN and the receiver for the proposed system is depicted in Figure 4.8. The transmitter structure for the proposed system is similar to the P2P FSO system with BICM-ID outlined in Section 4.5.1 except that $k \in (1,2)$. After NRS ENC and random bit-interleaving (Π), the binary signal is mapped onto BPSK symbol channels. The noisy output channel $y_r = RP_t \sum_{k=1}^{K} h_k x_k + w_r$ is received at the RN. The PNC mapping is processed on the received superimposed coded bits, where the network-coded bits are obtained as in (4.23). Thereafter, it modulated prior transmitted through the optical channel to the both source nodes as $y_{sk} = RP_t h_k x_R + w_k$. The iterative receiver works for the proposed system as described in the lower part of the Figure 4.8. Once the end nodes receive y_{sk}, they can use the iterative demapping and decoding process to obtain estimation transmitted bits D_k as described in Section 4.5.2. Then, the end nodes can recover the target information with the help of their self-information as in (4.27).

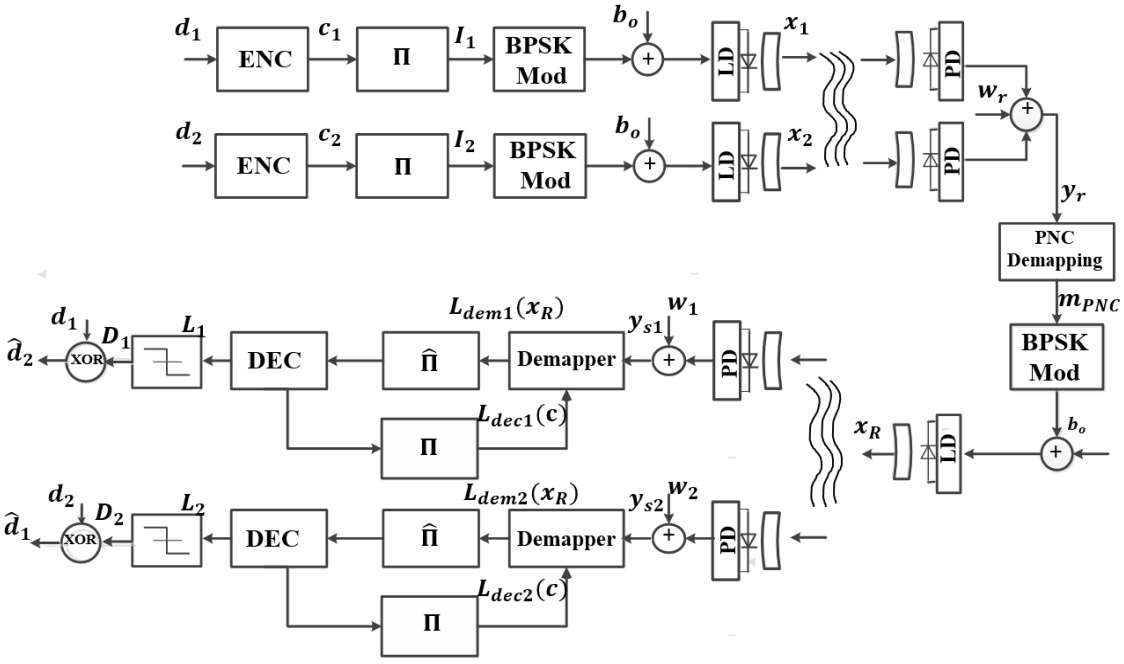

Figure 4.8 The block diagram for the TWR-FSO PNC system using iterative decoding.

4.7 Simulation Results

In this section, the simulated BER performance of the TWR-FSO PNC system with iterative decoding is investigated. Taking into account link impairments imposed by the atmospheric attenuation as a result of beam extinction and channel fading caused by turbulence, the BER is evaluated. Parameters of the TWR-FSO PNC system using BICM-ID iterative decoding are defined in Table 4.2. A comparative study between our proposed system against non-iterative CC and uncoded TWR-FSO PNC systems are also outlined in this section. The simulated BER results for the aforementioned systems under log-normal and gamma-gamma models are given in Figure 4.9 (a and b), respectively. However, for the TWR-FSO PNC, it is observed that the BER performance of BICM-ID outperforms the other both systems. For instance, there is an improvement about 10dB of SNR at a BER of 10^{-4} for the proposed system compared to that of CC as distinguished from figure over weak turbulence. Meanwhile, the coding gain is 14dB of SNR for the proposed system with respect to the uncoded one. Similarly, for the strong turbulence, it can be noticed that the performance of the BICM-ID also surpasses the other two systems. For example, at a BER of 10^{-4}, the SNR gains are 10 and 20dB for the proposed system compared to that of CC and uncoded TWR-FSO PNC systems, respectively, over strong turbulence. Nevertheless, the results show that BICM-ID codes with trellis-based

Table 4.2 Simulation parameters of the TWR-FSO PNC system with BICM-ID.

Parameter	**Typical value**
Code rate	$R_c = 0.5$
Constraint length	$K_c = 5$
Generator polynomial	$(23,35)_8$
Laser wavelength	$\lambda = 1550$ nm
Photodetector responsivity	$R = 0.5$ A/W
Visibility (clear weather condition)	$V = 10$ km
Link distance	$L = 2$ km
Rytov variance	$\sigma_R^2 = 0.3, 1.6$

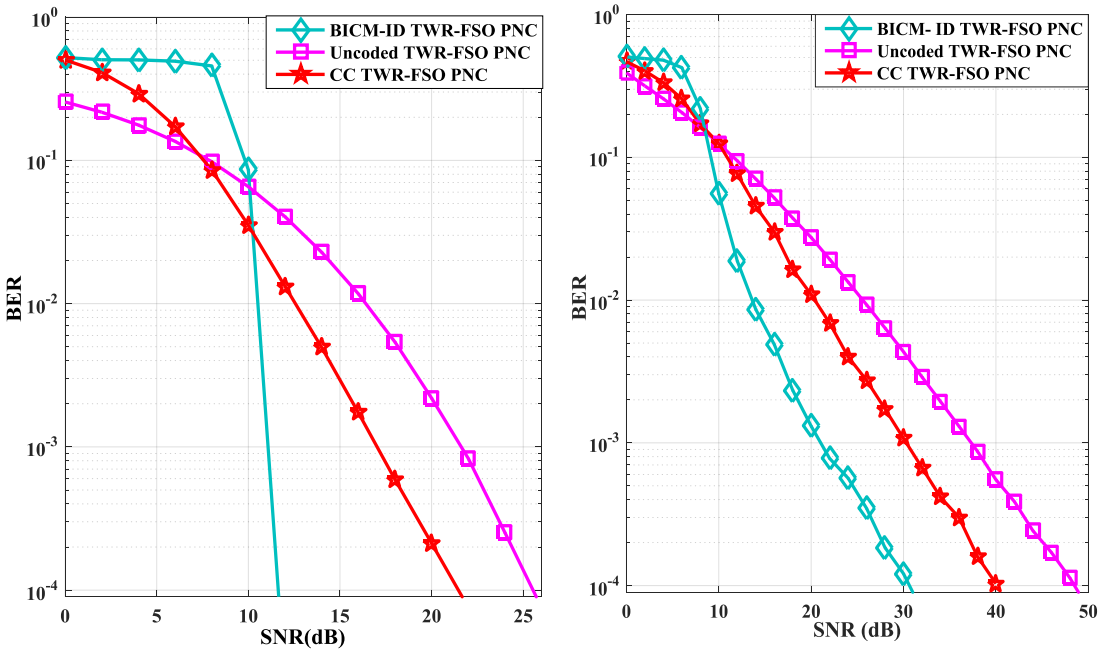

(a) (b)

Figure 4.9 The simulated BER performance against SNR for uncoded and coded TWR-FSO PNC using CC and BICM-ID over: (a) weak turbulence, and (b) strong turbulence with $R_c = 1/2, K_c = 5$, $L = 2$ km and $\lambda = 1550$ nm at clear weather condition at $V = 10$ km.

decoding algorithms is more suited to TWR-FSO PNC networks than CC on the fading channel. This is mainly because that in fading channel, introducing the interleaver produces a higher degree of diversity order and therefore guarantees significant improvement. The effects of iterative turbo-decoding are also detected in the simulation results.

4.8 Summary

This chapter began with an overview of the encoder and decoder for convolutional code, which will be used extensively throughout the rest of the thesis. The mathematical algorithms of the MAP, Max-Log-MAP and Log-MAP, which were used to decode the information bit streams, were also outlined in this chapter. The functionality of the encoder and decoder for the CC scheme for P2P FSO and TWR-FSO PNC

communication systems was demonstrated. The preliminary results showed that to achieve a BER of 10^{-4} , this scheme offered up to 4 and 9dB of SNR improvement over uncoded TWR-FSO PNC for both weak and strong turbulence environments, respectively. Furthermore, the fundamentals of coded modulation and BICM-ID code in particular were described. The BICM-ID scheme was a bandwidth efficient coded modulation scheme, which increased the time diversity and consequently was especially suited for Rayleigh fading channels. Hence, the implementation of the encoder and decoder for the BCIM-ID scheme for P2P FSO communication link was carried out. This part of the work was presented the effect of the channel coding on the P2P FSO links, which offered a coding gain about 18dB of SNR to achieve a BER of 10^{-4} for P2P FSO system using BICM-ID compared to that of uncoded P2P FSO under weak turbulence characterized by $\sigma_R^2 = 0.5$. The iterative decoding was a process when different modules in the receiver exchange information in an iterative fashion in order to improve system performance. Therefore, this chapter proposed an iterative demapping and decoding using BICM-ID and PNC joint processing framework in TWR-FSO PNC. The preliminary results for BICM-ID TWR-FSO PNC system were obtained in terms of the BER, which showed that the system had improved performance compared to that of uncoded and CC TWR-FSO PNC systems. It was delivered a coding gains about 14 and 20dB of SNR at a BER of 10^{-4} with respect to the uncoded TWR-FSO PNC system over weak and strong turbulence, respectively.

Chapter 5

MULTIUSER DETECTION WITH PNC

Although a significant amount of research has been focused on the PNC technique for TWRC, the number of users that can be simultaneously transmitted to the relay is still considered as the main constraint in such technique. Therefore, to overcome this challenge, a new scheme that integrates the iterative multiuser detection (I-MUD) technique with the PNC system is introduced. This scheme can accommodate the communications between multiple users via a single node, where each pair will transmit using the same chip-level interleaving. Another contribution is to evaluate the performance of this system that employs PNC technique at the intermediate node and iterative multi-user detection at the receiver over RF and FSO communication channels for TWRC. The software implementation of the system is investigated and compared with non-iterative multiuser (NI-MUD) detection in terms of BER. By iteratively updating the transmitted symbol pair probabilities, the MUD produces more accurate a priori probabilities of the XOR coded bits for the decoder, which can enhance the system performance. In the proposed system, both of the Gaussian and Rayleigh fading channels over RF links are implemented. A performance comparison over FSO links is also carried

out considering different levels of atmospheric turbulence with log-normal and gamma-gamma scintillation model for plane beam.

The reset of the chapter is organized as follow: Section 5.1 briefly reviews multiple access techniques and its characteristics on communication signals. While, Section 5.2 describes the optimal and sub-optimal turbo algorithms and compares between them in terms of its complexity. Emphasis is placed on multi-user PNC system with and without iterative multiuser decoding under BPSK modulation, which presents in Section 5.3. The mathematical representation of the multiuser detection function of user-specific interleaves is also discussed along with the chip-by-chip detection algorithm. The performance of TWR-FSO with multi-user PNC system using iterative detection is also realized in Section 5.4. Whereas Section 5.5 displays the simulation results, finally, conclude the chapter in Section 5.6.

5.1 Multiple Access Schemes

In the last two decades, with the ongoing integration of electronic circuits and growing computational power, wireless communication systems have brought great advances in the research and development of wireless technology such as paging systems, wireless data networks, satellite-based and cellular mobile system. However, the rapid worldwide growth in cellular telephone subscribers has evidently showed that the wireless communication is an effective means for transferring information in today's society [24]. Wireless access technologies have followed different evolutionary paths focused at unified target; performance and efficiency in high mobile environment. The first generation (1G) wireless systems were developed in the late 1970's - 1980's and were based on analogue technology, which is used to transport the voice information. As

demand increased and digital technology matured in the 1980's and 1990's, the second generation (2G) digital wireless systems were designed, which offer higher system capacity and improved QoS. Along with the rapid growth of increasing data and multimedia services, third generation (3G) were deployed to offer a variety of services to mobile users anywhere anytime by the end of 2000's and utilized many advanced techniques to more than double the spectral efficiency of the 2G systems. Whereas, the goal of 4G system was the high availability, global coverage, high quality, high network capacity, personalized service, user oriented service and low cost [80].

For all the applications in wireless communication, one of the primary objectives is to achieve reliable communication between wireless devices either in point-to-point links or multihop communication through relay devices. However, the performance of a system is subject to adverse physical factors such as limited transmit power, scarcity of the electromagnetic spectrum, signal attenuation and fluctuation in wireless links. Additionally, the performance of wireless communications systems is often limited or reduce due to the nature of the mobile radio channel, where multiple transmissions can be occurred at the same time and this phenomenon is caused the interference. Therefore, the functionality of such a network relies on the receiver's ability to work in the presence of severe interference. Consequently, research in this field has developed various system architectures for the mitigation such interference signals. Such architectures have been considered as a natural extension to the development of physical-layer systems. In order to deliver the performance necessary for supporting the different applications, it is essential for future wireless systems to utilize the available spectrum in a more efficient way. Thus, a cellular system divides any given area into cells, where a mobile unit in each cell communicates with a base station. As the spectrum is limited, so the sharing is

required to increase the capacity of the cell over a geographical area by allowing the available bandwidth to be used at the same time by different users.

Hence, multiple access techniques are used to allow a large number of mobile users to share the allocated spectrum. This sharing of spectrum must be done in a way such that the QoS does not degrade among the existing users. Multiple user channels require diversity so that each user can be identified by some unique characteristic in which this diversity can be done by time, frequency or code. The following sub-sections describe some of the popular multiple access techniques used in wireless communication.

5.1.1 Frequency division multiple access

In the 1G communication systems, FDMA was used, where the frequency is divided into multiple sub-bands as shown in Figure 5.1. Each sub-band occupies different frequency range [194]. These sub-bands, also referred to as channels, are allocated to different users. That allocated frequency is not used in the same cell or adjacent cells during the communication, therefore, the interference among users is very low when the frequency ranges of users are adequately separated and the guard band is wide enough [195]. This

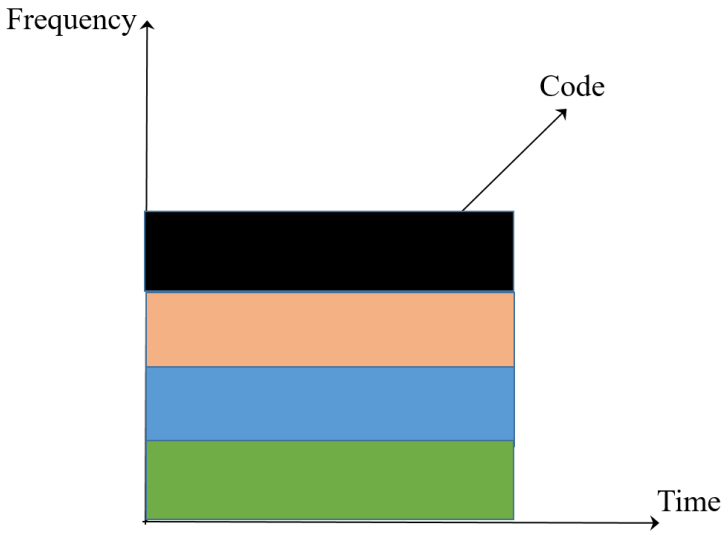

Figure 5.1 Frequency division multiple access (FDMA).

technique is also used in fiber optic communications systems, where a single fiber optic cable has enormous bandwidth that can be subdivided to provide FDMA. Different data or information sources are each assigned a different light frequency for transmission. Light generally isn't referred to by frequency but by its wavelength. As a result, fiber optic FDMA is called wavelength division multiple access (WDMA). In FDMA, the channel is allocated to a specific user and other users are not allowed to occupy the channel, therefore, the spectral efficiency is very low. Thus, the allowable number of users was difficult to satisfy the growing market of the wireless communications, and the only a few users can utilize the communication channel. So, this access scheme gradually obsolete due to the limited user number.

5.1.2 Time division multiple access

In digital systems, continuous transmission is not required because users do not use the allotted bandwidth all the time**.** In such cases, TDMA is a complimentary access technique to FDMA, which is widely used in 2G systems. A channel in TDMA system is defined according to time slots so different user will occupy different channels and

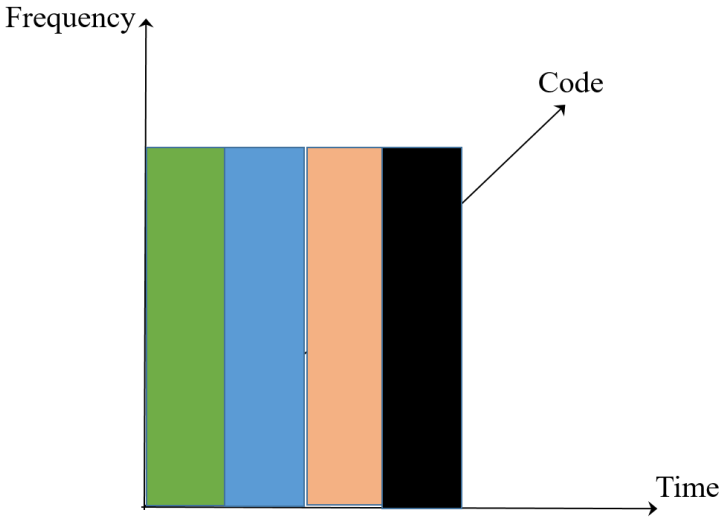

Figure 5.2 Time division multiple access (TDMA).

multiple access is achieved as shown in Figure 5.2. In FDMA, a user does not use the allocated channel all the time, so system will have some idle time, which leads to great waste of transmission time. TDMA can adequately exploit transmission time to maximize the number of the users. Furthermore, in FDMA, the limited frequency resource could provide services to only a few users, so the license fee to occupy the frequency band is very expensive. While TDMA technique changed this situation and initiated the revolution in wireless communication. The service fee to use a frequency band can be shared by a large number of users, so it can be affordable by more and more people. However, the disadvantage that TDMA used a higher power transmission than FDMA [196].

5.1.3 Code division multiple access

Although bandwidth is a valuable commodity in wireless systems, increasing the bandwidth of a transmitted signal can sometimes improve performance. Spread spectrum is a technique that the signal occupies a bandwidth much larger than is needed for the information signal. In 1978, spread spectrum signals was firstly used for the military applications because of its secrecy and improved immunity against multipath effects that are caused due to its inherent property of hiding the spread signal below the noise floor during transmission [101, 197]. However, CDMA is extensively used for achieving multiuser communication in the Radio-mobile environment, where several users simultaneously transmit information over the same channel at the same carrier frequency as shown in Figure 5.3. Each user modulates its data with a unique signature sequence. CDMA was considered as a dominant technology for the evolution of 3G. Unlike the FDMA and TDMA systems, that divide the spectrum into different frequency bands or time slots, CDMA approach overlaps every signal on the same carrier frequency by means

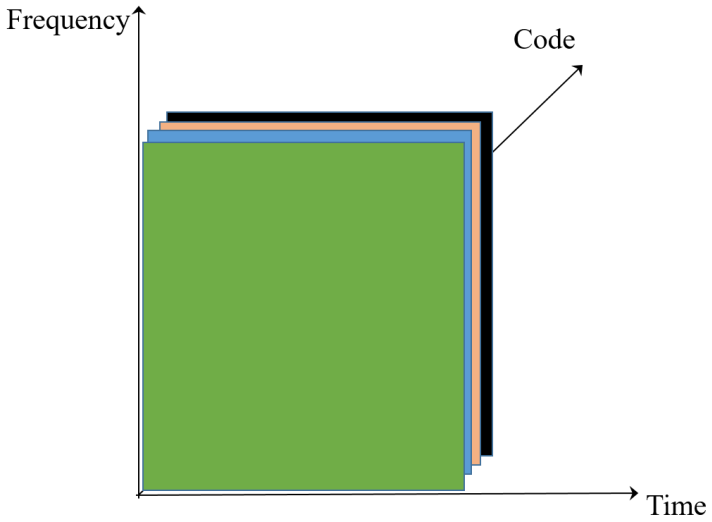

Figure 5.3 Code division multiple access (CDMA).

of a unique code, which is independent of the data signal. Therefore, the receiver is capable of detecting the data sequences from all active users in the network using the knowledge of all users' codes. In CDMA, the transmitted signal is spread over a frequency band much wider as compared to the minimum bandwidth required to transmit the input signal. Therefore, this redundancy of data plays a significant role and allows for the utilisation of many interesting features such as flexibility in the support of multiple users, allocation facilitates of different data rates, robustness against fading, supports of different diversity techniques and enhances the security.

5.1.3.1 The spreading codes for CDMA

In digital communication, coding technique increased the transmit signal bandwidth to a value much larger than the bandwidth needed for information data to be transmitted. A spread spectrum modulation is another method to increase the bandwidth of the information bits by using a spreading code [101]. In multiuser spread spectrum, the information signal of each user is assigned with an exclusive orthogonal or non-orthogonal spreading code depending on the code design. However, the best choice of

code design depends on the number of users in the system and the severity of the multipath and interference. Under ideal propagation conditions, the spreading codes are orthogonal, in which case users do not interfere with each other. On other hand, they can be non-orthogonal, in which interference between users will be occurred, but this interference is attenuated by the cross-correlation of the spreading codes. Additionally, spread spectrum multiuser systems can support an equal or larger number of users in a given bandwidth than other forms of spectral sharing [101].

In practical systems, the orthogonality is almost impossible to attain, thus the users will interfere with each other. If there is too much interference between users, the performance of all users degrades. To reduce the amount of MAI, it is desirable that the cross-correlation between different signatures be as small as possible, which is determined by the amount of interference between users modulated with these codes. Multiple access of the channel is accomplished by assigning each user a unique spreading code sequence, $s_k(t)$, with low cross-correlation values. Moreover, due to multipath, the spreading codes with small autocorrelation values are appropriate to reduce ISI and can be expressed as:

$$\rho_{auto}(\tau) = \frac{1}{T}\int_0^T s_k(t)\ s_k(t-\tau)\,dt, \tag{5.1a}$$

$$= \frac{1}{L_s}\sum_{l=1}^{L_s} s_k(lT_c)\ s_k(lT_c-\tau), \qquad l = 1,2,\ldots..,L_s \tag{5.1b}$$

where L_s is the number of chips over duration T and $s_k(t)$ is the spreading code of the k^{th} users and it is constant over a time duration T_c and has amplitude equal to 1 or -1, where T_c is the chip duration. By multiplying the information-bearing signal by the spreading signal, each information bit is chopped up into a number of small time

increment, which are usually referred to as chips, and $1/T_c$ is called the chip rate as it shown in Figure 5.4. In practice, spread spectrum systems have a processing gain or spreading factor $G = \beta_c/\beta_d$, which is define as the ratio of the spread signal bandwidth β_c to the information signal bandwidth β_d [101]. The bandwidth of the spreading code is around T_s/T_c times bigger than the bandwidth of the modulated signal, where T_s is the data symbol duration. Spreading factor plays a significant role in the design of the spreading spectrum system, which can be determined the number of the users that can be allowed in CDMA systems and the number of the chips per information bit and are supposed to be statistically independent, identically distributed random processes. Spreading code have many features such as very low correlation between time-shifted versions of the sequence and very low cross-correlation with any other interference signals [198]. However, the cross-correlation properties of different spreading codes determine the amount of MAI between users modulated with these codes assigned to user 1 and user 2 over one symbol time and it can be defined for synchronous users as:

$$\rho_{12}(\tau) = \int_{\tau}^{T_s} \mathbb{g}_1(t)\ \mathbb{g}_2(t-\tau)\, dt, \tag{5.2}$$

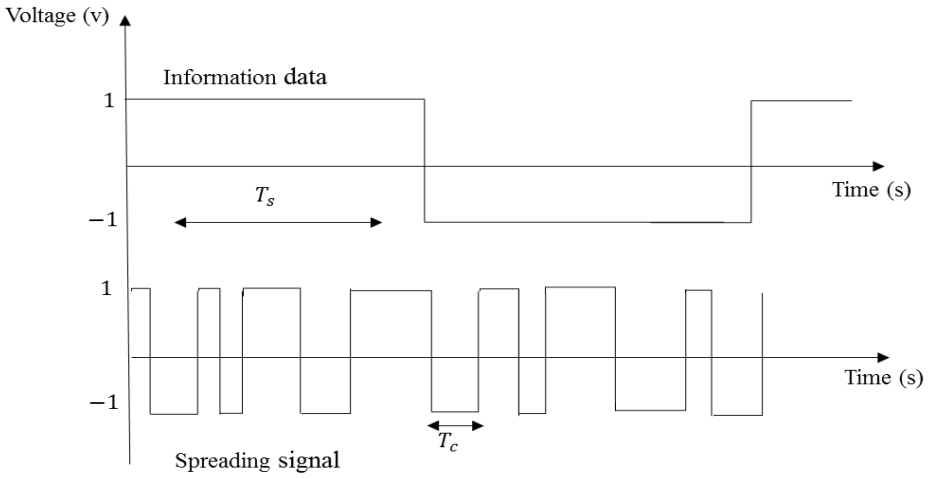

Figure 5.4 The relationship between the information data and the spreading signal.

where $\mathbb{g}_1(t)$ is the signature waveform and can be define as:

$$\mathbb{g}_1(t) = \sum_{l=-1}^{L_s} s_1(l)\, g(t - lT_c) \ , \qquad 0 \le t \le T_s \tag{5.3}$$

where $g(t)$ is a pulse-shaping function that is:

$$\int_{-\infty}^{\infty} g(t - lT_c) g(t) = 0 \ . \qquad l = 1,2, \ldots\ldots, L_s \tag{5.4}$$

In practical systems comprised of geographically separated transmitters, it is difficult to achieve the requirement that a signals remains bit-wise synchronous at the receiver. When transmission is bit asynchronous, orthogonal signalling becomes impossible. Therefore, reliable communication can be achieved in asynchronous CDMA by the use of signature sequence with low cross-correlation along with strong error correction code.

5.1.4 Interleave division multiple access

Interleaving is a process or methodology to make a system more efficient, fast and reliable by arranging data in a non-contiguous manner. The first used of the interleaver as specific user identification was proposed by F. N. Brom *et al.* for trellis-code multiple access (TCMA) [199]. Thereafter, the concept of the chip-interleaving with direct sequence spread spectrum (DS-SS) system was introduced by S. I. Tachikawa *et al.* and also studied by X. Gui *et al.* to combat burst noise [200, 201]. While M. Moher employed the chip-interleaving for user separation in CDMA systems to overcome the limitations of multiuser detectors when the user cross-correlations were high [202]. The possibility of using interleaving in CDMA to improve the BER performance with complexity detection at the receiver was demonstrated in [203, 204]. Chip-interleaving introduced in the CDMA cellular systems for high spectral efficiency, improved error performance under fading channel and low receiver complexity and was extensively studied by Y. N. Lin

and D. W. Lin [205, 206]. Based on the attitude of code-spread CDMA and chip-interleaved CDMA, IDMA was developed, which inherits many advantages from CDMA such as robustness against fading, dynamic channel sharing, mitigation of interferences, asynchronous transmission and mitigation of other-cell-user interference [207].

However, IDMA consists of three components, namely an encoder, spreading code and interleaver, which lead to chip-interleaving instead of bit-interleaving as in CDMA. Additionally, IDMA separates users by their unique user-specific interleaver combined with turbo-style iterative joint detection as well as channel decoding, unlike CDMA, which uses user-specific spreading codes. These features facilitate chip-based detection strategies and maintain good performance with far lower complexity than the CDMA scheme and was examined in [208].

As IDMA distinguishes users by using only random interleaver, a full bandwidth can be expanded for the channel coding. Due to low-rate coding and chip-level processing rather than spreading and bit-level processing in CDMA, the correlation between users is virtually eliminated. Therefore, the matrix inversion is avoided in IDMA, resulting in a low-complexity implementation that only grows linearly with the number of users. The price to pay is in terms of interleaver sizes, and thus in memory requirements. However, MAI is a major concern for CDMA cellular networks, which can be mitigated by using multiuser detection (MUD) technique. The high computational cost involved in MUD, which may increase in an exponential order with the number of users, limits its application in practical systems [62]. K. Kusume and G. Bauch provided a comprehensive comparison of the iterative MUD techniques for IDMA and CDMA in various scenarios such as user a synchronism, multipath channel, near-far problem and overloaded systems [209, 210]. Simulation results illustrated that in all the scenarios IDMA performs better

than CDMA. For instance, at a BER of 10^{-3} and for $K = 8$ users, the SNR penalty was 2dB for IDMA compared to that of CDMA. However, IDMA is one of the powerful multiple access schemes, which is considered one of the most promising candidates for the uplink in future wireless communication systems.

5.1.4.1 The choice of interleavers

Practically, a robust communication system should perform well not only in an AWGN but also in a fading channel. Hence, the emergence of interleaving in iterative turbo-code system, which is usually placed between FEC coding and spreading, has devised to reduce the effect of errors in fading channel [211]. The interleaver utilized at the transmitter performs the task of converting the burst errors into random errors by scrambling different sequence of bits, thus, decreased the bit error probability. The condition for IDMA to be successfully implemented is that the transmitter and receiver agree upon the same interleaver. However, the choice of interleaver is key component for IDMA in which the size of the interleaver must be large enough to make the fading independent across a received code word. In this case, the cost is an implementation complexity as the interleaver indices consume lots of memory to store. Therefore, the interleaver design for IDMA systems have attracted the attention of many researchers in which a set of interleaver must be satisfied the two conditions: (i) the set of interleavers are easy to specify and generate; and (ii) zero-correlation (or orthogonality) implied no collision among the set of interleaver. L. Ping *et al.* introduced random interleaver that are generated randomly and independently [207]. This method need to transmit the interleaver matrix to the receiver, which can be very costly. Thus, H. Wu devised a power interleaver, which used a master interleaver to generate a set of interleaver in order to reduce the memory consumption and the amount of information exchanged between

transmitter and receiver [212]. Whereas Pupae *et al.* analysed orthogonal interleaver, pseudo random interleaver and nested interleaver [63]. Additionally, they proposed a criterion for judging correlation between different interleaver so-called peak basis correlation (PBC) function, where the orthogonal interleaver designed based on pseudo random sequences. Different users utilize different primitive polynomials to obtain pseudo random interleaver, so each user only needs to store its own primitive polynomial to generate its interleaving sequence. Whereas Zhang *et al.* described shifting interleaver in [213]. The drawback of this method rose when the number of user increased so it is difficult to find enough primitive polynomials for pseudo random interleaver, and systems have to tolerate generation time for power or nested interleaver.

5.1.4.2 The mechanism of interleaving and correlation

The functionality of the interleaving is to rearrange the ordering of a data sequence by means of a deterministic bijective mapping [63]. Let $S = [s_0, s_1, \dots., s_{N-1}]$ be a sequence of length *N*. An interleaver maps S onto sequence $X = [x_0, x_1, \dots., x_{N-1}]$ such that X is a permutation of the elements of S as shown in Figure 5.5. The mapping function can be expressed as an ordered set called interleaving vector I:

$$I = \big[I[1], I[2], \dots \dots, I[N-1]\big]. \tag{5.5}$$

The i^{th}elements of the permuted sequence X are:

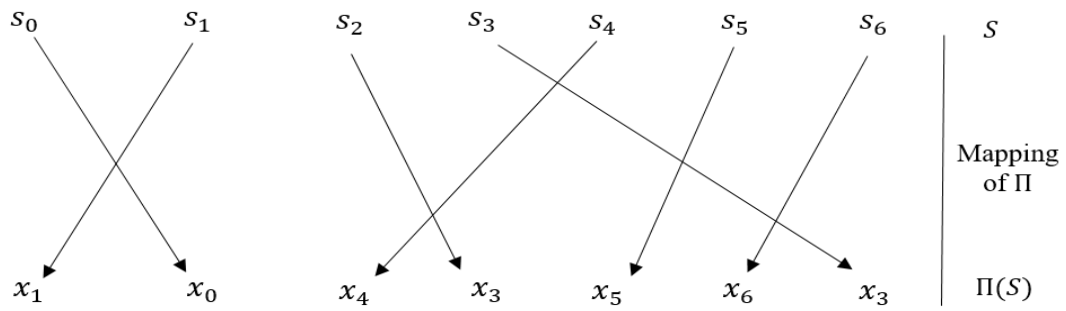

Figure 5.5 The mechanism of data interleaving.

$$X^i = S^{I[i]} . \tag{5.6}$$

The permuted elements with the proper deinterleaved $\hat{I}$ can be shifted back to their original positions:

$$\hat{I}\left[I[i]\right] = I\left[\hat{I}[i]\right] = i . \tag{5.7}$$

If i replaced by $\hat{I}[n]$, thus (5.6) will be:

$$X^{\hat{I}[n]} = S^{I[\hat{I}[n]]} = S^n . \tag{5.8}$$

The correlation between interleaver specified how strongly signals from other users affect the decoding process of a specific user. The de-correlation among the interleaver provides a mean to reduce the MAI from other users thus helping in the convergence of detection process.

In order to describe the cross-correlation for different interleaver, the correlation for the two interleaver I_i and I_j can be defined as:

$$\rho_{ij}\left(s_i , I_i, s_j, I_j\right) = \langle I_i(s_i), I_j\left(s_j\right)\rangle . \tag{5.9}$$

Thus, zero-correlation (or orthogonality) implies no "collision" among interleaver, hence, the two interleaver are called orthogonal if:

$$\rho_{ij}\langle I_i(s_i), I_j\left(s_j\right)\rangle = 0, \tag{5.10}$$

where $\langle s_i, s_j\rangle$ is the scalar product between two vectors. However, achieving the orthogonal interleavers in the practical IDMA systems is very computationally expensive, since correlation is affected by the coded data length. Therefore, to analyse the correlation issues, PBC function can be used.

5.2 Turbo Iterative-Multiuser Detection Technique

In a mobile cellular communication system, the performance of the system is restricted by MAI resulting from transmission of other interfering users and ISI caused by multipath

fading. Therefore, various MAI reduction schemes for synchronous and asynchronous systems have been developed and studied. In multiuser system, spread spectrum receiver that exploits the structure of the multiuser interference in signal detection is MUD, which was pioneered by Verdu [214]. A MUD is necessary to separate different users' signals that share the same propagation media and improve performance by jointly processing the signals from all of the users, therefore, the complexity involved $O\ (2^K)$, where K is the number of user. Therefore, the optimal MUD for the asynchronous users that consist of a bank of K single-user matched-filter detectors followed by a Viterbi sequence detection algorithm to jointly detect all users was shown in [215]. The VA has 2^{K-1} states and complexity that grows as 2^K assuming binary modulation. While such optimum MUD algorithms offer significantly improved performance by alleviating the disadvantages associated with the conventional scheme, they unfortunately suffer from the fact that their complexity grows exponentially with the number of users and the length of the sequence. Thus, numerous sub-optimal MUDs have been considered to mitigate the interference with respect to the performance, complexity, and requirements regarding channel knowledge such as de-correlator and minimum mean square error (MMSE) detectors. These linear sub-optimal MUDs are computed by measuring all cross-correlations between pairs of user codes and then inverting the resulting matrix of cross-correlations. In the asynchronous time dispersed case the complexity of the computation is further increased, thus, another popular approach is relying on the interference cancellation (IC) was proposed [216]. This technique employed a bank of single-user matched filters, whose outputs were processed by an iterative soft IC before demodulation of the desired data stream. However, the performance of the multiuser system could approach that of the single user bound (SUB) by applying the iterative decoding of turbo

codes [202]. Inspired by the success of turbo codes, iterative MUD (I-MUD) has been extensively studied. In the turbo processor, each decoder handles the data for a certain user only and disregards the others. Therefore, the complexity of the decoder is independent of K. Large improvements in the detection of CDMA signals were realized by performing the turbo I-MUD. In [217], the optimal I-MUD has been investigated and used a large interleaver with a conventional detector and channel decoder to show the I-MUD could achieve near single user performance, whereas BCJR algorithms with error correction code was used in [218], which has an exponential complexity of $O\ (2^K)$. In addition, MMSE based MUD has a complexity $O\ (K^3)$ due to the matrix operations. However, since the channel coding becomes common for practical systems and the optimal architecture with coding is more complex than that for uncoded systems, I-MUDs were alternative solutions to improve the system performance at a relatively low computational cost, which was widely used in multiuser systems to overcome the channel impairments and MAI between users.

5.3 Multiuser Detection in TWRC Employing PNC

PNC system improves the throughput in wireless networks by enabling two nodes to exchange their information with a minimum number of time slots. It is worth mentioning that constructing more efficient networks to support multiple users in PNC systems has been considered as an attractive area for research. This is due to that the main constraint is the number of users that can simultaneously transmit to the RN, where PNC mapping is processed. Therefore, to overcome this challenge, a new scheme that integrates low complexity MUD technique is introduced for PNC system as the main contribution of this chapter. This scheme can accommodate the communications between multiple pairs of user via a single node, where each pair of users wanting to swap their messages will

transmit using the same chip-level interleaver with the aim of maximizing the utilization of network resources.

However, the full structure of the transmitter, RN and the receiver of multi-user PNC system using non-iterative MUD (NI-MUD) and I-MUD receiver technique for RF link communication are described in the following sections. In both proposed systems, the BER performance is examined for both Gaussian and Rayleigh fading channels.

5.3.1 Multi-user PNC system with non-iterative decoding

The implementation of an end-to-end PNC system with NI-MUD receiver technique based PNC scheme is investigated in terms of BER performance. In this scheme, each pairs of users denoted by *P* exchange their information that is distinguished by a unique chip-level interleaving to accommodate the functionality of the user separation at the receiver side. Whereas all users employ the same spreading sequence using BPSK modulation is considered. PNC communication system is carried out in two phases; (i) the 1st phase MA is dedicated to the entire user to transmit to the RN; and (ii) the 2nd phase, where BC is responsible for transmission from RN back to the users. We assume that there is no direct link between users, all users' nodes operate over a half-duplex link and full transmissions synchronization between the nodes with the same transmits power for all nodes.

5.3.1.1 The transmitter structure for the NI-MUD based PNC system

A simplified view of the general transmitter structure for the proposed scheme is shown in Figure 5.6. The input binary bits sequence $(d_k)_{\ell=0}^{L_d-1} \in (0,1)$ of random data length L_d for each user k is encoded by NRS ENC producing a coded sequence $c_k = [c_k(1), \dots, c_k(N_c)]$ at a rate R_c, where $N_c = L_d/R_c$. The elements in c_k are then fed to a

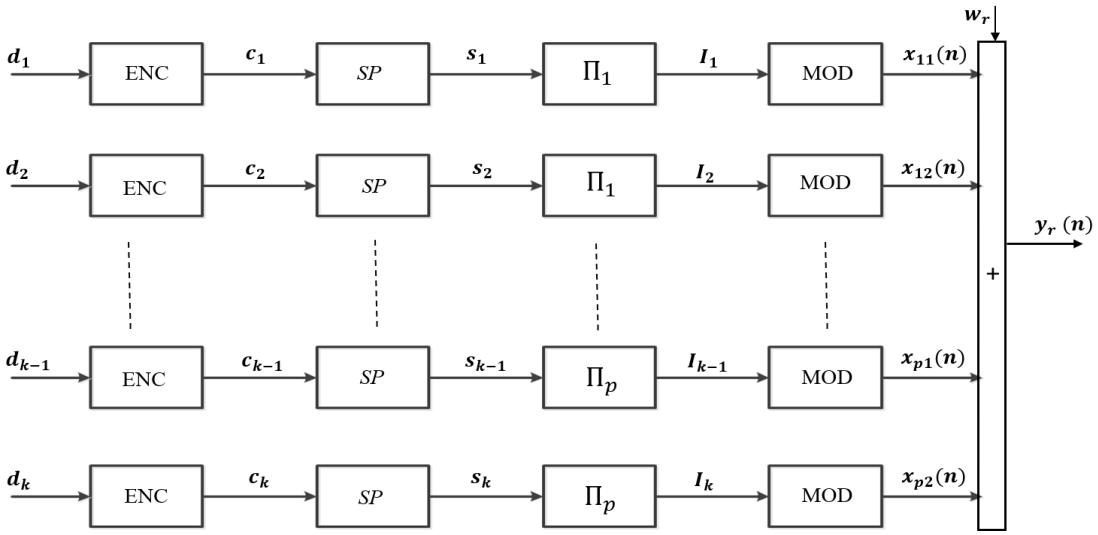

Figure 5.6 The block diagram of the transmitter structure for the NI-MUD based PNC system for *K* users.

simple spreading code (SP) module with length L_s. Assume all users employ the same spreading sequence $s(l_s)_{l=1}^{L_s} \in (0,1)$. Therefore, for the k^{th} user, the output chip sequence s_k with length $N = L_s \times N_c$ chips is given by:

$$s_k(\mathfrak{n} \times l) = s(l)\, c_k(\mathfrak{n}) \quad , \qquad l = 1,..,L_s \qquad \mathfrak{n} = 1,\dots,N_c \quad . \tag{5.11}$$

Afterward, s_k is permutated by a distinct chip-level interleaver Π_p for each *P*, producing an interleave sequence $I_k \in (0,1)$. The chip interleaver that generated independently and randomly, are used for user separation to ensure the adjacent chips are approximately uncorrelated. Next, the interleaved sequence is modulated using a BPSK symbol for transmission over the channel.

5.3.1.2 The relay structure for the NI-MUD based PNC system

The full block diagram of the RN structure for the proposed system is depicted in Figure 5.7. The received baseband signals at the RN are the superposition of the K user's signal plus the AWGN noise. After chip matched filtering and sampling at the chip rate, the transmitted signal from all K-user in the MA phase to the RN can be expressed as:

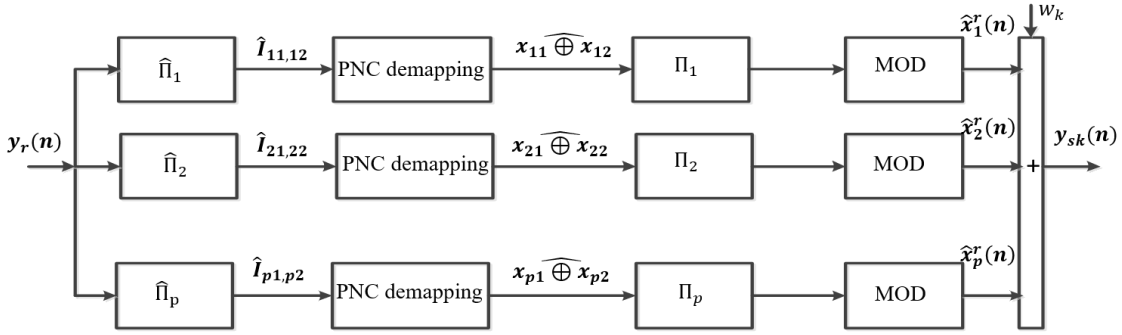

Figure 5.7 The RN structure for the NI-MUD based PNC system.

$$y_r(n) = \sum_{p=1}^{P} h_p x_p(n) + w_r(n), \tag{5.12}$$

where $x_p = x_{p1} + x_{p2}$ represents the superposition of the n^{th} partners' chip symbols transmitted. Upon receiving the signal at RN, $y_r(n)$, the deinterleaving procedure will be applied by inverting the permutation of the received signal with the same pair of *P* specific interleaver at the transmitter $\hat{I}_{p1,p2}$. Subsequently, PNC detection, based on a special hard decision for demodulation, is performed on the deinterleaving signal. The MED is used to map the deinterleaver superimposed symbol to a network-coded symbol for each *P* and can be written as:

$$(x_{p1} \widehat{\oplus} x_{p2}) = \arg \min_{x_{p1}, x_{p2} \in (1,-1)} \left| \hat{I}_{p1,p2} - (x_{p1} + x_{p2}) \right|. \tag{5.13}$$

Following this, the chips sequences for each *P* are permutated by a distinct chip-level interleaver in order to successfully distinguish the users at the receiver Π_p. The interleaver outputs in terms of BPSK symbols are summed, which can be forwarded to the prospective destination [61]. However, the broadcast signal to the destination for the BC phase from the RN is given by:

$$y_{sk}(n) = \sum_{p=1}^{P} h_p \hat{x}_p^r(n) + w_k, \tag{5.14}$$

where $\hat{x}_p^r(n) \in (+1, -1)$ is the n^{th} chip modulated transmitted signal for each *P*.

5.3.1.3 The receiver structure for the NI-MUD based PNC system

The computational complexity of the chip-by-chip I-MUD strategy is very low and independent of the K, in addition, it is essentially a low-cost iterative cancellation technique to remove jointly both MAI and ISI. It has been shown in [201, 213] that the algorithm can achieve near SUB performance with equal power control. Therefore, these meritorious properties provided the motivation to investigate the performance of such turbo chip detectors for real channel conditions. The receiver structure for the proposed system is described in Figure 5.8, where the soft demapper processes the received symbols $y_{sk}(n)$ from the channel output. The concept of the NI-MUD based PNC system depends on the demapper taking soft values from the channel output and producing extrinsic information $L_{dem}[\hat{x}_p^r(n)]$. The LLRs of the chip based on the received signal is given by:

$$L_{dem}[\hat{x}_p^r(n)] = \ln\left(\frac{p(y_{sk}(n)|\hat{x}_p^r(n) = +1)}{p(y_{sk}(n)|\hat{x}_p^r(n) = \quad 0\ )}\right). \tag{5.15}$$

Thus, the LLRs for the demapper can be computed as:

$$L_{dem}\left[\hat{x}_p^r(n)\right] = log\left[\frac{exp\left(-\frac{(y_{sk}(n)-h_k)^2}{2\sigma^2}\right)/\sqrt{2\pi\sigma^2}}{exp\left(-\frac{(y_{sk}(n)+h_k)^2}{2\sigma^2}\right)/\sqrt{2\pi\sigma^2}}\right]$$

$$L_{dem}(\hat{x}_p^r(n)) = (2\ h_k\ y_{sk}(n))/\sigma^2. \tag{5.16}$$

The output of the demapper is deinterleaved by user-specific interleaver $L_{dem}(\hat{x}_p^r(\hat{I}_p))$, which is used to calculate a priori LLR delivering to the despreading module (DSP) as shown in Figure 5.8. Therefore, the signal is integrated over the duration of one data symbol using DSP module. Based on the $L_{desp}(c_{p1} \oplus c_{p2})$ delivered from the DSP module and the spreading constraints, the module extracts the spreading factor and

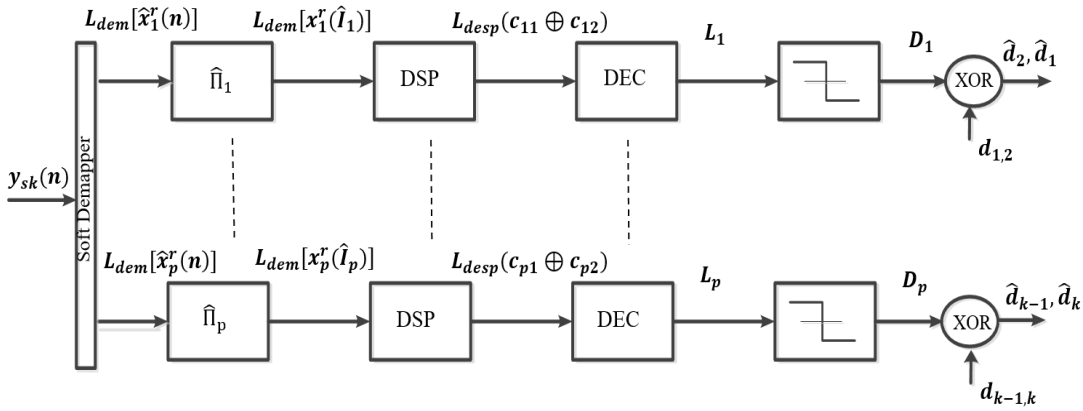

Figure 5.8 The receiver structure for the NI-MUD based PNC system.

performs the de-correlation process on each coded bit based on $L_{dem}(\hat{x}_p^r(\hat{I}_p))$ and the spreading constraint. Then, a prior LLR send to the DECs module can be calculated as:

$$L_{desp}(c_{p1} \oplus c_{p2}) = \sum_{j=(\ell-1)L_s+1}^{\ell L_s} s(j)\, L_{dem}\left[\hat{x}_p^r(\hat{I}(j))\right], \qquad \ell = 1, \dots L_d \tag{5.17}$$

Then, this extrinsic iformation is fed as a priori information to decoder channel for further eliminating from error. Finally, the channel decoder computes the a posteriori LLR for every information bits L_p, which is used to make a hard decision on the decoded bits to obtain D_p as:

$$D_p = \begin{cases} 1, & L_p \geq 0 \\ 0, & \text{otherwise} \end{cases} . \tag{5.18}$$

As the NI-MUD system employing PNC technique, the estimated information D_p is the superimposed signal for two users. Therefore, each user can acquire the estimation of the other user's information $(\hat{d}_1, \hat{d}_2, \hat{d}_3, \dots\dots, \hat{d}_k)$ by performing an XOR operation on the final signal and a copy of the original information as:

$$\hat{d}_{k-1} = D_p \oplus d_k \ , \ \ \hat{d}_k = D_p \oplus d_{k-1} \ . \tag{5.19}$$

5.3.2 Multi-user PNC system with iterative receiver

Turbo decoding principles showed that excellent performance could be obtained by using two decoders, concatenated and separated by a random interleaver. Decoding is achieved

by using SISO decoders that generate the soft APP. The two concatenated decoders pass this soft information between them, improving performance by iterating. Inspire from this principle, I-MUD receiver will utilize information from the channel code decoders to improve its estimate of the data sent by around the information between the MUD and decoder. The concept of the turbo code is that the MUD and decoders are assumed to exchange a priori information with each other via several iterations in order to enhance the performance of the system. The iterative receiver structure consists of two stages: SISO MUD followed by a bank of K single-user SISO decoders. The two stages are separated by K of deinterleaver/interleaver pairs, K of despreader /spreader pairs. Therefore, this section describes the effectiveness of I-MUD receiver coupled with the PNC system for TWRC. This scheme offers bi-directional communications between multiple pair of users via the RN with iterative decoding at the receiver. The transmitter and the RN structures for the I-MUD based PNC scheme as same as the structure for the previous system in Section 5.3.1. Thus, the next sub-section outlines the receiver structure of the I-MUD based PNC system.

5.3.2.1 The receiver structure of the I-MUD based PNC system

The block diagram of the I-MUD based PNC receiver structure is shown in Figure 5.9. The inputs to the MUD are the channel observation $y_{sk}(n)$ and the a posteriori LLR of a transmitted code bit of every pair P based on the multiple access constraint. Thus, the extrinsic LLRs provided by MUD can be computed as:

$$L(\hat{x}_p^r(n)) = log \frac{P_r\left[\hat{x}_p^r(n) = 1 \middle| y_{sk}(n)\right]}{P_r\left[\hat{x}_p^r(n) = 0 \middle| y_{sk}(n)\right]}. \tag{5.20}$$

Using Bayes rule, (5.20) can be written as:

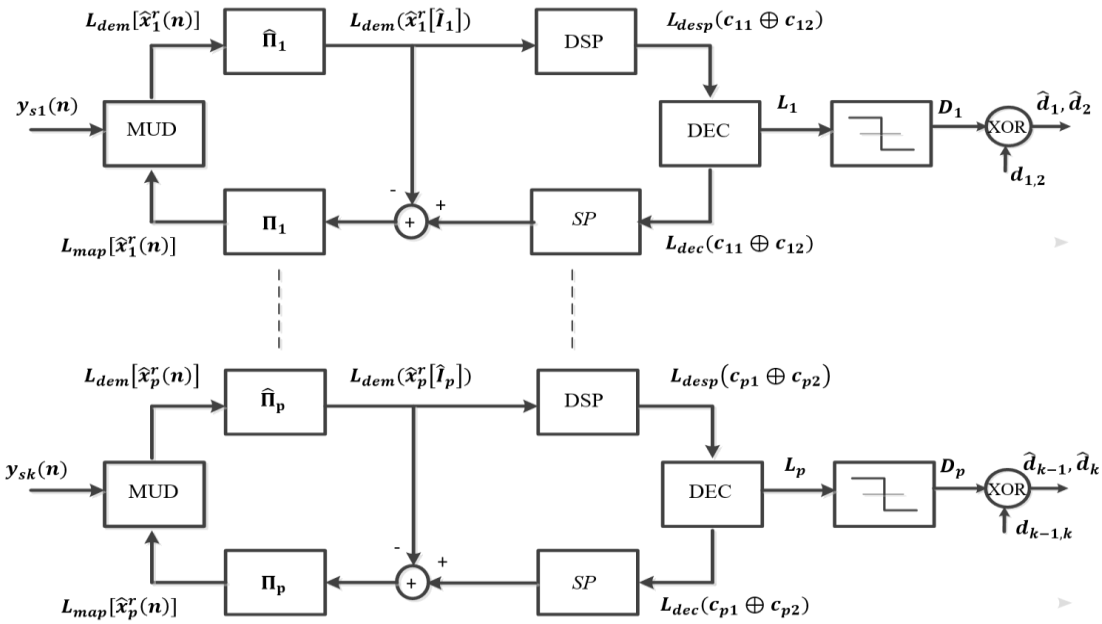

Figure 5.9 The receiver structure for the I-MUD based on PNC system.

$$L(\hat{x}_p^r(n)) = \underbrace{log\frac{p[y_{sk}(n)|\hat{x}_p^r(n)=1]}{p[y_{sk}(n)|\hat{x}_1^r(n)=0]}}_{L_{dem}[\hat{x}_p^r(n)]} + \underbrace{\frac{P_r[\hat{x}_p^r(n)=1]}{P_r[\hat{x}_p^r(n)=0]}}_{L_{map}[\hat{x}_p^r(n)]}, \tag{5.21}$$

where $p\left[y_{sk}\middle|\hat{x}_p^r(n) = 1 \text{ or } 0\right]$ represent the conditional probability distribution of the observed signal $y_{sk}(n)$, and $P_r\left[\hat{x}_p^r(n) = 1 \text{ or } 0\right]$ denotes the a priori probability of the n^{th} signal being transmitted. From the central limit theorem, the received signal can be approximated as a Gaussian distribution. Therefore, $p[.]$ of channel transition function can be defined as:

$$p[y|x] = \frac{1}{\sqrt{2\pi\sigma^2}}\ exp\left[\frac{[y - \sum_{k=1}^{K} h_k x_k]^2}{2\sigma^2}\right]. \tag{5.22}$$

Based on the BCJR algorithm, the estimation of the extrinsic LLRs can be computed as:

$$L[x_k(n)] = log\frac{\sum_{x_k=1} p(y|x_1(n), \ldots\ldots, x_k(n)) \prod_{\acute{k}\neq k} P_r(x_{\acute{k}}(n))}{\sum_{x_k=0} p(y|x_1(n), \ldots\ldots, x_k(n)) \prod_{\acute{k}\neq k} P_r(x_{\acute{k}}(n))}. \tag{5.23}$$

However, this optimum approach is usually prohibitively complicated and its complexity increases exponentially with K. Therefore, a sub-optimal low complexity chip-by-chip

approach is driven based on Gaussian Approach as follow. The chip-by-chip detection approach provides a coarse estimation of $\{x_k(n),\ \forall n,k\}$. To maintain low complexity, the coding and spreading are not considered in the MUD. For the first pair (i.e., P = 1), the (5.14) can be rewritten as:

$$y_{s1}(n) = \underbrace{h_1 \hat{x}_1^r(n)}_{\substack{The\ desired \\ signal}} + \underbrace{\sum_{\hat{p}\neq p}^{P} h_{\hat{p}}\ \ \hat{x}_{\hat{p}}^r(n) + w_k}_{\substack{The\ interference\ users \\ with\ noise}}, \tag{5.24a}$$

$$\eta_1(n) = \sum_{\hat{p}=1,\hat{p}\neq p}^{P} h_{\hat{p}}\ \hat{x}_{\hat{p}}^r(n) + w_k\ , \tag{5.24b}$$

where $\eta_1(n)$ indicates the distortion term that include MAI plus noise with respect to $\hat{x}_1^r(n)$. If the number of the users K is assumed to be large enough, the $\eta_1(n)$ can be approximated as a Gaussian random variable according to the central limit theorem. Thus, the total mean and variance of the distortion, respectively, for the p^{th} is expressed as:

$$E\big[\eta_p(n)\big] = \sum_{\hat{p}=1,\hat{p}\neq p}^{P} h_{\hat{p}}\ E\big[\ \hat{x}_{\hat{p}}^r(n)\big]. \tag{5.25a}$$

$$Var\big[\eta_p(n)\big] = \sum_{\hat{p}=1,\hat{p}\neq p}^{P} h_{\hat{p}}\ \ Var\big[\hat{x}_{\hat{p}}^r(n)\big] + \sigma^2. \tag{5.25b}$$

The mean and the variance of the random variable $\hat{x}_1^r(n)$ can be defined, respectively, as [202]:

$$\begin{aligned} E[\ \hat{x}_1^r(n)] &= \frac{P_r[\ \hat{x}_1^r(n)=1] - P_r[\ \hat{x}_1^r(n)=0]}{P_r[\ \hat{x}_1^r(n)=1] + P_r[\ \hat{x}_1^r(n)=0]} \\ &= \frac{\exp(\ \hat{x}_1^r(n)-1)}{\exp(\ \hat{x}_1^r(n)+1)} \\ &= tanh\big\{L_{map}\ [\ \hat{x}_1^r(n)]/2\big\}. \end{aligned} \tag{5.26a}$$

$$Var[\ \hat{x}_1^r(n)] = 1 - \{E[\ \hat{x}_1^r(n)]\}^2. \tag{5.26b}$$

By applying the Gaussian approximation to (5.24a), the estimation of the extrinsic LLRs can be computed as:

$$L_{dem}[\ \hat{x}_1^r(n)] = log\left[exp\left(-\frac{\big\{y_{s1}(n) - E\big(\eta_1(n)\big) - h_1\big\}^2}{2Var(\eta_1(n))}\right)/\sqrt{2\pi\sigma^2}\right]$$

$$- log\left[exp\left(-\frac{\{y_{s1}(n) - E(\eta_1(n)) + h_1\}^2}{2Var(\eta_1(n))}\right)/\sqrt{2\pi\sigma^2}\right],$$

$$L_{dem}[\hat{x}_1^r(n)] = 2\frac{h_1}{Var(\eta_1(n))}\left(y_{s1}(n) - E(\eta_1(n))\right). \quad (5.27)$$

However, the interference from the other users are eliminated by performing soft IC, the mean and variance (5.26a), (5.26b) respectively, are updated every iteration when the information exchange between the MUD and the DEC module. To restore the original ordering of sequences in the symbol, permutation of the received signal will be deinterleaving as ($L_{dem}[\hat{x}_1^r(\hat{I}_1)]$). Prior to deliver the priori LLR to the channel decoder, it is passed through the DSP module, where each group of deinterleaving chips within one-bit duration is summed up by means of the spreading factor and can be calculated as in (5.17). Based on the prior information, $L_{desp}[c_a(\ell)]$ from the k^{th} DSP module and the code constraints of the channel code, the k^{th} user's SISO channel decoder computes the a posteriori LLR of each code bit by performing APP decoding as:

$$L_{dec}[c_a(\ell)] = log\frac{p[c_a(\ell) = 1|L_{desp}[c_a(\ell)]]}{p[c_a(\ell) = 0|L_{desp}[c_a(\ell)]]}, \quad (5.28)$$

where c_a represents the XOR coded sequence($c_{11} \oplus c_{12}$). The output of decoder is then applied to *SP* module. This information is computed after interleaving as:

$$L_{map}[\hat{x}_1^r(I_1(j))] = s(l)L_{dec}[c_a(\ell)] - L_{dem}[\hat{x}_1^r(\hat{I}_1(j))]), \quad (5.29)$$

where $j = (\ell - 1)L_s + l$, $l = 1 \ldots L_s$ and $\ell = 1 \ldots . . L_d$. This functionality reduces the dependencies in the information flow and avoid that erroneous information propagates from iteration to another one. However, this extrinsic LLR are feedback to MUD to update a priori LLR by determining the new values for the mean and variance of the next iteration. The SISO channel decoder computes the a posteriori LLR of every information bits L_p, which is used to make a decision on decoded bits at the last iteration [208]. By performing

an XOR operation on the final estimation signal and a copy of the original information bit, each user can acquire the desired information send by other partner as in (5.19).

5.4 Multi-user PNC with iterative decoding over TWR-FSO link

The proposed system TWR-FSO PNC is extended to allow multiple pairs of user to swap their data between them within a single relay over FSO link when there is no direct link between them, with the aim of maximizing the utilization of network resources. Therefore, I-MUD for TWR-FSO PNC system alongside with chip-interleaving are also considered. This scheme referred to as I-MUD TWR-FSO PNC, which offers a bi-directional half-duplex relaying network that consists from K-users pairs communicate with each other via a single RN. Each pairs of users swap their information using RN during only two transmissions phases, the MA and BC. We further assume that each user node is equipped with single aperture antenna directed to the corresponding aperture at RN, whereas the RN consists of two directional antennas each having K antenna aperture directed to the corresponding users nodes. In the proposed system, the BER performance is evaluated for both log-normal and gamma-gamma fading channels.

5.4.1 The transmitter structure of the I-MUD TWR-FSO PNC system

The basic structure for the transmitter is shown in Figure 5.10. The input binary data sequence $d_k \in (0,1)$ is encoded by NRS ENC module at a rate R_c. The coded bit stream $c_k \in (0,1)$ is further encoded using SP module to produce s_k. The same spreading sequence is used for all user's node. Afterward, s_k is permutated by a unique user-specific interleave Π for each user, thus producing an interleave sequence $I_k \in (0,1)$. The interleave sequence is then used for modulating of an RF signal using BPSK modulation.

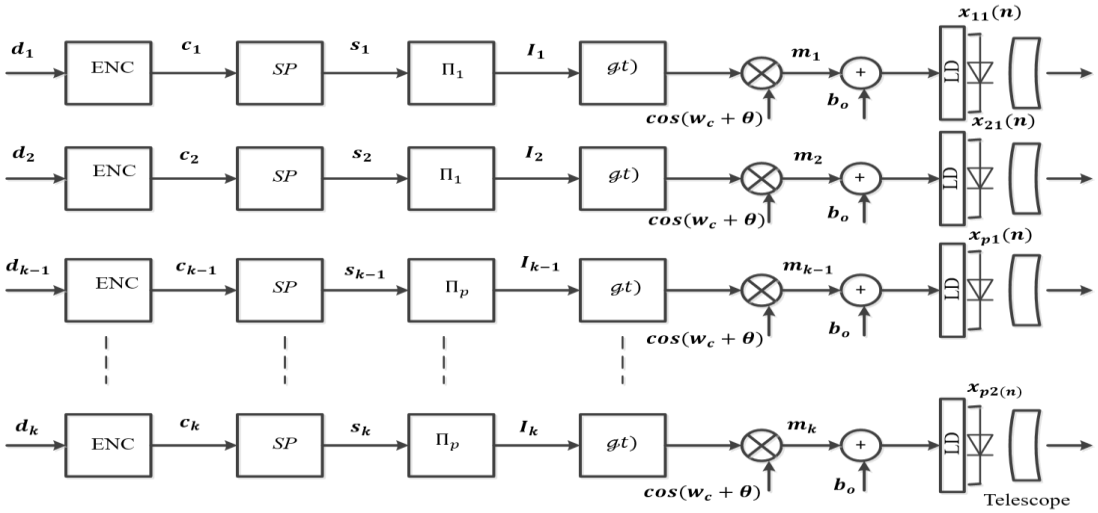

Figure 5.10 The transmitter structure for the I-MUD TWR-FSO PNC system, which consist from K users with unique interleaving sequence for each pairs.

An optical telescope is used to collimate and direct the optical beam into the channel for reception at the receiver.

5.4.2 The relay structure of the I-MUD TWR-FSO PNC system

In the MA phase all users are simultaneously transmitting to the RN, where the signals from all transmitters are collected and sent to the deinterleaved module. Figure 5.11 depicts the whole RN structure for the proposed system. Thus, the received electrical signal for the MA phase to the RN can be represented as:

$$y_r(n) = P_t R \sum_{k=1}^{K} h_k(1 + \zeta m_k(n)) + w_r(n). \tag{5.30}$$

Following the deinterleaving procedure, which is applied to the superimposed signal for each pairs of symbol, we have followed the same procedure in section 5.3.1.2 to extract the broadcast signal to the destination $\hat{x}_p^r$, which can combat the effects of the interference by performing network coding arithmetic at the physical layer on the received signal. However, the channel states from the RN to the destinations are assumed to be the same

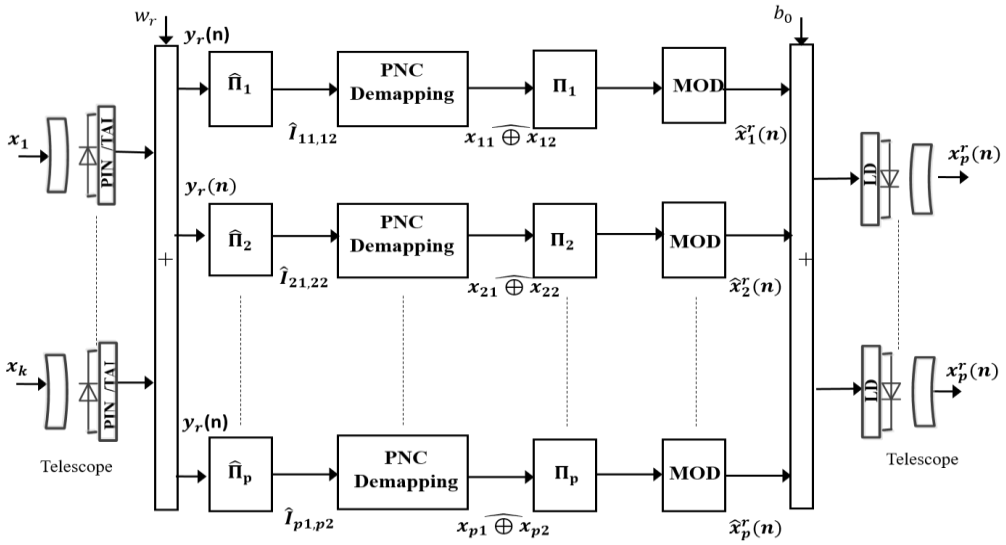

Figure 5.11 The RN structure for the proposed system, which is applied PNC demapping on the received signal after a pair of user seperated by their distict chip-level interleaving.

as in the first phase. A transmitter telescopes are used to collect, collimate and direct the optical radiation towards the receiver telescope at the other end of the channel.

5.4.3 The receiver structure of the I-MUD TWR-FSO PNC system

For the proposed system, the I-MUD technique is adopted to improve the system performance by eliminating the negative effect of each user on each other by iteratively exchanging the extrinsic information between the MUD and channel decoder. Figure 5.12 illustrates the receiver structure for I-MUD TWR-FSO PNC system. After receiving the optical signal and converted to the electrical, the I-MUD detection take place between the MUD and DEC units. All the procedure for the section 5.3.2.1 will be applied on the received signal to extract the desired information for each user.

5.5 Simulation Results

This section is carried out the comparative studies for both systems, namely, NI-MUD and I-MUD based PNC. Also, it presents the simulated BER performance of I-MUD

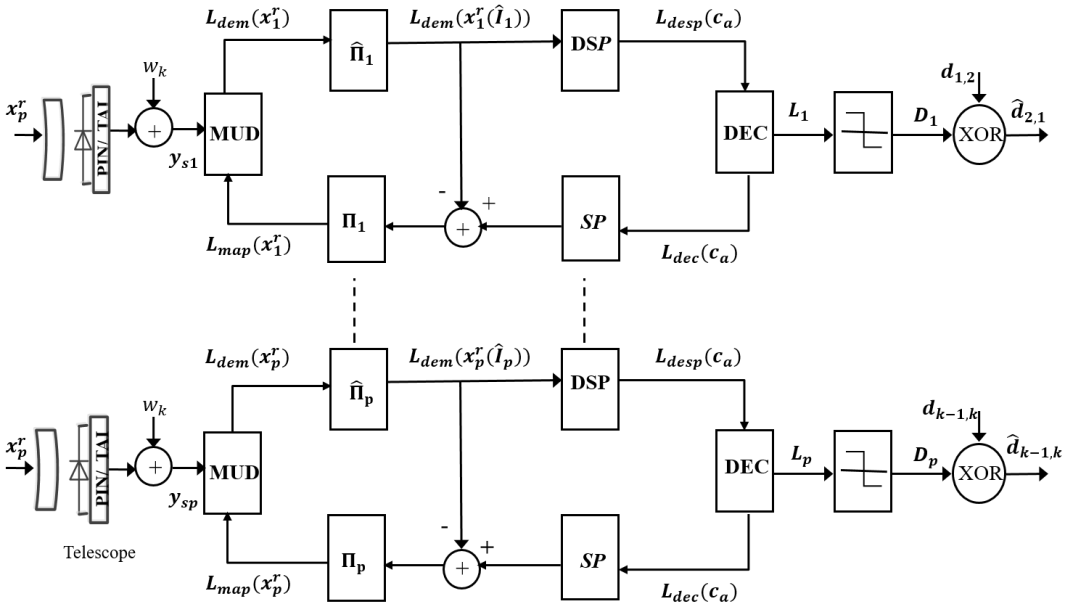

Figure 5.12 The block diagram of the receiver structure for the I-MUD TWR-FSO PNC system at BC phase. The input to the MUD model is the broadcast signal from the RN.

TWR-FSO PNC system. The simulation results reveal the ability of the proposed schemes to establish communication between the multiple nodes with a minimum number of transmission phases, even when the number of simultaneous users are increased. The simulation parameters considered in the BER analysis are defined in Table 5.1 for the aforementioned systems. The simulated BER performance of NI-MUD based PNC system is examined, where multiple users exchanging information via a RN over AWGN and Rayleigh fading channels as shown in Figure 5.13 (a and b), respectively. It can be

Table 5.1 Simulation parameters for the proposed systems under FSO link.

Parameter	**Typical value**
Code rate	$R_c = 0.5$
Constraint length	$K_c = 5$
Generator polynomial	$(23,35)_8$
Spreading rate	1/2,1/4,1/16
Laser wavelength	$\lambda = 1550$ nm
Photodetector responsivity	$R = 0.5$ A/W
Visibility (clear weather condition)	$V = 10$ km
Link distance	$L = 2$ km
Rytov variance	$\sigma_R^2 = 0.3, 1.6$
Number of users	$K = 4,6,8,10,12,14,16,20$

observed from the figures that BER performance improves with lower values of K. For example, at a BER of 10^{-3} and for $K = 6$, the SNR gains are ~7 and 18dB for the AWGN channel and Rayleigh fading channel, respectively. For $K = 10$, the SNR gains is much higher. Since there is no decoding process at the RN, therefore, any errors occurring at the RN within the MA phase is broadcasted to the destinations within the BC phase. However, the efficiency of NI-MUD system deteriorates with the growth of the number of users. To enhance the performance of NI- MUD system, the effectiveness of existence I-MUD technique with 5 iterations is investigated. The proposed I-MUD based PNC offers bi-directional communications between multiple pair of users via the RN with iterative decoding at the receiver. Thus, the simulated BER performance against the SNR for I-MUD PNC over AWGN and Rayleigh fading channels for a number of simultaneous users are presented in Figure 5.14 (a and b). It can be observed the positive effect of the I-MUD technique on the BER performance by reducing the effects of the Rayleigh fading channel.

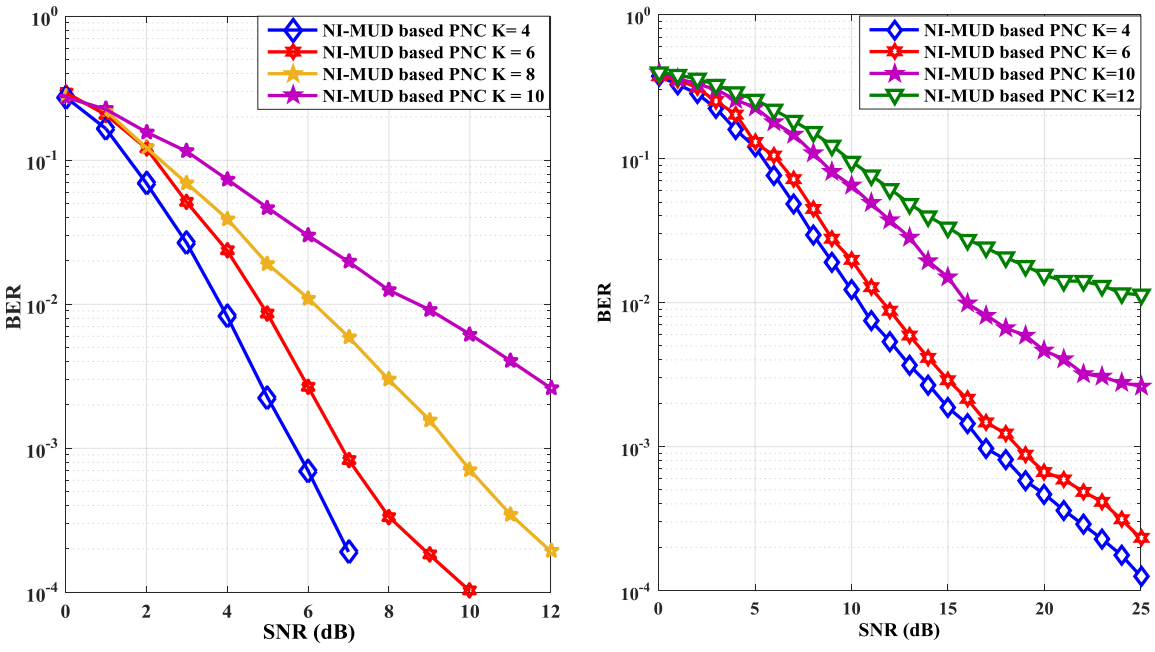

(a) (b)

Figure 5.13 The simulated BER performance against SNR for the NI-MUD-PNC system for $K = 4,6,8,10$ and 12 at $R_c = 1/2$ and spreading rate $= 1/8$ over: (a) AWGN, and (b) Rayleigh fading channel.

For example, at a BER of 10^{-3} for $K = 6$, the SNR gain is 18dB for NI-MUD over Rayleigh channel as shown in Figure 5.13(b). To achieve the same BER, 8dB of SNR is required for I-MUD over Rayleigh fading channel with $K = 6$, as displayed in Figure 5.14(b). Moreover, at higher values of K, the SNR penalties are higher for Rayleigh fading channel compared with AWGN channel. For example, at a BER of 10^{-4} and for $K = 16$, the SNR value for AWGN channel is 5.2dB, while for the same BER, the SNR value for Rayleigh fading is 11dB with $K = 20$, as shown in Figure 5.14 (a and b), respectively. However, for both systems, the sequence of the *SP* and the chip-level interleaving modules lead to propagate the signal over the channel in terms of bit-interleaving instead of symbol-interleaving. This feature is an advantage for the de-mapping process on the received superimposed signal at the RN. Furthermore, it can be seen that the simulated results for the I-MUD based PNC offer improved BER performance compared to the NI-MUD based PNC system. This is because the new model

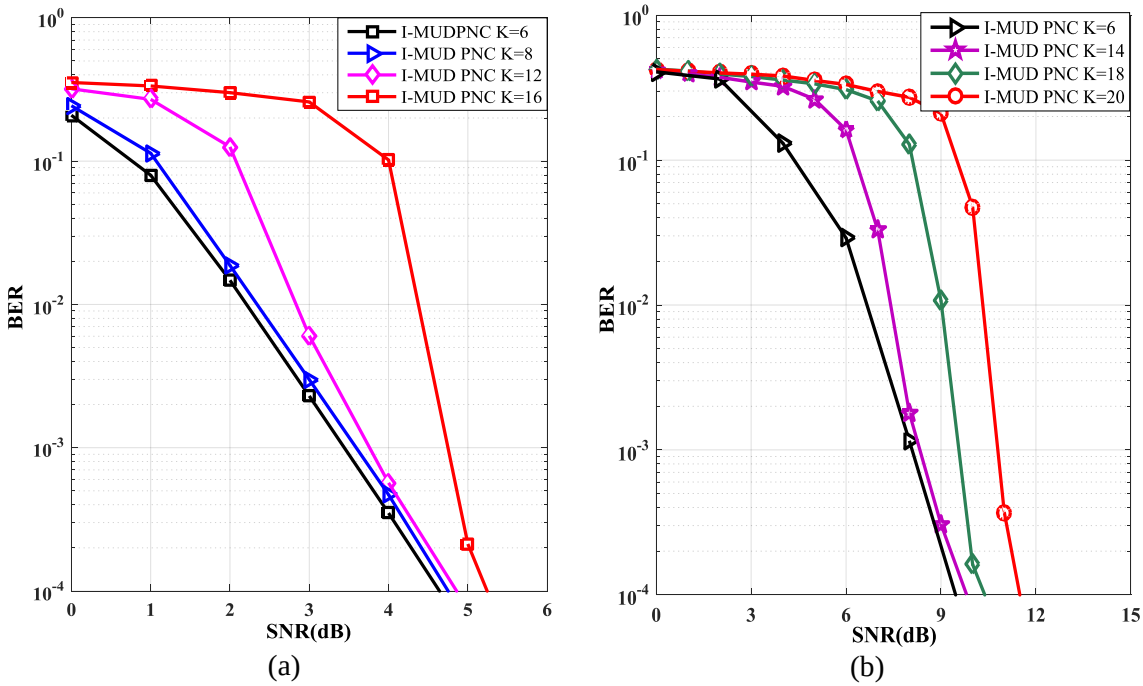

(a) (b)

Figure 5.14 The simulated BER performance against SNR of the I-MUD PNC for $K = 6,8,12,14,16,20$ at $R_c = 1/2$ and spreading rate $= 1/4$ with 5 iterations over : (a) AWGN, and (b) Rayleigh fading channels.

not only depends on the PNC exclusive demodulation at the RN but also on the iterative detection processing to mitigate the interference. For instance, to achieve a BER of 10^{-4} and for $K = 6$ users, SNR of ~4.5 and 10dB are needed for I-MUD and NI-MUD based PNC system for AWGN channel, as shown in Figures 5.14(a) and 5.13(a), respectively. Additionally at a BER of 10^{-3} and $K = 6$, the I-MUD based PNC system require 8dB of lower SNR compared to the NI-MUD based PNC system for Rayleigh fading channel. Finally, the performance of I-MUD TWR-FSO PNC in terms of BER is also investigated, where multiple source nodes exchanging information via a single RN over FSO link when there is no direct link between them. Figure 5.15(a) presents the simulated BER performance as a function of SNR for the proposed system with different number of users $K = 4, 12, 20$. The simulated BER performance of the TWR-FSO PNC is also plotted as reference. The simulation is carried out under the weak atmospheric turbulence regime characterized by $\sigma_R^2 = 0.3$ considering the atmospheric loss and pointing errors. The simulation result shows that there is an improvement in the BER performance for the proposed system compared to TWR-FSO PNC albeit the increased number of simultaneous users. For instance, at a BER of 10^{-4} and for $K = 4$ for I-MUD FSO based PNC, the SNR gain is ~14dB compared with the TWR-FSO PNC system. The SNR penalties are lower by ~10 and ~7dB for $K = 12$ and 20, respectively, with respect to TWR-FSO PNC. Furthermore, Figure 5.15(b) shows the system performance under strong turbulence for different number of users $K = 4, 8, 14$. It can be observed that the proposed system provides a good performance although the number of the concurrent users is growing. For example, at BER 10^{-4}, the SNR gains are 28, 25 and 22dB with respect to the TWR-FSO PNC system. The improvement detected is because the proposed model uses

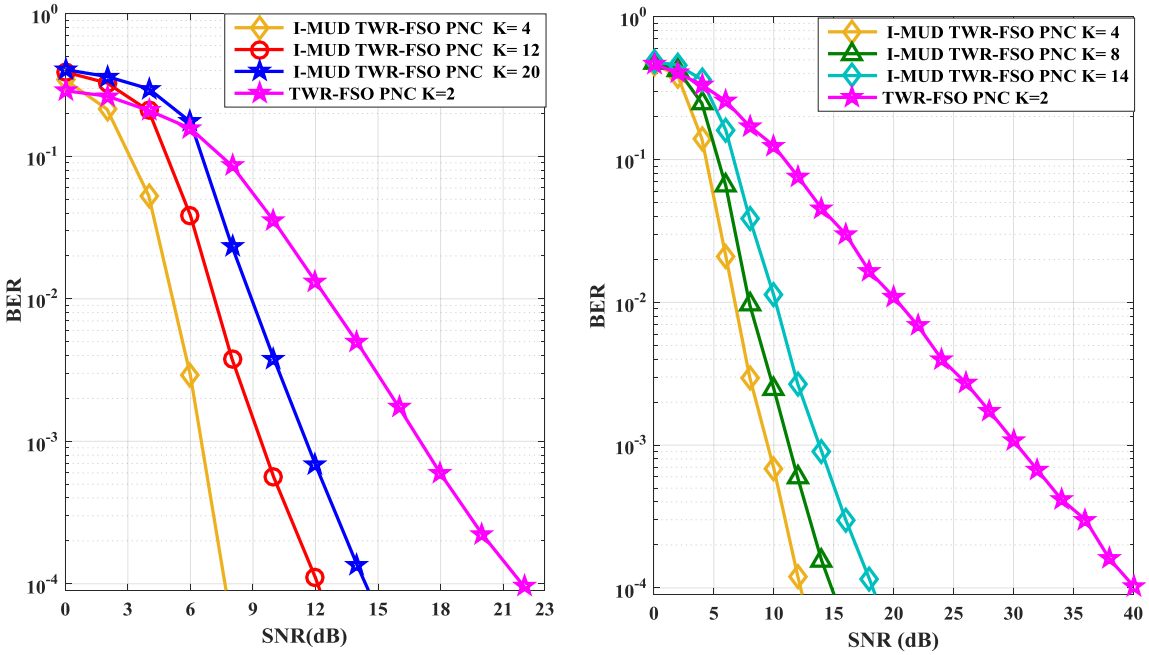

(a) (b)

Figure 5.15 The simulated BER performance against SNR for TWR-FSO PNC and I-MUD TWR-FSO PNC systems for $K = 4,8,12,14,20$, $L = 2$ km, $\lambda = 1550$ nm under clear weather condition at $V = 10$ km over :(a) weak turbulence, and (b) strong turbulence.

relay-assisted FSO, which performs PNC mapping at the RN. This is leads to enhanced channel capacity by reducing the transmitting information between multiple users in two phases. Additionally, adopting the I-MUD and interleaving techniques in the proposed system does reduce the error rate at the destination.

5.6 Summary

The challenge of increasing the number of communication nodes in PNC system that exchanges their information through an intermediate node was considered the main contribution of this chapter. Towards this goal, iterative channel decoding with chip-interleaving were adopted. One of the powerful of MUD technique was embraced owing to its ability to mitigate the interference, which is independent of the number of the communication nodes by utilizing chip-by-chip detection. The role of the interleaver alongside with its mechanism was described in this chapter. The most popular multiple

access techniques and its characteristics on communication signals were also reviewed in this chapter. Emphasis was placed on the I-MUD with TWRC employing PNC mapping at the intermediate node. The basic structure of the NI-MUD based PNC was described and the fundamental architecture of I-MUD based PNC and its performance in AWGN and Rayleigh fading channel were also highlighted. From the preliminary simulation results, the combination of PNC technique with the chip-level interleaving and iterative decoding showed an improved BER performance compared to the NI-MUD PNC and effectively alleviated the interference due to multiple users in the MA phase. For example, at a BER of 10^{-3} and $K = 6$, the I-MUD based PNC system required 8dB of lower SNR compared to the NI-MUD based PNC system for Rayleigh fading channel. The same structure was extended to perform I-MUD on the TWR-FSO PNC system, where multiple users exchanging information via a single RN over FSO link. The block diagram of the I-MUD TWR-FSO PNC together with the performance of the system under log-normal and gamma-gamma distribution channel in terms of the BER were furthermore illustrated in this chapter. The results showed that the proposed relaying strategy was a viable solution for heavy loaded multiuser TWR-FSO to mitigate the interference and the scintillation effects when the relay applied the strategy of the PNC mapping for FSO channels combined with I-MUD and chip-interleaving techniques. It was also demonstrated that a larger number of simultaneous users could be supported with this new scheme in establishing a communication link between multiple pairs of nodes in two time slots, thereby improving the channel capacity. For instance, at a BER of 10^{-6} and for $K = 14$, the SNR gain was 18dB compare to that of TWR-FSO PNC system over strong turbulence under clear weather condition.

Chapter 6

CONCLUSIONS AND FUTURE WORK

6.1 Conclusions

In this research project, the communication technologies in relaying system with physical layer network coding were considered, especially for TWRC system. For end-to-end PNC technique, a special demodulation-and-forward strategy was applied, where the RN did not perform any encoding or decoding of the demapped binary vector, which reduced the complexity of the system for constructing larger networks. When PNC scheme is applied in TWRC systems, the transmission time slot needing to complete data exchange between two nodes can be reduced, which in turn boosts the network throughput.

On other hand, FSO communication is a LOS optical transmission technique through the atmosphere, which provides a cost-effective and easy-to-install alternative to fiber optics. However, a major degrading factor in FSO communication links is the atmospheric turbulence. To mitigate the degrading effect of turbulence-induced fading, TWR-FSO was proposed in the literature as a very promising technique to overcome atmospheric turbulence degradations. The fact that fading variance is distance-dependent in FSO systems constitutes a major difference between wireless RF and wireless optical systems.

Therefore, multi-hop FSO transmission elegantly exploit the shorter distance in the resulting hops and brings substantial improvements against the degrading effects of turbulence-induced fading. However, this thesis started by reviewing and discussion the fundamental principles of P2P FSO and PNC technique with its building blocks to be able to carry out the objectives of this research.

To benefit from the advantage of the PNC technique, TWR-FSO based PNC technique over a Gaussian channel model of the IM/DD system was proposed. The BER performance of the new model was carried out to investigate the TWR-FSO communication link impairments imposed by the combined effects of atmospheric loss, turbulence and pointing errors. In particular, important link design criteria were jointly considered, which consist of the transmitter beam width, link range, and optical wavelength under clear weather conditions. Turbulent atmospheric channel causes the intensity of an optical beam travelling through it was further reviewed and two most reported models, namely, log-normal and gamma-gamma, were described and their respective PDFs presented. These models were later used to model the statistical behaviour of the received signal for short to very long range TWR-FSO system. It was observed from the preliminary results that the performance of the proposed system had a slightly worse BER compared to that of P2P FSO system. However, it increased the network throughput by reducing the transmission time slot needing to complete data exchange between the two FSO nodes by exploiting the functionality of the PNC technique. In this research work, the end-to-end basis was considered in PNC technique, where the RN performed demapping/modulation on the superimposed received signal, which reduced the complexity of the system but results in a degradation of performance at the destination nodes due to un-corrected errors at the RN. Therefore, this project

addressed coded end-to-end PNC for the TWR-FSO system. CC was adopted for P2P FSO and TWR-FSO PNC systems to combat the deleterious effect of the wireless channels by saving the message being transmitted, so increasing the reliability of the information. The simulation results showed that substantial gains in SNR were obtained, especially under weak turbulence conditions for coded P2P FSO. For instance, at a BER of 10^{-4}, the coding gain were 10dB and 5dB of SNR over weak and strong turbulence, respectively. Similarly, an enhancement BER performance was obtained for the coded TWR-FSO PNC system. The proposed system offered coding gains about 4dB and 10dB of SNR at a BER 10^{-4} compared with uncoded one over weak and strong turbulence, respectively. Thereafter, an iteratively coding was used, where the iteration takes place between the soft demapper and decoder. Therefore, joint investigation of the effects of BICM-ID combined with PNC on the performance of P2P FSO and TWR-FSO communication systems was also presented, in order to examine the resulting impact of the iterative coding on the BER of the TWR-FSO link, under the influences of atmospheric turbulence. The numerical results were obtained in terms of the BER, which showed that the system had improved performance compared to that of uncoded and convolutional code systems for TWR-FSO PNC. It was delivered a coding gain about 10dB and 16dB of SNR with respect to the uncoded and convolutional code systems, respectively. The issue of increasing the number of users in PNC model that exchanged their data information simultaneously was manipulated. This is done by adopting the functionality of I-MUD technique joint with chip-level interleaving. Comparative studies between the I-MUD and NI-MUD systems based PNC was also outlined when the number of communication nodes increased up to two. The proposed scheme was simulated to investigate the impact of combination the PNC technique with the chip-level interleaving

and iterative decoding showed an improved BER performance compared to the NI-MUD based PNC. It effectively alleviated the interference due to multiple users in the MA phase and combats the effect of fading channel. From the preliminary results, it showed that at BER of 10^{-4}, SNR improvement of ~5.5dB was observed for I-MUD based PNC with respect to the NI-MUD system over AWGN channel. Whereas over Rayleigh fading channel for I-MUD based PNC, at a BER of 10^{-3}, the SNR improvement was 8 dB compared to that of NI-MUD system when the $K = 6$. Additionally, I-MUD technique was also adopted with the proposed system TWR-FSO PNC, where multiple nodes could exchange their information through the RN over NLOS FSO link. The proposed system showed improved BER performance compared to TWR-FSO PNC even for higher number of simultaneous users. For instance, for weak turbulence regime and at a BER of 10^{-4}, we observed ~8dB gain for SNR with respect to TWR-FSO PNC when the $K = 20$.

6.2 Recommendations for Future Work

This thesis has contributed to study the design of the TWR-FSO communication system that employing PNC mapping at the intermediate node based upon plane beam and IM/DD technique with BPSK modulation, which has progressively uncovered more research opportunities and areas of improvement pertaining to the system under study.

- As a straight forward progression of the proposed TWR-FSO PNC system presented here, the study and experimental demonstration of the proposed system can prove very useful. This, potentially, will provide interesting findings regarding the integration of PNC technique with TWR-FSO links. This experiment can further prove the suitability/viability of PNC technique as a tool for increasing communication systems throughput.

- A comprehensive design benchmark of TWR-FSO PNC links was presented in Chapter 3, taking into account the effect of different link design criteria (beam width, link range and wavelength). However, another mitigation approaches, namely, aperture averaging, can be incorporated to the existing system, in order to obtain the best BER performance under different atmospheric channel effects resulting from turbulence-induced scintillations and pointing error. Thereafter, more extensive simulation studies are required to observe and validate the performance of the proposed system.

- In the proposed system presented in Chapter 4, the trade-off between the system performance and interleaver size can be exploited to offer variable QoS suitable for wireless multimedia systems. Adaptability can also be achieved by varying the code rate, the encoder constraint length, and the number of decoder iterations. More advanced iterative FEC techniques such as LDPC and TC codes for TWR-FSO PNC can be used and their performance should be compared against BICM-ID.

- Another future work is the design of the component encoders using an ExIT chart to predict the performance of the iterative decoding, where the BER estimation based ExIT chart was originally used to design the encoder of the iterative turbo-code.

- This research project concentrated primarily on multi-user communication for both downlink and uplink in Chapter 5. The emphasis should be placed on techniques such as OFDM to mitigate multipath and the results should be compared with single carrier PNC system.

References

[1] H. Willebrand and B. S. Ghuman, *Free space optics: enabling optical connectivity in today's networks*: SAMS publishing, 2002.

[2] L. C. Andrews and R. L. Phillips, *Laser beam propagation through random media* vol. 52: SPIE press Bellingham, WA, 2005.

[3] A. Tympas, "The Victorian Internet: The Remarkable Story of the Telegraph and the Nineteenth Century's On-Line Pioneers [Book Review]," *IEEE Annals of the History of Computing,* vol. 23, pp. 63-64, 2001.

[4] J. M. Dilhac, "The telegraph of glaud chappe-an aoptical telecommunication network for the XVIIITH century," *Institut National des Sciences Appliquées de Toulouse.*

[5] A. G. Bell, "Selenium and the photo phone," *Nature,* pp. 500–503, 1880.

[6] S. Hranilovic, *Wireless optical communication systems*: Springer Science & Business Media, 2006.

[7] F. E. Goodwin, "A review of operational laser communication systems," *Proceedings of the IEEE,* vol. 58, pp. 1746-1752, 1970.

[8] H. Hemmati, "Interplanetary laser communications," *Optics and Photonics News,* vol. 18, pp. 22-27, 2007.

[9] Z. Sodnik, B. Furch, and H. Lutz, "Free-space laser communication activities in europe: SILEX and beyond," *19th Annual Meeting of the IEEE* in *Lasers and Electro-Optics Society (LEOS),*pp. 78-79, 2006.

[10] H. Hemmati, *Deep space optical communications* vol. 11: John Wiley & Sons, 2006.

[11] J. Montgomery, "Free-space optics seen as viable alternative to cable," *Lightwave (Analyst corner),* pp. 43-44, 2004.

[12] I. I. Kim, B. McArthur, and E. Korevaar, "Comparison of laser beam propagation at 785 nm and 1550 nm in fog and haze for optical wireless communications," in *proc. SPIE,* pp. 26-37, 2001.

[13] M. Bettayeb and S. F. A. Shah, "State of the art ultra-wideband technology for communication systems: a review," *10th IEEE International Conference on Electronics, Circuits and Systems (ICECS),* vol. 3, pp. 1276-1279, 2003.

[14] I. K. Son, "Design and optimization of free space optical networks," Auburn University, 2010.

[15] M. O. Zaatari, "Wireless optical communications systems in enterprise networks," *The Telecommunications Review,* pp. 49-57, 2003.

[16] I. Kim, "10 G FSO systems position technology for the future,"" *Lightwave online,* pp. 19-21, 2009.

[17] D. K. Borah, A. C. Boucouvalas, C. C. Davis, S. Hranilovic, and K. Yiannopoulos, "A review of communication-oriented optical wireless systems," *Journal on Wireless Communications and Networking* (*EURASIP),* vol. 2012, pp. 1-28, 2012.

[18] M. Ijaz, "Experimental characterisation and modelling of atmospheric fog and turbulence in FSO," Northumbria University, 2013.

[19] G. Nykolak, P. F. Szajowski, G. Tourgee, and H. Presby, "2.5 Gbit/s free space optical link over 4.4 km," *Electronics Letters,* vol. 35, pp. 578-579, 1999.

[20] P. L. Eardley and D. R. Wisely, "1 Gbit/s optical free space link operating over 40 m system and applications," *IEEE Proceedings - Optoelectronics,* vol. 143, pp. 330-333, 1996.
[21] S. R. Forrest, "Optical detectors: Three contenders: Depending on the application, the photoeonductor, p-i-n diode, or avalanche photodiode may prove the best choice," *IEEE Spectrum,* vol. 23, pp. 76-85, 1986.
[22] K. Wilson and M. Enoch, "Optical communications for deep space missions," *IEEE Communications Magazine,* vol. 38, pp. 134-139, 2000.
[23] O. Bouchet, H. Sizun, C. Boisrobert, and F. De Fornel, *Free-space optics: propagation and communication* vol. 91: John Wiley & Sons, 2010.
[24] T. S. Rappaport, *Wireless Communications : Principles and Practice,* Prentic Hall, 2001.
[25] L. Ly-Minh-Duy, T. Kah Chan, and K. H. Li, "Survey on diversity-combining techniques for interference suppression in fast frequency hopping systems," *IET Communications,* vol. 9, pp. 1501-1509, 2015.
[26] A. Andrawes and R. Nordin, "Survey on performance of adaptive modulation scheme with cooperative diversity in wireless systems," *1st International Conference on Telematics and Future Generation Networks (TAFGEN),* pp. 65-70, 2015.
[27] Q. Zhang, E. Liu, and K. K. Leung, "Cooperative communication and networking," *Johns Hopkins APL Technical Digest,* vol. 30, pp. 144-150, 2011.
[28] V. D. Meulen and C. Edward, "Three-terminal communication channels," *Advances in Applied Probability,* pp. 120-154, 1971.
[29] T. Cover and A. E. Gamal, "Capacity theorems for the relay channel," *IEEE Transactions on Information Theory,* vol. 25, pp. 572-584, 1979.
[30] J. N. Laneman, D. N. C. Tse, and G. W. Wornell, "Cooperative diversity in wireless networks: Efficient protocols and outage behavior," *IEEE Transactions on Information Theory,* vol. 50, pp. 3062-3080, 2004.
[31] M. N. Tehrani, M. Uysal, and H. Yanikomeroglu, "Device-to-device communication in 5G cellular networks: challenges, solutions, and future directions," *IEEE Communications Magazine,* vol. 52, pp. 86-92, 2014.
[32] P. Li and S. Guo, "Literature survey on cooperative device-to-device communication," in *Cooperative Device-to-Device Communication in Cognitive Radio Cellular Networks,* pp. 7-12, 2014.
[33] Q. Li, R. Q. Hu, Y. Qian, and G. Wu, "Cooperative communications for wireless networks: techniques and applications in LTE-advanced systems," *IEEE Wireless Communications,* vol. 19, p. 1, 2012.
[34] M. Nokleby and B. Aazhang, "Cooperative compute-and-forward," *IEEE Transactions on Wireless Communications,* vol. 15, pp. 14-27, 2016.
[35] F. Mansourkiaie and M. H. Ahmed, "Cooperative routing in wireless networks: a comprehensive survey," *IEEE Communications Surveys & Tutorials,* vol. 17, pp. 604-626, 2015.
[36] A. Sendonaris, E. Erkip, and B. Aazhang, "User cooperation diversity. Part I. system description," *IEEE Transactions on Communications,* vol. 51, pp. 1927-1938, 2003.
[37] S. I. Bross and M. A. Wigger, "On the relay channel with receiver-transmitter feedback," *IEEE Transactions on Information Theory,* vol. 55, pp. 275-291, 2009.

[38] D. Gunduz, A. Yener, A. Goldsmith, and H. V. Poor, "The multiway relay channel," *IEEE Transactions on Information Theory*, vol. 59, pp. 51-63, 2013.
[39] C. E. Shannon, "Two-way communication channels," *4th Berkeley Symp. Math. Stat. Prob*, pp. 611-644, 1961.
[40] E. Yilmaz, R. Knopp, and D. Gesbert, "Interference two-way relay channel with three end-nodes," *ArXiv preprint arXiv:1102.3120*, 2011.
[41] B. Rankov and A. Wittneben, "Spectral efficient protocols for half-duplex fading relay channels," *IEEE Journal on Selected Areas in Communications*, vol. 25, pp. 379-389, 2007.
[42] B. Rankov and A. Wittneben, "Achievable rate regions for the two-way relay channel," *IEEE International Symposium on Information Theory*, pp. 1668-1672, 2006.
[43] R. Ahlswede, N. Cai, S. Y. R. Li, and R. W. Yeung, "Network information flow," *IEEE Transactions on Information Theory*, vol. 46, pp. 1204-1216, 2000.
[44] S. L. Zhang, S. C. Liew, and P. P. Lam, "Hot topic: physical-layer network coding," *Mobicom*, pp. 358-365, 2006.
[45] S. Katti, S. Gollakota, and D. Katabi, "Embracing wireless interference: analog network coding," *ACM SIGCOMM Computer Communication Review*, pp. 397-408, 2007.
[46] C. E. Shannon, "A mathematical theory of communication," *The Bell System Technical Journal*, vol. 27, pp. 379-423, 1948.
[47] S. C. Liew, S. Zhang, and L. Lu, "Physical-layer network coding: tutorial, survey, and beyond," *Physical Communication*, vol. 6, pp. 4-42, 2013.
[48] S. Zhang and S. C. Liew, "Channel coding and decoding in a relay system operated with physical-layer network coding," *IEEE Journal on Selected Areas in Communications*, vol. 27, pp. 788-796, 2009.
[49] D. To and J. Choi, "Convolutional codes in two-way relay networks with physical-layer network coding," *IEEE Transactions on Wireless Communications*, vol. 9, pp. 2724-2729, 2010.
[50] X. Wu, C. Zhao, and X. You, "Joint LDPC and physical-layer network coding for asynchronous bi-directional relaying," *IEEE Journal on Selected Areas in Communications*, vol. 31, pp. 1446-1454, 2013.
[51] K. Xu, Z. Lv, Y. Xu, D. Zhang, X. Zhong, and W. Liang, "Joint physical network coding and LDPC decoding for two way wireless relaying," *Physical Communication*, vol. 6, pp. 43-47, 2013.
[52] N. Balasuriya and C. B. Wavegedara, "Low-complexity LDPC decoder for physical layer network coded multi-way wireless relay systems," *10th IEEE International Conference on Industrial and Information Systems (ICIIS)*, pp. 226-231, 2015.
[53] L. Xu, Z. Shengli, and Q. Gongbin, "Mapping and coding design for channel coded physical-layer network coding," *International Workshop on High Mobility Wireless Communications (HMWC)*, pp. 120-125, 2013.
[54] Z. Chen, B. Xia, and H. Liu, "Multi-level physical-layer network coding for Gaussian two-way relay channels," *IEEE Wireless Communications and Networking Conference (WCNC)*, pp. 2422-2427, *2013*,.
[55] C. Li, Y. Yakufu, Y. Xiaojun, and S. Zichao, "Design of BICM-ID for two-way relay channels," *International Workshop on High Mobility Wireless Communications (HMWC)*, pp. 11-15, *2015*.

[56] L. C. Zhou and C. D. Xiu, "A joint design of physical layer network coding and channel coding for wireless networks," *International Conference on Computer Science and Electronics Engineering (ICCSEE)*, pp. 312-316, 2012.

[57] S. Shukla, V. T. Muralidharan, and B. S. Rajan, "Wireless network-coded three-way relaying using Latin Cubes," *23rd International Symposium on Personal Indoor and Mobile Radio Communications (PIMRC)*, pp. 197-203 , 2012.

[58] S. Shukla and B. S. Rajan, "Wireless network-coded four-way relaying using Latin Hyper-Cubes," in *Wireless Communications and Networking Conference (WCNC)*, pp. 2410-2415, 2013.

[59] M. Chen and A. Yener, "Multiuser two-way relaying for interference limited systems," *8th IEEE International Conference on Communication (ICC)*, pp. 3883-3887, 2008.

[60] S. Mao, J. Kim, and J. Lee, "Multi-user analog network coding with spread spectrum," *75th IEEE* in *Vehicular Technology Conference (VTC)*, pp. 1-5, 2012.

[61] F. Dong, L. Peng, A. Burr, and R. d. Lamare, "Physical-layer network coding based interference exploitation strategy for multi-user hierarchical wireless networks," *18th European Wireless Conference* (*EW)*, pp. 1-6, 2012.

[62] H. Qian, S. C. Chan, K. King-Tim, P. Li, and W. Peng, "A QoS architecture for IDMA-based multi-service wireless networks," *7th IEEE International Conference on Communications (ICC)*, pp. 5070-5075, 2007.

[63] I. Pupeza, A. Kavcic, and L. Ping, "Efficient generation of interleavers for IDMA," *6th IEEE International Conference on Communications (ICC)*, pp. 1508-1513, 2006.

[64] F. Lenkeit, C. Bockelmann, D. Wubben, and A. Dekorsy, "IRA code design for IDMA-based multi-pair bidirectional relaying systems," *IEEE Globecom Workshops (GC Wkshps)*, pp. 241-246, *2013*.

[65] L. K. Chen, M. Li, and S. C. Liew, "Breakthroughs in photonics 2014: optical physical-layer network coding, recent developments, and challenges," *IEEE Photonics Journal*, vol. 7, pp. 1-6, 2015.

[66] W. Qike, T. Kam-Hon, C. Lian-Kuan, and L. Soung-Chang, "Physical-layer network coding for VPN in TDM-PON," *IEEE Photonics Technology Letters*, vol. 24, pp. 2166-2168, 2012.

[67] C. C. K. Chan and L. Zhixin, "Physical-layer network coding in optical networks," *12th International Conference on Optical Communications and Networks (ICOCN)*, pp. 1-4, 2013.

[68] Z. Liu, M. Li, L. Lu, C. K. Chan, S. C. Liew, and L. K. Chen, "Optical physical-layer network coding," *IEEE Photonics Technology Letters*, vol. 24, pp. 1424-1427, 2012.

[69] L. Zhixin, L. Lu, Y. Lizhao, C. Chun-Kit, and L. Soung-Chang, "Optical physical-layer network coding over fiber-wireless," *39th European Conference and Exhibition on Optical Communication (ECOC)*, pp. 1-4, 2013.

[70] A. Nosratinia, T. E. Hunter, and A. Hedayat, "Cooperative communication in wireless networks," *IEEE Communications Magazine*, vol. 42, pp. 74-80, 2004.

[71] R. Huang, C. Feng, T. Zhang, and W. Wang, "Energy-efficient relay selection and power allocation scheme in AF relay networks with bidirectional asymmetric traffic," *14th International Symposium on Wireless Personal Multimedia Communications (WPMC)*, pp. 1-5, 2011,.

[72] Y. Li, Z. Zheng, M. Zhao, Y. Chen, and C. Liu, "Energy efficient design for two-way AF relay networks," *International Journal of Antennas and Propagation*, vol. 2014, 2014.
[73] R. Hu, C. Hu, J. Jiang, X. Xie, and L. Song, "Full-duplex mode in amplify-and-forward relay channels: Outage probability and ergodic capacity," *International Journal of Antennas and Propagation*, vol. 2014, 2014.
[74] A. Sheikh and A. Olfat, "Diversity achieving schemes for two-way multi-antenna relay networks in Nakagami-m fading," *IET Communications*, vol. 9, pp. 1561-1574, 2015.
[75] S. Sahin and U. Aygolu, "Physical-layer network coding with limited feedback based on decoding at relay," *5th International Conference on Signal Processing and Communication Systems (ICSPCS)*, pp. 1-8, 2011.
[76] A. A. A. Haija and M. Vu, "Improving transmission rate for the two-way relay channel by user cooperation," *14th IEEE Canadian Workshop on Information Theory (CWIT)*, pp. 195-199, 2015.
[77] A. C. T. Wang, G. Giannakis, and J. Laneman, "High-performance cooperative demodulation with decode-and-forward relays," *IEEE Transactions on Communications*, vol. 55, pp. 830-830, 2007.
[78] E. Soleimani-Nasab, A. Kalantari, and M. Ardebilipour, "Performance analysis of selective DF relay networks over Rician fading channels," *IEEE Symposium on Computers and Communications (ISCC)*, pp. 117-122, 2011.
[79] R. Baldemair, E. Dahlman, G. Fodor, G. Mildh, S. Parkvall, Y. Selen, *et al.*, "Evolving wireless communications: addressing the challenges and expectations of the future," *IEEE Vehicular Technology Magazine*, vol. 8, pp. 24-30, 2013.
[80] L. Hanzo, H. Haas, S. Imre, D. O. Brien, M. Rupp, and L. Gyongyosi, "Wireless myths, realities, and futures: from 3G/4G to optical and quantum wireless," *IEEE Proceedings*, vol. 100, pp. 1853-1888, 2012.
[81] K. Tsukamoto, A. Hashimoto, Y. Aburakawa, and M. Matsumoto, "The case for free space," *IEEE Microwave Magazine*, vol. 10, pp. 84-92, 2009.
[82] A. Bekkali, C. B. Naila, K. Kazaura, K. Wakamori, and M. Matsumoto, "Transmission analysis of OFDM-based wireless services over turbulent radio-on-FSO links modeled by gamma-gamma distribution," *IEEE Photonics Journal*, vol. 2, pp. 510-520, 2010.
[83] N. H. M. Noor, A. W. Naji, and W. Al-Khateeb, "Theoretical analysis of multiple transmitters/receivers on the performance of Free Space Optics (FSO) link," *IEEE International Conference on Space Science and Communication (IconSpace)*, pp. 291-295, 2011.
[84] T. Plank, M. Czaputa, E. Leitgeb, S. S. Muhammad, N. Djaja, B. Hillbrand, *et al.*, "Wavelength selection on FSO-links," *Proceedings of the 5th European Conference on Antennas and Propagation (EUCAP)*, pp. 2508-2512, 2011.
[85] A. K. Majumdar and J. C. Ricklin, *Free-space laser communications: principles and advances* vol. 2: Springer Science & Business Media, 2010.
[86] X. Wu, P. Liu, and M. Matsumoto, "A Study on atmospheric turbulence effects in full-optical free-space communication systems," *6th International Conference on Wireless Communications Networking and Mobile Computing (WiCOM)*,pp. 1-5, 2010.
[87] M. S. Khan, M. S. Awan, S. S. Muhammad, V. Kvicera, M. Grabner, C. Capsoni, *et al.*, "Linearity in optical attenuations for Free-space optical links in continental

fog," *Proceedings of the 5th European Conference on Antennas and Propagation (EUCAP),* pp. 2504-2507, 2011.
[88] S. A. Zabidi, M. R. Islam, W. A. Khateeb, and A. W. Naji, "Investigating of rain attenuation impact on free space optics propagation in tropical region," *4th International Conference On Mechatronics (ICOM),*pp. 1-6, 2011.
[89] M. N. Khan and W. G. Cowley, "Signal dependent Gaussian noise model for FSO communications," in *Communications Theory Workshop (AusCTW),* pp. 142-147, 2011.
[90] J. Libich and S. Zvanovec, "Utilization of route diversity in free-space optical networks," *IEEE Avionics, Fiber- Optics and Photonics Technology Conference (AVFOP),* pp. 65-66, 2011.
[91] A. Hashmi, A. Eftekhar, S. Yegnanarayanan, and A. Adibi, "Analysis of optimal adaptive optics system for hybrid RF-wireless optical communication for maximum efficiency and reliability," *4th International Conference on Emerging Technologies(ICET),* pp. 62-67, 2008.
[92] R. M. Gagliardi and S. Karp, *Optical communications*, 2nd Edition: New York: John Wiley, 1995.
[93] V. R. Gudimetla, R. B. Holmes, C. Smith, and G. Needham, "Analytical expressions for the log-amplitude correlation function of a plane wave through anisotropic atmospheric refractive turbulence," *JOSA A,* vol. 29, pp. 832-841, 2012.
[94] Z. Ghassemlooy, W. Popoola, and S. Rajbhandari, *Optical wireless communications: system and channel modelling with MATLAB*: CRC Press, 2012.
[95] I. E. Lee, "Free-space optical communication systems with a partially coherent gaussian beam and media diversity," Northumbria University, 2014.
[96] W. K. Pratt, *Laser communication systems*, 1969.
[97] S. Betti, G. De Marchis, and E. Iannone, *Coherent optical communications systems*: Wiley-Interscience, 1995.
[98] J. C. Palais, *Fiber optic communication, 5th Edition . Prentice Hall, UK, 2005*.
[99] M. A. Khalighi, N. Aitamer, N. Schwartz, and S. Bourennane, "Turbulence mitigation by aperture averaging in wireless optical systems," *10th International Conference on Telecommunications (ConTEL),* pp. 59-66, 2009.
[100] E. Ip, A. P. T. Lau, D. J. Barros, and J. M. Kahn, "Coherent detection in optical fiber systems," *Optics Express,* vol. 16, pp. 753-791, 2008.
[101] A. Goldsmith, *Wireless communications*: Cambridge University Press, 2005.
[102] R. H. Clarke, "A statistical theory of mobile-radio reception," *The Bell System Technical Journal,* vol. 47, pp. 957-1000, 1968.
[103] T. Singal, *Wireless communications*: Tata McGraw-Hill Education, 2010.
[104] M. Ju and I. M. Kim, "Error performance analysis of BPSK modulation in physical layer network coded bidirectional relay networks," *IEEE Transactions on Communications,* vol. 58, pp. 2770-2775, 2010.
[105] D. MADUIKE, "Design and implementation of physical layer network coding protocols," Texas A&M University, 2009.
[106] J. G. Proakis, *Digital communications*, 2001.
[107] S. Haykin, *Communication systems*: John Wiley & Sons, 2008.
[108] Z. Shengli, S. C. Liew, and P. P. K. Lam, "Physical layer network coding," *ArXiv Preprint ArXiv:0704.2475,* 2007.

[109] H. Yang, W. Meng, B. Li, and G. Wang, "Physical layer implementation of network coding in two-way relay networks," *IEEE International Conference on Communications (ICC)*, pp. 671-675, 2012.
[110] L. B. Stotts, L. C. Andrews, P. C. Cherry, J. J. Foshee, P. J. Kolodzy, W. K. McIntire, *et al.*, "Hybrid optical RF airborne communications," *IEEE Proceedings*, vol. 97, pp. 1109-1127, 2009.
[111] L. C. A. a. R. L. Philips, *Laser Beam Propagation through Random Media , Bellingham, WA: SPIE Optical Engineering Press*, 2005.
[112] A. A. Farid and S. Hranilovic, "Outage capacity optimization for free-space optical links with pointing errors," *Journal of Lightwave Technology*, vol. 25, pp. 1702-1710, 2007.
[113] M. Uysal, L. Jing, and Y. Meng, "Error rate performance analysis of coded free-space optical links over gamma-gamma atmospheric turbulence channels," *IEEE Transactions on Wireless Communications*, vol. 5, pp. 1229-1233, 2006.
[114] M. Czaputa, T. Javornik, E. Leitgeb, G. Kandus, and Z. Ghassemlooy, "Investigation of punctured LDPC codes and time-diversity on free-space optical links," *11th International Conference on Telecommunications (ConTEL)*, pp. 359-362, 2011.
[115] H. G. Sandalidis, "Coded free-space optical links over strong turbulence and misalignment fading channels," *IEEE Transactions on Communications*, vol. 59, pp. 669-674, 2011.
[116] J. A. Anguita, J. Herreros, and I. B. Djordjevic, "Coherent multimode OAM superpositions for multidimensional modulation," *IEEE Photonics Journal*, vol. 6, pp. 1-11, 2014.
[117] I. B. Djordjevic, J. A. Anguita, and B. Vasic, "Error-correction coded orbital-angular-momentum modulation for FSO channels affected by turbulence," *Journal of Lightwave Technology*, vol. 30, pp. 2846-2852, 2012.
[118] I. B. Djordjevic, "Heterogeneous transparent optical networking based on coded OAM modulation," *IEEE Photonics Journal*, vol. 3, pp. 531-537, 2011.
[119] M. M. Ibrahim and A. M. Ibrahim, "Performance analysis of optical receivers with space diversity reception," *IEE Proceedings - Communications*, vol. 143, pp. 369-372, 1996.
[120] A. Farid and S. Hranilovic, "Outage capacity for MISO intensity-modulated free-space optical links with misalignment," *IEEE/OSA Journal of Optical Communications and Networking*, vol. 3, pp. 780-789, 2011.
[121] M. Abaza, R. Mesleh, A. Mansour, and E. H. M. Aggoune, "Spatial diversity for FSO communication systems over atmospheric turbulence channels," *IEEE Wireless Communications and Networking Conference (WCNC)*, pp. 382-387, 2014.
[122] R. Boluda-Ruiz, A. García-Zambrana, B. Castillo-Vázquez, and C. Castillo-Vázquez, "On the capacity of MISO FSO systems over gamma-gamma and misalignment fading channels," *Optics Express*, vol. 23, pp. 22371-22385, 2015.
[123] H. Kazemi, Z. Mostaani, M. Uysal, and Z. Ghassemlooy, "Outage performance of MIMO free-space optical systems in gamma-gamma fading channels," *Proceedings of the 2013 18th European Conference on Network and Optical Communications & 2013 8th Conference on Optical Cabling and Infrastructure (NOC-OC&I)*, pp. 275-280, 2013.

[124] M. M. Abadi, Z. Ghassemlooy, D. Smith, W. P. Ng, M. A. Khalighi, and S. Zvanovec, "Comparison of different combining methods for space-diversity FSO systems," *9th International Symposium on Communication Systems, Networks & Digital Signal Processing (CSNDSP)*,pp. 1023-1028, 2014.

[125] W. O. Popoola, "Subcarrier intensity modulated free-space optical communication systems," Northumbria University, 2009.

[126] A. Chaman-Motlagh, V. Ahmadi, and Z. Ghassemlooy, "A modified model of the atmospheric effects on the performance of FSO links employing single and multiple receivers," *Journal of Modern Optics*, vol. 57, pp. 37-42, 2010.

[127] M. A. Kashani, M. Uysal, and M. Kavehrad, "On the performance of MIMO FSO communications over double generalized gamma fading channels," *IEEE International Conference on Communications (ICC)*, pp. 5144-5149, 2015.

[128] C. K. Datsikas, K. P. Peppas, N. C. Sagias, and G. S. Tombras, "Serial free-space optical relaying communications over gamma-gamma atmospheric turbulence channels," *IEEE/OSA Journal of Optical Communications and Networking*, vol. 2, pp. 576-586, 2010.

[129] T. Xuan, W. Zhaocheng, X. Zhengyuan, and Z. Ghassemlooy, "Multihop free-space optical communications over turbulence channels with pointing errors using heterodyne detection," *Journal of Lightwave Technology*, vol. 32, pp. 2597-2604, 2014.

[130] A. S. Acampora and S. V. Krishnamurthy, "A broadband wireless access network based on mesh-connected free-space optical links," *IEEE Personal Communications*, vol. 6, pp. 62-65, 1999.

[131] J. Akella, M. Yuksel, and S. Kalyanaraman, "Error analysis of multi-hop free-space optical communication," *IEEE International Conference on Communications (ICC)*, vol. 3, pp. 1777-1781, 2005.

[132] M. Safari and M. Uysal, "Relay-assisted free-space optical communication," *Forty-First Asilomar Conference on Signals, Systems and Computers (ACSSC)*, pp. 1891-1895, 2007.

[133] C. Abou-Rjeily and A. Slim, "Cooperative diversity for free-space optical communications: transceiver design and performance analysis," *IEEE Transactions on Communications*, vol. 59, pp. 658-663, 2011.

[134] M. Karimi and M. Nasiri-Kenari, "Free space optical communications via optical amplify-and-forward relaying," *Journal of Lightwave Technology*, vol. 29, pp. 242-248, 2011.

[135] M. R. Bhatnagar, "Average BER analysis of differential modulation in DF cooperative communication system over gamma-gamma fading FSO links," *IEEE Communications Letters*, vol. 16, pp. 1228-1231, 2012.

[136] R. Boluda-Ruiz, A. Garcia-Zambrana, B. Castillo-Vazquez, and C. Castillo-Vazquez, "MISO relay-assisted FSO systems over gamma-gamma fading channels with pointing errors," *IEEE Photonics Technology Letters*, vol. 28, pp. 229-232, 2016.

[137] A. E. Kamal, ""1+N network protection for mesh networks: network coding-based protection using P-cycles," *IEEE/ACM Transactions on Networking*, vol. 18, pp. 67-80, 2010.

[138] O. M. Al-Kofahi and A. E. Kamal, "Network coding-based protection of many-to-one wireless flows," *IEEE Journal on Selected Areas in Communications*, vol. 27, pp. 797-813, 2009.

[139] R. C. Menendez and J. W. Gannett, "Efficient, fault-tolerant all-optical multicast networks via network coding," *Conference on Optical Fiber communication/National Fiber Optic Engineers Conference (OFC/NFOEC)*, pp. 1-3, 2008.
[140] E. D. Manley, J. S. Deogun, L. Xu, and D. R. Alexander, "All-optical network coding," *IEEE/OSA Journal of Optical Communications and Networking*, vol. 2, pp. 175-191, 2010.
[141] X. Zhou, D. Zhang, Y. Yang, and M. S. Obaidat, "Network- coded multiple-source cooperation aided relaying for free- space optical transmission," *International Journal of Communication Systems*, vol. 25, pp. 1465-1478, 2012.
[142] C. Abou-Rjeily, "All-active and selective FSO relaying: do we need inter-relay cooperation?," *Journal of Lightwave Technology*, vol. 32, pp. 1899-1906, 2014.
[143] Y. Tang, X. Zhou, Z. Zhang, and Q. Tian, "Performance analysis of a two-way network-coded free space optical relay scheme over strong turbulence channels," *IEEE Vehicular Technology Conference (VTCl)*, pp. 1-5, 2011.
[144] P. Puri, P. Garg, M. Aggarwal, and P. K. Sharma, "Outage analysis of two-way relay assisted FSO systems over weak turbulence region," *Annual IEEE India Conference (INDICON)*, pp. 1-5, 2013.
[145] P. Puri, P. Garg, and M. Aggarwal, "Outage and error rate analysis of network-coded coherent TWR-FSO systems," *IEEE Photonics Technology Letters*, vol. 26, pp. 1797-1800, 2014.
[146] W. O. Popoola and Z. Ghassemlooy, "BPSK subcarrier intensity modulated free-space optical communications in atmospheric turbulence," *Journal of Lightwave Technology*, vol. 27, pp. 967-973, 2009.
[147] I. E. Lee, Z. Ghassemlooy, W. P. Ng, and M. Uysal, "Performance analysis of free space optical links over turbulence and misalignment induced fading channels," *8th International Symposium on* in *Communication Systems, Networks & Digital Signal Processing (CSNDSP)*, pp. 1-6, 2012.
[148] J. C. Ricklin, S. M. Hammel, F. D. Eaton, and S. L. Lachinova, "Atmospheric channel effects on free-space laser communication," *Journal of Optical and Fiber Communications Reports*, vol. 3, pp. 111-158, 2006.
[149] A. García-Zambrana, C. Castillo-Vázquez, and B. Castillo-Vázquez, "Outage performance of MIMO FSO links over strong turbulence and misalignment fading channels," *Optics Express*, vol. 19, pp. 13480-13496, 2011.
[150] N. D. Chatzidiamantis, D. S. Michalopoulos, E. E. Kriezis, G. K. Karagiannidis, and R. Schober, "Relay selection protocols for relay-assisted free-space optical systems," *IEEE/OSA Journal of Optical Communications and Networking*, vol. 5, pp. 92-103, 2013.
[151] W. O. Popoola, Z. Ghassemlooy, C. G. Lee, and A. Boucouvalas, "Scintillation effect on intensity modulated laser communication systems—a laboratory demonstration," *Optics & Laser Technology*, vol. 42, pp. 682-692, 2010.
[152] H. E. Nistazakis, T. A. Tsiftsis, and G. S. Tombras, "Performance analysis of free-space optical communication systems over atmospheric turbulence channels," *IET Communications*, vol. 3, pp. 1402-1409, 2009.
[153] J. Goodman, *Statistical optics* vol. 1: New York, Wiley-Interscience, 1985.
[154] L. C. Andrews, R. L. Phillips, and C. Y. Hopen, *Laser beam scintillation with applications* vol. 99: SPIE press, 2001.

[155] S. Karp, R. M. Gagliardi, S. E. Moran, and L. B. Stotts, *Optical channels: fibers, clouds, water, and the atmosphere*: Springer Science & Business Media, 2013.
[156] Z. Xiaoming and J. M. Kahn, "Free-space optical communication through atmospheric turbulence channels," *IEEE Transactions on Communications, ,* vol. 50, pp. 1293-1300, 2002.
[157] T. A. Tsiftsis, H. G. Sandalidis, G. K. Karagiannidis, and M. Uysal, "Optical wireless links with spatial diversity over strong atmospheric turbulence channels," *IEEE Transactions on Wireless Communications,* vol. 8, pp. 951-957, 2009.
[158] H. G. Sandalidis, T. A. Tsiftsis, G. K. Karagiannidis, and M. Uysal, "BER performance of FSO links over strong atmospheric turbulence channels with pointing errors," *IEEE Communications Letters,* vol. 12, pp. 44-46, 2008.
[159] H. Yang, W. Shiqiang, S. Qingyang, G. Lei, and A. Jamalipour, "Synchronous physical layer network coding: a feasibility study," *IEEE Transactions on Wireless Communications,* vol. 12, pp. 4048-4057, 2013.
[160] M. K. Simon and M.-S. Alouini, *Digital communication over fading channels,* vol. 95: John Wiley & Sons, 2005.
[161] J. M. Borwein and R. E. Crandall, "Closed forms: what they are and why we care," *Notices of the AMS,* vol. 60, 2013.
[162] M. A. a. I. S. Stegun, "Handbook of mathematical functions with formulars, graphs and mathematical tables," *Dover,* 1977.
[163] W. O. Popoola, Z. Ghassemlooy, J. I. H. Allen, E. Leitgeb, and S. Gao, "Free-space optical communication employing subcarrier modulation and spatial diversity in atmospheric turbulence channel," *IET Optoelectronics,* vol. 2, pp. 16-23, 2008.
[164] K. Prabu, D. S. Kumar, and R. Malekian, "BER analysis of BPSK-SIM-based SISO and MIMO FSO systems in strong turbulence with pointing errors," *Optik - International Journal for Light and Electron Optics,* vol. 125, pp. 6413-6417, 2014.
[165] R. W. Hamming, "Error detecting and error correcting codes," *The Bell System Technical Journal,* vol. 29, pp. 147-160, 1950.
[166] M. J. Golay, "Notes on digital coding," *Proceedings of the Institute of Radio Engineers,* vol. 37, no. 6, pp: 657-657, 1949.
[167] J. Daniel and J. Costello, *Error control coding, fundamentals and applications,* Prentice Hall, Inc. Englewood Cliffs, New Jersey, 1983.
[168] P. Elias, "Predictive coding--I," *IRE Transactions on Information Theory,* vol. 1, pp. 16-24, 1955.
[169] A. Viterbi, "Error bounds for convolutional codes and an asymptotically optimum decoding algorithm," *IEEE Transactions on Information Theory,* vol. 13, pp. 260-269, 1967.
[170] K. Moon Todd, *Error correction coding, mathematical methods and algorithms*: John Wiley & Sons, Ltd, 2005.
[171] L. Bahl, J. Cocke, F. Jelinek, and J. Raviv, "Optimal decoding of linear codes for minimizing symbol error rate (Corresp.)," *IEEE Transactions on Information Theory,* vol. 20, pp. 284-287, 1974.
[172] S. Benedetto, D. Divsalar, G. Montorsi, and F. Pollara, "A soft-input soft-output APP module for iterative decoding of concatenated codes," *IEEE Communications Letters,* vol. 1, pp. 22-24, 1997.

[173] J. P. Woodard and L. Hanzo, "Comparative study of turbo decoding techniques: an overview," *IEEE Transactions on Vehicular Technology,* vol. 49, pp. 2208-2233, 2000.
[174] J. Erfanian, S. Pasupathy, and G. Gulak, "Reduced complexity symbol detectors with parallel structure for ISI channels," *IEEE Transactions on Communications,* vol. 42, pp. 1661-1671, 1994.
[175] P. Robertson, E. Villebrun, and P. Hoeher, "A comparison of optimal and sub-optimal MAP decoding algorithms operating in the log domain," *IEEE International Conference on Communications (ICC),* vol. 2, pp. 1009-1013, 1995.
[176] F. Xu, A. Khalighi, P. Caussé, and S. Bourennane, "Channel coding and time-diversity for optical wireless links," *Optics Express,* vol. 17, pp. 872-887, 2009.
[177] M. I. Petkovic, N. M. Zdravkovic, and G. T. Dordevic, "Error performance of uncoded and convolutional coded SC receiver over FSO channel with pointing errors," *21st Telecommunications Forum (TELFOR),* pp. 283-286, 2013.
[178] J. G. Proakis, *Digital communications* : *McGraw-Hill, New York, 1995*.
[179] G. D. Forney, and G. David Forney, *Concatenated codes*: vol. 11, MIT Press, Cambridge, 1966.
[180] C. Berrou, A. Glavieux, and P. Thitimajshima, "Near shannon limit error-correcting coding and decoding: turbo-codes. 1," *IEEE International Conference on Communications (ICC),* vol. 2, pp. 1064-1070, 1993.
[181] J. L. Massey, "Coding and modulation in digital communications," 3rd *International Zurich Seminar on Digital Communications,* 1974.
[182] G. Ungerboeck, "Channel coding with multilevel/phase signals," *IEEE Transactions on Information Theory,* vol. 28, pp. 55-67, 1982.
[183] C. E. W. Sundberg and N. Seshadri, "Coded modulations for fading channels: an overview," *European Transactions on Telecommunications,* vol. 4, pp. 309-324, 1993.
[184] E. Zehavi, "8-PSK trellis codes for a Rayleigh channel," *IEEE Transactions on Communications,* vol. 40, pp. 873-884, 1992.
[185] B. He and R. Schober, "Bit-interleaved coded modulation for hybrid RF/FSO systems," *IEEE Transactions on Communications,* vol. 57, pp. 3753-3763, 2009.
[186] L. Xiaodong and J. A. Ritcey, "Trellis-coded modulation with bit interleaving and iterative decoding," *IEEE Journal on Selected Areas in Communications,* vol. 17, pp. 715-724, 1999.
[187] S. X. Ng, T. H. Liew, L. L. Yang, and L. Hanzo, "Comparative study of TCM, TTCM, BICM and BICM-ID schemes," *53rd IEEE Vehicular Technology Conference (VTC),* vol. 4, pp. 2450-2454, 2002.
[188] F. Xu, M. A. Khalighi, and S. Bourennane, "Coded PPM and multipulse PPM and iterative detection for free-space optical links," *IEEE/OSA Journal of Optical Communications and Networking,* vol. 1, pp. 404-415, 2009.
[189] K. Kumar and D. K. Borah, "Hybrid symbols for parallel optical/rf channels using BICM-ID," *Electronics Letters,* vol. 47, pp. 1189-1190, 2011.
[190] K. Kumar and D. K. Borah, "Hybrid FSO/RF symbol mappings: merging high speed FSO with low speed RF through BICM-ID," *IEEE Global Communications Conference (GLOBECOM),* pp. 2941-2946, 2012.
[191] K. Kumar, "Pulse position modulation using BICM-ID for FSO channels," *International Telemetering Conference Proceedings*, 2013.

[192] M. C. Castro, B. F. Uchoa-Filho, T. T. V. Vinhoza, M. Noronha-Neto, and J. Barros, "Improved joint turbo decoding and physical-layer network coding," *IEEE Information Theory Workshop (ITW)*, pp. 532-536, 2012.
[193] T. Ferrett, M. C. Valenti, and D. Torrieri, "An iterative noncoherent relay receiver for the two-way relay channel," *IEEE International Conference on Communications (ICC)*, pp. 5903-5908, 2013.
[194] R. Steele and L. Hanzo, *Mobile Radio Communications*: IEEE Press-John Wiley, 1999.
[195] W. C. Y. Lee, "Comparison of spectrum efficiency between FDMA and TDMA in digital cellular," *39th IEEE Vehicular Technology Conference (VTC)*, vol. 1, pp. 165-168, 1989.
[196] K. Fazal and S. Kaiser, *Multi-carrier and spread spectrum systems: from OFDM and MC-CDMA to LTE and WiMAX* : 2008.
[197] G. R. Cooper and R. W. Nettleton, "A spread-spectrum technique for high-capacity mobile communications," *IEEE Transactions on Vehicular Technology*, vol. 27, pp. 264-275, 1978.
[198] W. Tranter, K. Shanmugan, T. Rappaport, and K. Kosbar, *Principles of communication systems simulation with wireless applications*: Prentice Hall Press, 2003.
[199] F. Brannstrom, T. M. Aulin, and L. K. Rasmussen, "Iterative detectors for trellis-code multiple-access," *IEEE Transactions on Communications*, vol. 50, pp. 1478-1485, 2002.
[200] S. I. Tachikawa, K. Toda, T. Isikawa, and G. Manibayashi, "Direct sequence/spread spectrum communication systems using chip interleaving and its applications for high- speed data transmissions on power lines," *Electronics and Communications in Japan (Part I: Communications)*, vol. 75, pp. 46-58, 1992.
[201] G. Xiang and N. Tung Sang, "A novel chip-interleaving DS SS system," *IEEE Transactions on Vehicular Technology*, vol. 49, pp. 21-27, 2000.
[202] M. Moher, "An iterative multiuser decoder for near-capacity communications," *IEEE Transactions on Communications*, vol. 46, pp. 870-880, 1998.
[203] L. Lihai, W. K. Leung, and P. Li, "Simple iterative chip-by-chip multiuser detection for CDMA systems," *57th IEEE Semiannual Vehicular Technology Conference(VTC)*, vol. 3, pp. 2157-2161, 2003.
[204] D. Garg and F. Adachi, "Performance of DS-CDMA with chip interleaving and frequency domain equalisation in a fading channel," *IEEE Proceedings-Communications*, vol. 152, pp. 757-763, 2005.
[205] L. Yu-Nan and D. W. Lin, "Novel analytical results on performance of bit-interleaved and chip-interleaved DS-CDMA with convolutional coding," *IEEE Transactions on Vehicular Technology*, vol. 54, pp. 996-1012, 2005.
[206] L. Yu-Nan and D. W. Lin, "Chip interleaving for performance improvement of coded DS-CDMA systems in Rayleigh fading channels," *58th IEEE Vehicular Technology Conference (VTC)*, vol. 2, pp. 1323-1327, 2003.
[207] P. LI, "Interleave-division multiple-access," *IEEE Transaction Wireless Communication*, vol. 5, pp. 938-947, 2006.
[208] W. Xiaodong and H. V. Poor, "Iterative (turbo) soft interference cancellation and decoding for coded CDMA," *IEEE Transactions on Communications*, vol. 47, pp. 1046-1061, 1999.

[209] K. Kusume, G. Bauch, and W. Utschick, "IDMA Vs. CDMA: detectors, performance and complexity," *IEEE Global Telecommunications Conference (GLOBECOM)*, pp. 1-8, 2009.
[210] K. Kusume, G. Bauch, and W. Utschick, "IDMA vs. CDMA: analysis and comparison of two multiple access schemes," *IEEE Transactions on Wireless Communications*, vol. 11, pp. 78-87, 2012.
[211] A. Dudkov and V. Ipatov, "Chip-interleaved decorrelation in asynchronous DS CDMA," *8th IEEE Workshop* in *Signal Processing Advances in Wireless Communications(SPAWC)*, pp. 1-5, 2007.
[212] H. Wu, L. Ping, and A. Perotti, "User-specific chip-level interleaver design for IDMA systems," *Electronics Letters*, vol. 42, pp. 233-234, 2006.
[213] C. Zhang and J. Hu, "2-Dimension interleaver design for IDMA systems," *4th IEEE International Conference on Circuits and Systems for Communications (ICCSC)*, pp. 372-376, 2008.
[214] S. Verdu, "Minimum probability of error for asynchronous Gaussian multiple-access channels," *IEEE Transactions on Information Theory*, vol. 32, pp. 85-96, 1986.
[215] D. Divsalar, M. K. Simon, and D. Raphaeli, "Improved parallel interference cancellation for CDMA," *IEEE Transactions on Communications*, vol. 46, pp. 258-268, 1998.
[216] C. Berrou and A. Glavieux, "Near optimum error correcting coding and decoding: turbo-codes," *IEEE Transactions on Communications*, vol. 44, pp. 1261-1271, 1996.
[217] M. C. Reed, C. B. Schlegel, P. D. Alexander, and J. A. Asenstorfer, "Iterative multiuser detection for CDMA with FEC: near-single-user performance," *IEEE Transactions on Communications*, vol. 46, pp. 1693-1699, 1998.
[218] R. H. Mahadevappa and J. G. Proakis, "Mitigating multiple access interference and intersymbol interference in uncoded CDMA systems with chip-level interleaving," *IEEE Transactions on Wireless Communications*, vol. 1, pp. 781-792, 2002.